A Novel Boundary Element Method for Low Reynolds Number External Flow of Biological Fluid Dynamics

Bwebum Cleofas Dang

A Thesis Submitted for the Award of Doctor of Philosophy

School of Computing, Science and Engineering

University of Salford Manchester

United Kingdom

May, 2020

Contents

List of Figures

Acknowledgement

I appreciate everyone that supported me during this research period. Particularly, I would like to thank my supervisor, Dr Edmund Chadwick, who has been very resourceful and generous by giving his time to answer my many questions. You have helped me to discover my potential–I truly appreciate you, Sir. Thanks to Dr Mohammed Mahmood who assist with useful advice during the early stage of model formulation. I am grateful to Professor O. Anwar Beg for pointing out specific things I needed to know for a good research output and for always willing to help whenever I come with questions.

Thanks to my wonderful siblings and extended family members back home in Nigeria for their patience during my absence and busy life throughout this period. I especially want to acknowledge my mum, Dcn Grace C Dang, and my late dad, Mr Cleofas I Dang, for their support and upbringing. I know if my dad were still here today, he would be very proud of who I am. Thanks to my girlfriend Deborah who supported me through this journey.

Thanks to everyone in our research office Newton Building for your support and friendship, I will never forget our time together which encourages me so much. Thanks to Dr Thomas Walsh for your useful suggestions: you have always supported me. You are patient, kind hearted, and always willing to help–thank you.

Thanks to all who at one point or another added value to my life: you all contributed to who I am today. All of my teachers in Plateau State, Nigeria: from LGEA primary school, Bokkos; Government Secondary School Bokkos, COCIN Comprehensive College, Gindiri; and the Department of Mathematics, University of Jos. I

would also like to thank the Department of Mathematics at the Federal University of Technology, Yola.

Special thanks to Nigerian government and the University of Jos, Nigeria, for giving me this life time opportunity to develop myself in research–God bless Nigeria.

Finally, I would like to thank all my friends and well wishers here in the UK, in Nigeria, and all over the world. Thank you all.

Declaration

I declare that there is no conflict of interest and that this research is carried out by me, Bwebum Cleofas Dang, under the supervision of Dr Edmund Chadwick.

Dedication

I dedicate this to the maker of the universe, the giver of life, without whom nothing could be that it is; God I exalt you now and forever, Amen.

Abstract

Consider two dimensional low Reynolds number flow past a body. In this thesis, the problems of steady flow past a circular cylinder, steady flow past an elliptical cylinder, and the motion of a generic tail-like body are investigated. The theoretical treatment by Chadwick (Chadwick, 2013) is detailed and elaborated upon. A boundary integral representation that matches an outer Oseen flow and inner Stokes flow is given, and the matching error is shown to be smallest when the outer domain is as close as possible to the body. Also, it is shown that as the origin of the Green's function is approached, the oseenlet becomes the stokeslet to leading order and has the same order of magnitude error as the matching error. This means that a novel boundary integral representation in terms of oseenlets is possible. To test this, we have developed a corresponding boundary element code that uses point collocation weighting functions, linear shape functions, and two-point Gaussian quadrature with analytic removal of the Green's function singularity for the integrations.

First, we compare against various methods for the benchmark problems of flow past a circular cylinder and also a cylinder with an elliptical cross-section. The other methods are: representations using stokeslets (that suffer from Stokes' paradox giving an unbounded velocity); Lamb's (Lamb, 1932) treatment; Yano and Kieda's Oseen flow treatment (Yano & Kieda, 1980); and the matched asymptotic formulations of Kaplun (Kaplun & Lagerstrom, 1957) and Proudman and Pearson (Proudman & Pearson, 1957) which Lee and Leal (Lee & Leal, 1986) later used. In particular we use the drag coefficient for the comparison. The advantage of this method over existing ones is that it is accurate, uncomplicated to use, and this is demonstrated and discussed. Finally, we consider the steady forward motion of a generic tail-like body and how the frequency varies against body thickness, amplitude, wavelength and Reynolds number, and then discuss the results.

Chapter 1

Introduction

1.1 Introduction of the Study

Integral equations have been in use for almost two centuries. After their introduction by Abel in 1823 (Abel, 1823), many engineers, mathematicians and scientists have found them very useful in solving physical problems associated with differential equations. To be able to apply an integral equation to a differential equation, it has to first be reformulated as the convolution of a kernel-which is referred to as the Green's function density. When the Green's function of a particular partial differential equation is known, then the most efficient method for solving such partial differential equations is the Boundary Integral Method (BIM), provided the integral formulation can be established (Hao, Hu, Li, & Song, 2018). The Green's function is specific to the differential operator. For instance, the kernel of the Oseen equation is called *oseenlet* and similarly the kernel of the Stokes equation is called *stokeslet*, a name that was coined by Hancock (Hancock, 1953). It was later realised from the independent proofs given by Ehrenpreis (Ehrenpreis, 1954, 1955) and Malgrange (Malgrange, 1956) that only a limited class of differential operators can have a representation using the Green's function. This therefore limits integral equations to only specific differential equations whose integral representation can be found. With development of quadratures and stable discretisation, evaluation of integrals becomes more accurate and efficient (Hao et al., 2018).

Over the past five decades, a numerical method called the Boundary Element Method (BEM) has been developed to solve integral equations. BEM can be traced back to the 1960s (Cheng & Cheng, 2005) where its numerical implementation was made robust with the advent of powerful computers which aid in solving large sets of equations. BEM becomes very useful for solving partial differential equations whose integral equations are known and can be evaluated. It can be seen that BEM performs numerical discretisation on the boundary and so on a reduced spatial dimension. For example, for problems in three spatial dimensions (that is, a volume), by application of BEM, the problem will reduce the discretisation to be performed on the bounding surface only. Also for two spatial dimensions (that is, a surface), by application of BEM, the problem will reduce to the boundary curve only. It is worth noting that in the field of fluid mechanics, not all problems can be transformed to integral form. Those which can be transformed are governed by linear equations, some of which include irrotational and inviscid potential flow, and creeping flow such as Stokes flow and Oseen flow.

1.2 Aim and Objectives

1.2.1 Aim of the Study

The aim of this thesis is to provide an accurate and uncomplicated-to-use method for low Reynolds number flows used in biological fluid dynamics. Currently, the existing methods are: Stokes flow (Stokes, 1851), Yano and Kieda's (Yano & Kieda, 1980) Oseen flow (Oseen, 1910), Lamb's (Lamb, 1932) approximation, the matched asymptotic procedure of Proudman and Pearson (Proudman & Pearson, 1957) and, separately, Kaplun and Lagerstrom (Kaplun & Lagerstrom, 1957) and Navier-Stokes Computational Fluid Dynamics (CFD) solvers. All of these methods have disadvantages: Stokes flow suffers from Stokes' paradox of unbounded velocity; Yano and Kieda's approach is unclear in how to extend to complicated geometries; Lamb's approximation suffers from lack of accuracy; the matched asymptotic procedures are complicated to implement and the CFD solvers are highly computer-intensive,

particularly for exterior domain problems which must be truncated. In contrast, it will be demonstrated that our method is the most accurate, fastest, and also uncomplicated to implement and use. This means it shows great promise for modelling complex geometries for low Reynolds number flow in biological fluid dynamics problems. In particular, this is achieved by developing a novel BEM and testing it against the following benchmark problems of flow pass a circular cylinder and flow past an elliptic body.

1.2.2 Objectives of the Study

The objectives that will be achieve by this studies are as follows:

1. Investigate the existing theory and numerical approaches for low Reynolds number viscous fluid flow
2. Present a matched asymptotic expansion for Stokes flow in the near field and Oseen flow in the far field for the solution of viscous fluid flow.
3. Use the matched asymptotic expansion formulation and develop a BEM that will provide solution to a low Reynolds flow in an unbounded domain.
4. Validate the BEM developed using flow past a circular cylinder and flow past an elliptical cylinder.
5. Model a tail-like body shape for motion in an exterior domain.

1.3 Statement of Problem

In this thesis, an unbounded domain will be considered for a flow past a circular cylinder in two dimensions, steady flow past an elliptical cylinder, and the motion of a generic tail-like body using Oseen equations for both the near-field and the far-field (Hao et al., 2018), (Pozrikidis, 2002, 1992). Studies of slow motion of viscous fluid flow past a body in an unbounded domain date back to the work

of Stokes in 1851 (Stokes, 1851). Because of the difficulty in satisfying boundary conditions both at the cylinder surface and the far-field, Stokes drew a conclusion that such a solution does not exist(Stokes' paradox). Several analytical studies began to emanate, seeking a solution to Stokes' paradox. This includes the approximation given by Oseen (Oseen, 1910), further approximated by Lamb (Lamb, 1911, 1932), and later Imai (Imai, 1954). However, Oseen's approximation assumes linearisation of the free stream velocity which breaks down on the body boundary. To overcome this, the method of matched asymptotic expansions, which combines linearisation to Stokes flow in the near-field matched to linearisation to Oseen flow in the far-field region was presented by Proudman and Pearson (Proudman & Pearson, 1957) and Kaplun and Lagerstrom (Kaplun & Lagerstrom, 1957). Experimental studies (Tritton, 1959) with different qualitative and quantitative results have also been presented, in particular for the benchmark problem of steady flow past a circular cylinder.

Further to the numerical methods discussed above, Yano and Kieda (Yano & Kieda, 1980) applied a discrete singularity method to solve a two-dimensional flow by distributing oseenlets, sources, sinks and vortices in the interior of an obstacle with a least square criterion to satisfy the boundary condition. Their result was benchmarked against the analytic results of Lamb (Lamb, 1932), Kaplun and Lagerstrom (Kaplun & Lagerstrom, 1957), and the experimental results of Tritton (Tritton, 1959) for the drag coefficient. It was revealed that when the Reynolds number is below one ($Re < 1$) there is good agreement between theory and experiment, but when the Reynolds number is in the range 1 to 4 the analytical results do not align very closely with experiment, except in the numerical studies presented by Yano and Kieda (Yano & Kieda, 1980). The analytical results work well for body surfaces with simple geometries, but as soon as the geometry becomes complicated numerical approaches provided better basis for analysis. For application to more complicated geometries, Lee and Leal (Lee & Leal, 1986) considered a matched asymptotic expansion method that used Green's integral representations of the velocity. Chadwick (Chadwick, 2013) took this approach and matched Stokes and Oseen flows within a boundary integral formulation. He found that the error is least if the matching boundary is on the body itself. It is important to note that this

approach does not break down on the body boundary because in this formulation the oseenlet approximates to the stokeslet.

In this thesis, the approach of Chadwick (Chadwick, 2013) is tested by developing a BEM using point collocation weighting functions, linear shape functions, and two-point Gaussian quadrature with analytic removal of the Green's function singularity for the integrations. The purpose is to develop a new numerical technique for low Reynolds number flows up to $Re = 1$ that deals with complex geometries and moving bodies.

1.4 Outline of the Thesis

This thesis will take the following outline

- First chapter present general introduction and background of the studies. The aim and objectives is stated in this chapter and also the problem statement will also be giving here.
- Second chapter will present survey of relevant literatures, this will comprise the basic equation governing fluid flows and in particular the equations for viscous fluid flow. In this chapter, some examples of models of viscous fluid flow with applications in biology will also be presented. Stokes paradox and a comparison between some numerical methods will be presented.
- Third chapter will discuss the general theoretical background, derivation of equations that will be use in this thesis. Navier-Stokes equation will be derived and Green's integral representation of Oseen and Stokes velocity will be presented.
- Fourth chapter is the model formulation, this is where boundary element formulation for Stokes and Oseen equation is detailed with analytic removal of the Green's function singularity.
- Fifth chapter is dedicated for validation of the model developed, validation for flow past a circular cylinder and flow past an elliptic cylinder. Plots for the

drag coefficient against the Reynolds number will be presented, this is going to be compare with different other existing results.

- Sixth chapter is where the model is design for flow past a circular cylinder, elliptical cylinder, and to mimic a moving tail-like body shape in motion. The data for the tail-like body here is hypothetical, but a sensitivity analysis is carried out on the data used.

- The last chapter is summary, conclusion, and suggestion for future studies.

1.5 Summary of Chapter

In this chapter, Integral equations and BEM are introduced. The aim of the study and objectives that will be achieved are also stated in this chapter, followed by statement of the problem. The motivation is from the fact that at very low Reynolds number, stokes paradox holds for two dimensional flow. In this studies, a method that matches the near-field Stokes with the far-fields Oseen will be presented. An Outline for the thesis is presented at the closing of this chapter.

Chapter 2

Background of Study and Literature Reviews

2.1 Fluid Flows and their Classification

Fluid flows can be classified into two different categories. The first category is referred to as $external flow$: this comprises a flow which is of infinite extent, that is, flow past a body in an exterior domain. One example of such flow includes problems associated with the motion of self propelled micro-organisms. The second is referred to as $internal flow$: this has to do with flows in the confined boundaries of a container, and so it is of finite extent within an interior domain (Shankar, 2007).

The main focus of this thesis will be on external flows. One feature of such systems is that the outer boundary conditions usually consist mainly of a decay condition which eliminates the problem of singularities in the boundary. Two dimensional flow past a circular cylinder for low Reynolds number falls under the category of external flow. In this study, attention will be focused on such external flows in an unbounded domain.

2.2 Stokes Paradox

Work on slow flow viscous fluids can be dated as far back as the work of Stokes in 1851 (Stokes, 1851), wherein he was investigating slow motion of fluid around an infinite cylinder. Stokes considered external flows in an effectively infinite ambient viscous fluid. While conducting his research, it was difficult for Stokes to be able to correctly compute boundary conditions that are either near or on the cylinder's surface or far away from the cylinder in a two dimensional regime using the Stokes equation. This caused him to postulate that such solutions did not exist, and this was later called Stokes' Paradox (Khalili & Liu, 2017). Stokes' paradox implies that there does not exist a bounded solution to the Stokes equation in two-dimensional flow past a finite body. This is because the velocities tend to grow as the distance away from the finite body increases, such growth is logarithmic because of the singular nature of the stokeslet as can be seen in (2.1). In three dimensions, the velocity does not vary logarithmically, but rather contains a decay property as seen in (2.2):

$$\text{Two-dimensional stokeslet: } u_i^{(j)} = \frac{Re}{4\pi\mu}\left(\delta_{ij}\ln r - \frac{x_i x_j}{r^2}\right), \tag{2.1}$$

$$\text{Three-dimensional stokeslet: } u_i^{(j)} = \frac{Re}{8\pi\mu}\left(\frac{1}{r} - \frac{x_i x_j}{r^3}\right), \tag{2.2}$$

where Re is the Reynolds number, r is the radial distance, μ is viscosity, δ_{ij} is the Kronecker delta function such that $\delta_{ij} = 1$ if $i = j$ and $\delta_{ij} = 0$ if $i \neq j$, x_i is a Cartesian coordinate (x_1, x_2, x_3) and $u_j^{(i)}$ is velocity of the stokeslet, where the direction $i = (1, 2, 3)$, and j is the order of stokeslet.

Stokes' paradox prompted many applied mathematicians to start work on a way to solve the problem of finding a solution to the two-dimensional Stokes equation. Some useful results that attempt to solve it include the method of matched asymptotic expansion used by Proudman and Pearson (Proudman & Pearson, 1957) and Kaplun and Lagerstrom (Kaplun & Lagerstrom, 1957). In their method, the Stokes equation provided a solution to the inner boundaries near the finite body, while far away from the body the Oseen equation for a uniform stream flow at infinity (which include a convective term) described the flow field. Matching the Stokes and the Oseen equations using matched asymptotic expansions (Proudman & Pearson,

1957; Kaplun & Lagerstrom, 1957; Lee & Leal, 1986) yields an approximation to two dimensional flow past a circular cylinder. The equivalent formulation of this same problem in three dimensions does not require matched asymptotic expansion, because it does not posses any non-uniformity (S. H. Smith, 1987).

2.2.1 Flow Past a Circular Cylinder

As discussed above, previous to the work by Proudman and Pearson and Kaplun and Lagerstrom in 1957 there was no solution to the Stokes equation for flow past a circular cylinder in two dimensions. Their matched asymptotic expansion approach prompted other authors to begin work on that area of research. Below is a discussion of some research into the problem that Stokes encountered in 1851.

Studies of Yano and Kieda: Yano and Kieda (Yano & Kieda, 1980) solve a low-Reynolds number flow past cylindrical bodies for an incompressible viscous fluid that is formulated based on the Oseen equation. They proposed a discrete singularity method inspired by the work of Imai (Imai, 1954) to model an Oseen flow past a circular cylinder. This method of a discrete singularity for the solution of a potential flow problem in Yano and Kieda (Kieda & Yano, 1978) was based on a least square criterion for the boundary conditions to model a two-dimensional potential flow problem. It was the extension of this method to low Reynolds number flow that yielded the next paper by the same authors (Yano & Kieda, 1980) for an external flow in two-dimensions. To establish this method, oseenlets, sources, sinks, and vortices were distributed in the interior of the body surface using least square criterion for the boundary condition. This method was applied to calculate the drag acting on a circular cylinder, the forces acting on an inclined elliptic cylinder, the forces acting on two circular cylinders, and forces acting on an inclined square cylinder. For a Reynolds number of less than one, the results of Yano and Kieda compared favourably with the analytical results of Lamb (Lamb, 1932) and Imai (Imai, 1954), but as the Reynolds number began to increase greater than one ($Re > 1$), the results of Yano and Kieda gave a better match with experimental results (Tritton, 1959). In contrast, Lamb's result diverges in this limit.

Studies of Proudman and Pearson: In the work of Proudman and Pearson

(Proudman & Pearson, 1957), they assumed a uniform flow field at infinity with a velocity of order $\frac{1}{\log Re}$, which gives a velocity on the matching boundary between Stokes flow and the far field of order one, which in turn gives a velocity on the body of order $\frac{1}{\log Re}$. This means that the Stokes flow velocity is bounded on the matching boundary.

Studies of Kaplun and Lagerstrom: Kaplun and Lagerstrom (Kaplun & Lagerstrom, 1957) used the method of matched asymptotic expansion to solve a flow past a circular cylinder for an incompressible viscous fluid in two dimensions. In the matched asymptotic expansion that Kaplun and Lagerstrom presented, it is assumed that a far-field uniform flow field velocity of order one was assumed. Rescaling, however, gave a representation equivalent to Proudman and Pearson. Further, Kaplun and Lagerstrom did not model a near-field Stokes region, unlike Proudman and Pearson. Hence, they considered a complete expansion valid everywhere in the flow region both on the body and the far-field.

Studies of Chadwick: Chadwick (Chadwick, 2013) also used matched asymptotic expansion to match Stokes and Oseen flow within a boundary integral formulation. He found that the error is least if the matching boundary is on the body itself (this is because the error in the matching is of order $\mathcal{O}\left(\frac{1}{\ln Re\frac{L^*}{L}}\right)$ where L^* is the distance to the boundary and L is the length of the body. So the error is smallest when the L^* is smallest, that is $L^* = L$.). It is noted that this approach does not break down on the body boundary because in the formulation the oseenlet approximates to the stokeslet.

Studies of Tomotika: In their studies, Tomotika and Aoi (Tomotika & Aoi, 1951) considered an expansion formula for the drag experienced by a circular cylinder in motion through a viscous fluid for a low Reynolds number. The expansion formula was represented in a power series of the Reynolds number for a steady flow. It was revealed that up to the fourth order, their power series representation correctly express the approximation with high accuracy as long as the Reynolds number is not more than four ($Re \leq 4$).

Studies of Tritton: Experimental studies for flow past a circular cylinder at low Reynolds number was carried out by Tritton (Tritton, 1959). The experiment present description for measurement of drag coefficient experience by a moving body

at a low Reynolds number in the range 0.5 to 100 ($0.5 \leq Re \leq 100$). The experiment was observed for bending of quartz fibres in a stream flow. Tritton was able to compare his work with other experimental values and various theoretical results which shows good agreement.

2.3 The Equation Governing Fluid Flow

Motion of any continuous medium, whether fluid or solid, is governed by the Cauchy equation given by

$$\rho \frac{Du_i}{Dt} = \frac{\partial}{\partial x_j}\sigma_{ij} + f_i \tag{2.3}$$

$$\frac{\partial \rho}{\partial t} + \frac{\partial}{\partial x_i}\left(\rho u_i\right) = 0, \tag{2.4}$$

where u_i is the fluid velocity, x_i is the Cartesian coordinate in the Einstein tensor suffix notation, σ_{ij} is the stress tensor, f_i is a body force acting on the fluid (such as gravity), t is time, ρ is the density of the substance and the material derivative is given by

$$\frac{Du_i}{Dt} \equiv \frac{\partial u_i}{\partial t} + u_j \frac{\partial u_i}{\partial x_j}. \tag{2.5}$$

If the fluid is Newtonian, the stress tensor is related to the pressure p, and also to the rate of deformation tensor by the linear constitutive equation

$$\sigma_{ij} = -p\delta_{ij} + 2\mu\left(e_{ij} - \frac{1}{3}\Delta\delta_{ij}\right). \tag{2.6}$$

Here $e_{ij} = \frac{1}{2}\left(\frac{\partial u_i}{\partial x_j} + \frac{\partial u_j}{\partial x_i}\right)$, $\Delta = e_{ii}$, and μ is the dynamic viscosity. The first term on the right hand side of equation (2.6) is the sum of the isotropic part, $-p\delta_{ij}$, and the remaining anisotropic part $2\mu\left(e_{ij} - \frac{1}{3}\Delta\delta_{ij}\right)$ that can be termed the deviatoric stress tensor which contributes to the tangential stresses. Its diagonal elements sum to zero. This deviatoric term depends on the motion of the fluid. Though viscosity depends significantly on temperature (and on the presence of temperature differences), then it can also be regarded as function of position. Nevertheless, in most cases temperature differences are so small as to be negligible, thus enabling the viscosity to be regarded as uniform throughout the fluid and therefore considered constant (Batchelor, 1967). In this approximation, substituting the stress

tensor back into the Cauchy equation (2.3) yields the Navier-Stokes equation for an incompressible fluid with constant viscosity:

$$\rho\frac{Du_i}{Dt} = f_i - \frac{\partial p}{\partial x_i} + \mu\left(\frac{\partial^2 u_i}{\partial x_j \partial x_j} + \frac{1}{3}\frac{\partial \Delta}{\partial x_i}\right). \tag{2.7}$$

If the density is constant as is usually the case with incompressible fluid, the Navier-Stokes and mass conservation equations become, respectively,

$$\rho\frac{\partial u_i}{\partial t} + \rho u_j\frac{\partial u_i}{\partial x_j} = f_i - \frac{\partial p}{\partial x_i} + \mu\frac{\partial^2 u_i}{\partial x_j \partial x_j} \tag{2.8}$$

and

$$\frac{\partial u_i}{\partial x_i} = 0. \tag{2.9}$$

Linearisation of the Navier-Stokes equation results in the Stokes and Oseen equations (Shankar, 2007). Detailed derivation and further discussion of the above will be presented in the next Chapter.

Stokes Equation: A linearisation of the Navier-Stokes equation for low Reynolds number (see section 2.3.2) yields the Stokes equation, which describes the motion of a slow viscous fluid. Generally, this type of fluid is characterised by the dominance of viscous forces over inertial forces, rendering its velocity very low as the viscosity becomes very large (creeping flow). The Stokes equation can be traced back to the early work of Stokes, with creeping flow first studied to understand lubrication problems (Stokes, 1851). After that, its application became very popular. A key property of the Stokes equation includes instantaneity, which is to say that Stokes flow does not depend on time except through time-dependent boundary conditions. This instanteinity means that a flow that is generated due to varying time boundary condition, if the opposite boundary condition is applied in reverse, exactly the same flow will be obtained, for example when trying to pull something from a sticky surface. Additionally, and due to being time independent, the Stokes equation is time reversible. As a result, if one were to solve the time-reversed Stokes equation they would obtain the same result as solving the original non-time reversed equation. In practice, this is demonstrated in the difficulty of mixing two different viscous fluids together. The last property that will be mentioned here is the Stoke's paradox, a situation involving the absence of a solution for the Stokes equation considering two-dimensional flow around an infinitely long circular cylinder. Examples of creeping

flow where the Stokes equation can be applied include the swimming of micro-organisms, movement of sperm cells through the convoluted geometry of the fallopian tube and in industry where creeping flow occurs in paint, MicroElectroMechanical System (MEMS) devices, and in the flow of viscous polymers. To solve the Stokes equation, different well-known methods for solving linear differential equations can be used. To utilise the BIM, the fundamental solution of the Stokes equation is called *stokeslet* which is the Green's function of the Stokes equation (Hancock, 1953) is employed.

Oseen Equation: The Oseen equation was first proposed by Oseen (Oseen, 1910) as a linearisation of the non-linear convective terms of the Navier-Stokes equation. By approximating the forces acting on the body at low Reynolds number, a solution for homogenous fluid flow problems can be achieved using the Oseen equation. However, the Oseen equation is not valid for flows that are very near to the body surfaces. Because of Stokes' paradox, Oseen proposed an improvement to Stokes equation in order to find a solution for two dimensional flows around an infinitely long cylinder. Oseen flow, just like Stokes flow, describes the flow of incompressible viscous fluid at low Reynolds number (Oseen, 1910). Oseen's approach makes an approximation to the convective acceleration terms of the Navier-Stokes equation in that the velocity becomes a uniform stream flow far away from the two dimensional circular cylindrical body. The fundamental solution of the Oseen equation is called *oseenlet*. These oseenlets arise due to the singular point force embedded in the Oseen flow. Applications of the Oseen equation include bio-engineering and blood flow in small vessels with low Reynolds number.

The fact low Reynolds number flow past a circular cylinder in two dimensions has no exact solution due to Stokes paradox is the main inspiration behind the present work. While other authors have found approximate solutions, our approach provides more rigorous solutions while expanding the potential scope of such research due to the lower computational complexity of our method. Here, a boundary-only approach shall be presented and compared against the methods of Lamb (Lamb, 1932), Imai (Imai, 1951) and Kaplun (1957). Most of the existing work focuses mostly on internal flow, while less attention has been given to external flow in

two dimensions because for internal flows Stokes paradox is not an issue while for external flows stokes paradox holds.

2.3.1 Divergence Theorem

The divergence theorem is key in the Boundary Integral Method (BIM). BIM depends on the use of the divergence theorem, which allows the conversion of a volume integral to a surface integral or a surface integral to a line integral. Let V_c be an arbitrary volume in a given space bounded by a closed surface D. The divergence theorem states that the volume integral of the divergence of any differentiable vector function, $\mathbf{F} = (f_x, f_y, f_z)$, over V_c is equal to the flow rate of $\mathbf{F}$ across D (Pozrikidis, 2011), that is

$$\iiint_{V_c} \nabla \cdot \mathbf{F} dV = \iint_D \mathbf{F} \cdot \mathbf{n} dS. \tag{2.10}$$

2.3.2 Reynolds Number

The Reynolds number (Re) of a fluid is a dimensionless quantity that arises from scaling the Navier-Stokes equation. It is the ratio of inertial forces to viscous forces. At low Reynolds number, flow tends to be laminar, while large Reynolds number corresponds to turbulent flow. Reynolds carried out an experiment entitled 'an experimental investigation of the circumstances which determine whether the motion of water in parallel channels shall be direct or sinuous'.

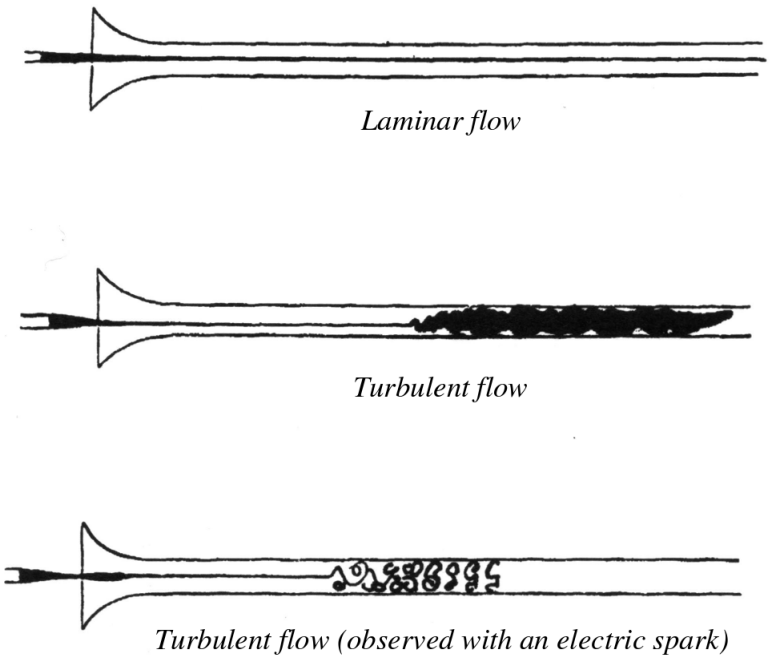

Figure 2.1: Experiment by Reynold showing flow at different rates. Original drawing from (Reynolds, 1883)

The investigation is shown in figure (2.1) (Reynolds, 1883). His methodology involved injecting dyed water into a clear glass pipe and then allowing it to flow at different rates. He noticed that the flow could be characterised as laminar or turbulent based on a critical value of the dimensionless number he called 'R'. In laminar flow (see figure 2.1 top), the liquid moves in parallel layers: the injected dye moves in streak lines with the water in the pipe at low flow rates. After a certain critical number at higher flow rate, however, the flow becomes turbulent (see figure 2.1 middle). The dye moves in an irregular manner mixing up with the fluid inside the tube (see figure 2.1 bottom) when the flow was observed with a stroboscopi light thereby creating those multiple eddies of different scales were observed. Sommerfeld was the first to call the proposed dimensionless number the "Reynolds number", as he added it in his equation called the "Orr-Sommerfeld equation" during an international congress of mathematicians in Rome (Sommerfeld, 1908). The Reynolds number is given as

$$Re = \frac{\rho U L}{\mu}, \tag{2.11}$$

or equivalently

$$Re = \frac{UL}{\nu}, \tag{2.12}$$

where $\nu = \frac{\mu}{\rho}$ is the kinematic viscosity, L is a characteristic length scale associated with the body, and U is a characteristic velocity. This determines whether the flow is laminar or turbulent based on the properties of the fluid including velocity, density, and viscosity. For a viscous fluid, the Oseen equation describes the flow field far from the body while the Euler equation describes the flow field in an inviscid flow.

2.4 Application of the Boundary Element Method in Biology

In biological fluids, numerical methods can be used to model motion in fluid flow. For instance, cilia and flagella (see figure 2.2) which are hair-like structures on the free ending of cells are locomotive organelle of micro-organisms. Flagella are very useful motile organelle for many organisms that navigate in biological fluids, ranging from the microscopic to some macroscopic organisms (Fawcett, 2014). Beside their locomotive importance, flagella also help in food gathering and response to environmental changes (Witman, 1990). At a very low Reynolds number, the flow of a fluid is very slow because of the dominance of viscous forces over inertial forces (Reynolds, 1883). Some common examples of models (among many) that describe such flows include the motion of micro-organisms in viscous fluid (Montenegro-Johnson, Smith, Smith, Loghin, & Blake, 2012). One example of this is the movement of mammalian spermatozoa to reach the fallopian tube where fertilisation will eventually take place (Fauci & Dillon, 2006).

Studies of the active movement of cells and transport of fluids at the microscopic level have been target problems in the field of theoretical biology. They attract the interest of many researchers in applied mathematics. Microscopic swimming of biological organisms has been studied by many biologists in detail (Parker, 1905; Gray, 2015; Verworn, 1891). As collaboration between experimentalists and theoreticians began, it gave meaningful development to this area of research. In

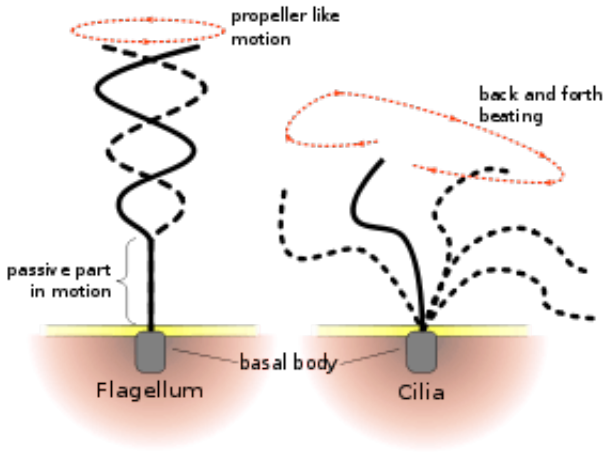

Figure 2.2: Flagella and cilia demonstrating beat pattern. Original photo on Wikipedia licensed CC-BY-3.0

return, the collaboration gave way for the development of models of slender body theory (a model through distribution of force singularities) to study, so-called "thin body" swimmers (Hancock, 1953). Different numerical methods have been used to solve problems regarding fluid motion of micro-swimmers. These include the popular *Finite Element Method* (FEM) (Montenegro-Johnson et al., 2012; Zhu, Lauga, & Brandt, 2012). Using this method to run numerical simulations, Zhu et al., studied the kinematic changes in swimming microorganism (?, ?; Montenegro-Johnson, Smith, & Loghin, 2013). They considered two cases: the first was swimming in Newtonian fluid and the second was swimming in viscoelastic fluid for pusher-type swimmers and puller-type swimmers. Some of the results revealed show that swimming speed in viscoelastic fluid is less than that in a Newtonian one (Zhu et al., 2012). In mammals, flagella help in reproduction by propelling the sperm swim to meet the ovum for fertilisation (Henkel, Bittner, Weber, Hüther, & Miska, 1999; Nonaka et al., 1998; D. Smith, Gaffney, Blake, & Kirkman-Brown, 2009). D. Smith et al. also used BEM to carry out a simulation study on the accumulation of human sperm near surfaces (D. Smith et al., 2009).

On the other hand, plankton (which uses flagella for movement) can also be modelled using BEM. Plankton are moving organisms living mostly in the sea, ponds, streams or large rivers. There are many different species of planktons and to

a large extent they are aquatic and therefore their motion is mostly by swimming using flagella (Baretta-Bekker, Duursma, & Kuipers, 1992; Suthers & Rissik, 2009). Different species of plankton come in different sizes ranging from picoplankton with a size of less than $3\mu m$ (Kress, 2019) to megaplankton with size of greater than $20cm$. They are of particular interest due to their position in the food chain; their size and distribution also contribute to their usefulness. Some of them, such as phytoplankton are primary producers (autotrophs), while others such as bacterio plankton and zoo plankton are consumers (heterotrophs). Jelly fish and krill also fall into the latter category (Raymont, 1980; Suthers & Rissik, 2009).

In addition, plankton plays a vital role in the carbon cycle (Falkowski, 2012) serving as the largest source of food for aquatic animals. Phytoplankton are free-floating photosynthetic micro-organisms. As a result of their natural life cycle, phytoplankton are important contributors to oceanic carbon fixing (Falkowski, 2012; Weber & Deutsch, 2010). Since the size of the resulting carbon is dependant on the phytoplankton population (and population density), it is important to understand their motion (A. Longhurst, Sathyendranath, Platt, & Caverhill, 1995; A. R. Longhurst & Harrison, 1989).

2.5 Comparison of Some Important Numerical Methods

Several numerical methods have been developed for solving partial differential equations. The most popular numerical methods used in fluid mechanics are the Finite Difference Method (FDM), Finite Element Method (FEM), Finite Volume Method (FVM), and BEM. Detail of These methods including their advantages and disadvantages will be discuss next.

2.5.1 Finite Difference Method

FDM is a domain method for solving differential equation through discretisation. It does not however finds solutions at the nodes, but rather it solves the problem by storing the values of the function only at the grid points. Taylor's theorems are used for the approximation of the differential equations in the finite difference method. The underlying principle of FDM is that the regions over which the independent variables of the partial differential equation is defined has been replaced by a finite grid of points at which the dependent variable is approximated (Causon & Mingham, 2010).

Advantages of the Finite Difference Method:

1. The main advantage of FDM is the fact that it is a very exact method. The solutions obtained from FDM are usually significantly closer to the solution, as the results obtained from, e.g., weighted residual methods (Rapp, 2017).

2. Finite difference method is computationally efficient if the simulation can be discretise in a square or rectangular geometry using a regular grid. In such case FDM is more efficient to easily implement than for finite-element and finite-volume methods.

3. Finite difference method has a simple code structures that is easy to implement.

4. The finite-difference method is defined dimension per dimension; this makes it easy to increase the "element order" to get higher-order accuracy.

Disadvantages of the Finite Difference Method:

1. When geometry becomes complex, FDM does not cope with such complexity because it requires a known familiar grid structuring like square and rectangle.

2. FDM becomes computationally expensive with complex and multiscale geometries (Rapp, 2017).

3. With the finite-difference method, defining boundary conditions becomes a problem particularly when handling curve boundaries and as a result it could lead to large computational errors.

4. When there is discontinuity on a material, finite difference method is poor in handling such discontinuity.

5. Unlike in FEM, FDM does not allow for adaptive mesh refinement or local grid refinement. Grid refinement is necessary when there are corners or complex shapes that might cause variation in solution.

2.5.2 Finite Element Method

FEM is a domain discretisation method which is a common technique used in finding the numerical solution to differential equations. The basic underlying principle of FEM is that it partitions the domain of the differential equation into smaller parts called elements (Whiteley, 2017) based on an irregular (e.g. triangular) mesh that can easily resolve complex geometries (Neill & Hashemi, 2018). These elements then form a mesh that will be used to find the solution to the differential equation in question using a low-order or high-order polynomial function. The solution on each of the elements is approximated. So, given any partial differential equation, the finite element method is regarded as a general method that can be use to find its approximate solution.

Advantages of Finite Element Method:

1. FEM is the most popular numerical method used for solving differential equations in engineering. One of the main advantage of the method is that it is applicable to both linear and non-linear differential equations in two and three dimensions.

2. Unlike FDM, FEM can model complex and Irregular geometric shapes. Because the designer is able to model both the interior and exterior, he or she can determine how critical factors might affect the entire structure and why

failures might occur.

3. FEM is flexible to adapt certain specifications to enable reduction in the need to have a physical prototype in the design process. Therefore using FEM software, the time to spend on designing prototype will be reduced because computer simulations can do same in far less time than designing a prototype.

4. Physical deformity can make modelling by hand impossible, but a numerical approximation with FEM can solve any deformity to a high degree of accuracy.

Disadvantages of Finite Element Method:

1. For a body with complex geometry, such as body geometry with corners, notches, or holes, mesh refinement can be difficult since discretisation is carried out in the entire domain. Generation of the finite element mesh therefore becomes laborious and time consuming.

2. When dealing with problems in the exterior domain where the boundary is infinite, the FEM uses a fictitious closed boundary condition to find a solution. This then leads to great compromise of the accuracy of the method, and in some cases yields completely erroneous results. Examples of such infinite domains include half-spaces or complementary domains to a finite one.

3. Making modifications on the mesh that will accommodate changes in the geometry of the body becomes difficult and time consuming with the FEM.

4. FEM has computational inefficiency because of domain discretisation and also it has a complex code structure that is difficult to implement.

2.5.3 Finite Volume Method

This is another numerical method for solving partial differential equations (Rapp, 2017). In FVM, the domain is first discretised into a number of non overlapping finite volumes or cells. Usually, these finite volumes are triangles (2D) or prisms (3D). Next, conservation laws are applied to each individual cell to form enough

algebraic equations, which can be solved to compute the state variables (Neill & Hashemi, 2018). FVM, like FEM, is based on an unstructured (e.g. triangular) mesh. Therefore, it is suitable for irregular and complex geometries unlike FDM that is based on regular grid geometry.

Advantages of the Finite Volume Method: All the advantages of FEM and FDM also holds for FVM and in addition, the following also add to the advantages.

1. FVM is based on the integral form of the conservation laws, rather than their differential form. This leads to more accuracy/stability, especially for sharp gradients (i.e. large derivatives) inside a domain, which is also called shock-capturing property.
2. A region of the geometry could be resolved at significant higher accuracy while relaxing the resolution throughout the rest of the region (Rapp, 2017).
3. FVMs have less strict requirements on grid structuring
4. Compared to the finite difference method, one further advantage of the finite-volume method is that it is very flexible—it can be rather easily implemented on structured as well as on unstructured grids. This renders the finite-volume method particularly suitable for the simulation of flows in or around complex geometries.
5. FVM allows locally adapting the grid to suit the geometry.
6. This leads to another important feature of the approach, namely the ability to compute weak solutions of the governing equations correctly (Blazek, 2015).

Disadvantages of the Finite Volume Method:

1. The local accuracy of the FVM, such as close to a corner of interest, can be increased by refining the mesh around that corner, similar to FEM. However, the functions that approximate the solution when using FVM cannot be easily made of higher order. This is a disadvantage of the FVM compared to the finite-element and finite-difference methods.

2. Finite volume methods work fine in multiple dimensions, but to go higher than second order for general flow structures, one needs extra face quadrature points and/or transverse Riemann solves, greatly increasing the cost relative to FD methods. However, these FV methods can be applied to non-smooth and unstructured meshes and can use arbitrary Riemann solvers.

3. FVM: Getting high-order schemes is a pain, it is extremely cumbersome.

4. However, in some cases, it is difficult to design schemes which give enough precision. Indeed, the FEM can be much more precise than FVM when using higher order polynomials, but it requires an adequate functional framework which is not always available in industrial problems (Eymard, Gallouët, & Herbin, 2000).

2.5.4 Boundary Element Method

BEM is not a domain method like FEM, but rather a boundary-only method (Katsikadelis, 2016). However, BEM uses similar shape functions to FEM for the distribution of variables over the boundary. Its basis, however, can be traced to the theory of integral equations (Brebbia, 2017).

The Advantages of the Boundary Element Method:

1. The discretisation of the Boundary Element Method is only over the boundary. Since this method allows for the reduction of the dimension of the domain by order one and hence also reducing the number of unknown factors by order of one, this makes the Boundary Element Method more suited in handling algebraic equations than the Finite Element Method.

2. With BEM, evaluation of the solution can be done at any point of the domain and at any instant in time because the integral representation of the solution is a continuous function whose derivative can be found. Conversely, solutions found via the FEM can only be obtained at nodal points-therefore, the points at which the system is evaluated are not arbitrary.

3. BEM can accurately solve problems with concentrated forces which result from derivatives of field functions such as stresses and moments.

4. Peculiar geometries, such as cracks, can be handled by BEM, since the discretization need only be done on the boundary of the crack.

5. When considering an infinite domain, BEM can be used if the problem is formulated as an exterior problem. This is because the boundary condition that will be suitable at infinity will satisfy the fundamental solution.

Disadvantages of the Boundary Element Method:

1. When the differential equation is non linear, application of BEM on the integral representation is not possible.

2. BEM results in a dense matrix which is usually non symmetric. Therefore the populated matrix can be difficult to solve. Conversely, in FEM, the system of algebraic linear equations are diagonally dominant which makes it easier to handle.

3. In the event where singularity is encounter, evaluating such singularity can be a difficult procedure using BEM.

4. BEM requires fundamental solution to the partial differential equation be known, otherwise it will be impossible to get a BEM formulation of the PDE and not all PDE's fundamental solution are known.

2.6 Summary of Chapter

In this chapter, general literature surveys are carried out for low Reynolds number flow past a body. It was stated clearly that this study is for two dimensional flow in an exterior domain for which Stokes' paradox holds, a match asymptotic expansion will be used in later chapters. Studies for two dimensional flow past a circular cylinder from Yano and Kieda ((Yano & Kieda, 1980)), Proudman and Pearson

((Proudman & Pearson, 1957)), Kaplun and Lagerstrom ((Kaplun & Lagerstrom, 1957)), and Chadwick ((Chadwick, 2013)) has been reviewed in this chapter. Oseen and Stokes equation has been clearly stated and the Reynolds number with diagram showing the first experiment carried out by Osborne Reynolds in 1883. Some few examples of low Reynolds number flow applied in biology are presented and the chapter ended by comparing four different numerical methods: FDM, FEM, FVM, and BEM.

Chapter 3

Theoretical Background and Governing Equations

3.1 Introduction

In this chapter the classical equations that govern the general fluid flow and particularly the equations that describe the near-field and the far-field behaviour of fluid flow shall be discussed. Using mathematical analysis, there will be matching of the near-field and far-field. In solving problems in fluid mechanics, certain conditions must be taken into account, such as conservation of mass, and conservation of momentum. This chapter will begin by deriving equations for the mass conservation and momentum, from this two all other equations will be deduce from them.

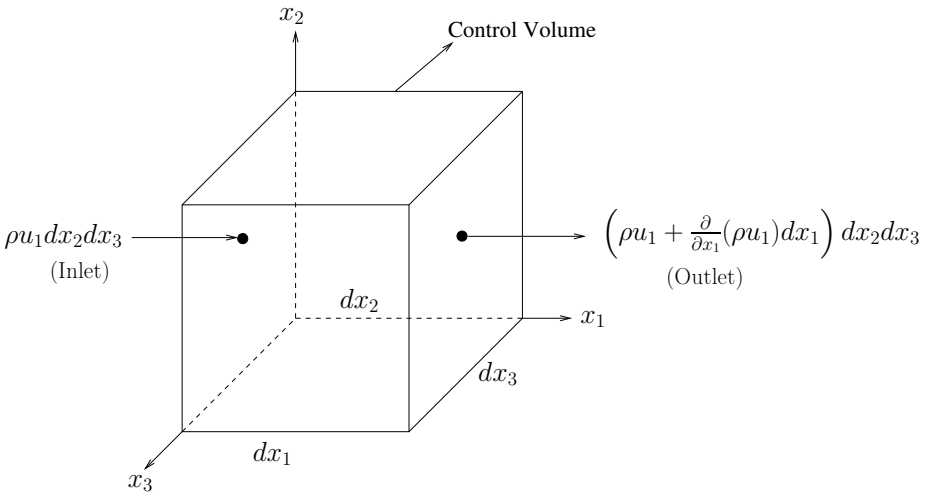

Figure 3.1: Fixed control volume showing inflow and outflow

3.2 Derivation of Continuity Equation and Navier-Stokes Equation

3.2.1 Continuity Equation

Conservation of mass m, which is commonly referred to as the continuity equation, states that the mass of the fluid cannot change in a closed system (White, 2011). In the following analysis, m is therefore regarded as a constant, that is

$$\frac{dm}{dt} = 0, \tag{3.1}$$

where t is time. Consider a control volume of infinitesimal size (dx_1, dx_2, dx_3) (see figure 3.1). The flow through each element is balanced, with mass conservation given as

$$\int_{cv} \frac{\partial \rho}{\partial t} d\Sigma + \sum_i (\rho_i A_i u_i)_{\text{outlet}} - \sum_i (\rho_i A_i u_i)_{\text{inlet}} = 0, \tag{3.2}$$

where cv represents the control volume, ρ_i is the density, $d\Sigma$ is an element of volume, A_i is the cross sectional area, and u_i is the velocity. Because equation (3.2) describes an infinitesimal fluid element, the full volume integral simply reduces to a differential term

$$\int_{cv} \frac{\partial \rho}{\partial t} d\Sigma \approx \frac{\partial \rho}{\partial t} dx_1 dx_2 dx_3. \tag{3.3}$$

In the x_1 direction, the inlet for the mass flow rate is $(\rho u_1) dx_2 dx_3$, while for the outlet, the mass flow rate is $\left(\rho u_1 + \frac{\partial}{\partial x_1}(\rho u_1)dx_1\right) dx_2 dx_3$. Similar procedures apply

for the remaining directions, x_2 and x_3. Substituting all these into (3.2) gives

$$\frac{\partial \rho}{\partial t}dx_1dx_2dx_3 + \frac{\partial}{\partial x_1}(\rho u_1)dx_1dx_2dx_3 + \frac{\partial}{\partial x_2}(\rho u_2)dx_1dx_2dx_3 + \frac{\partial}{\partial x_3}(\rho u_3)dx_1dx_2dx_3 = 0. \tag{3.4}$$

The volume element $dx_1dx_2dx_3$, from the equation (3.4) cancels out, hence, the conservation of mass for an infinitesimal control volume which is the continuity equation and is given as

$$\frac{\partial \rho}{\partial t} + \frac{\partial}{\partial x_1}(\rho u_1) + \frac{\partial}{\partial x_2}(\rho u_2) + \frac{\partial}{\partial x_3}(\rho u_3) = 0 \tag{3.5}$$

or it can be written using index notation as

$$\frac{\partial \rho}{\partial t} + \frac{\partial}{\partial x_i}(\rho u_i) = 0. \tag{3.6}$$

Equation (3.6) is called the continuity equation for compressible and unsteady flow, while for an incompressible and steady flow it is given as

$$\frac{\partial u_i}{\partial x_i} = 0. \tag{3.7}$$

3.2.2 Momentum Equation

Using the same control volume shown in figure 3.1, the force balance for the linear momentum will be (Munson, 2002; White, 2011),

$$\sum_i F = \frac{\partial}{\partial t}\left(\int_{cv}(u_i\rho)d\Sigma\right) + \sum_i(m_iu_i)_{\text{outlet}} - \sum_i(m_iu_i)_{\text{inlet}} \tag{3.8}$$

just like when deriving the continuity equation, when it was an infinitesimal volume been considered, the integral in the above equation will simply be reduced to a derivative term giving

$$\frac{\partial}{\partial t}(u_i\rho)d\Sigma \approx \frac{\partial}{\partial t}(u_i\rho)dx_1dx_2dx_3\ , \tag{3.9}$$

considering the momentum fluxes from all the six faces consisting of three inlet and three outlet (see figure 3.1) (White, 2011). In the x_1 direction, the inlet for the mass flow rate is $(\rho u_1u_i)dx_2dx_3$, while for the outlet, the mass flow rate is

$\left(\rho u_1 u_i + \frac{\partial}{\partial x_1}(\rho u_1 u_i)dx_1\right) dx_2 dx_3$. Similar procedures apply for the remaining directions, x_2 and x_3. Substituting all these and (3.9) into (3.8) gives

$$\sum F = \left(\frac{\partial}{\partial t}(u_i\rho) + \frac{\partial}{\partial x_1}(u_i u_1 \rho) + \frac{\partial}{\partial x_2}(u_i u_2 \rho) + \frac{\partial}{\partial x_3}(u_i u_3 \rho)\right) dx_1 dx_2 dx_3, \quad (3.10)$$

which is simplified to

$$\begin{aligned}\frac{\partial}{\partial t}(u_i\rho) + \frac{\partial}{\partial x_1}(u_i u_1 \rho) + \frac{\partial}{\partial x_2}(u_i u_2 \rho) + \frac{\partial}{\partial x_3}(u_i u_3 \rho) &= u_i \left(\frac{\partial \rho}{\partial t} + \frac{\partial}{\partial x_i}(\rho u_i)\right) \\ &+ \rho\left(\frac{\partial u_i}{\partial t} + u_1\frac{\partial u_i}{\partial x_1} + u_2\frac{\partial u_i}{\partial x_2} + u_3\frac{\partial u_i}{\partial x_3}\right),\end{aligned} \quad (3.11)$$

where the right hand side of (3.11) is simply the continuity equation and the total acceleration of a particle that instantaneously occupies the control volume, hence

$$\sum F = \rho\frac{du_i}{dt}dx_1 dx_2 dx_3 \ . \quad (3.12)$$

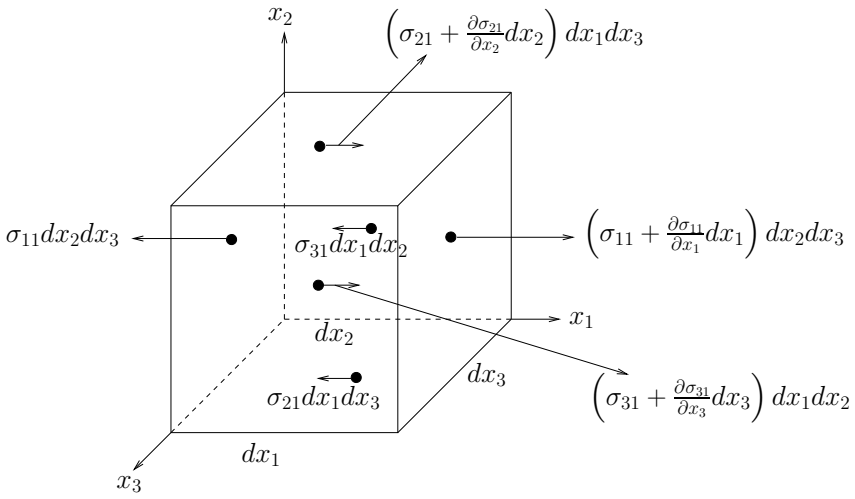

Figure 3.2: Control volume for a differential element

Equation (3.12) above shows that the net force must be of differentiable size on the control volume and proportional to the element volume. Consider figure 3.2, the net surface forces for only the x_1-direction is given by

$$dF_{1,surf} = \left(\frac{\partial}{\partial x_1}(\sigma_{11}) + \frac{\partial}{\partial x_2}(\sigma_{21}) + \frac{\partial}{\partial x_3}(\sigma_{31})\right) dx_1 dx_2 dx_3, \quad (3.13)$$

where $F_{1,surf}$ is the surface force in the x_1-direction. Putting the above equation in terms of pressure and viscous forces gives

$$\frac{dF_1}{d\Sigma} = -\frac{\partial p}{\partial x_1} + \frac{\partial}{\partial x_1}(\tau_{11}) + \frac{\partial}{\partial x_2}(\tau_{21}) + \frac{\partial}{\partial x_3}(\tau_{31}), \quad (3.14)$$

where the stresses are the sum of hydrostatic pressure plus viscous stresses τ_{ij} that arise from motion with velocity gradient given as

$$\sigma_{ij} = \begin{pmatrix} -p + \tau_{11} & \tau_{21} & \tau_{31} \\ \tau_{12} & -p + \tau_{22} & \tau_{32} \\ \tau_{13} & \tau_{23} & -p + \tau_{33} \end{pmatrix} \tag{3.15}$$

where σ_{ij} is the stress in $j-$direction on a face normal to i axis. This now leads us to the basic differential momentum equation given for an infinitesimal fluid element with gravitational force (the only body force that will be considered here), given as

$$\rho f_i - \frac{\partial p}{\partial x_i} + \frac{\tau_{ij}}{\partial x_j} = \rho \frac{\partial u_i}{\partial t} + u_1 \frac{\partial u_i}{\partial x_1} + u_2 \frac{\partial u_i}{\partial x_2} + u_3 \frac{\partial u_i}{\partial x_3}, \tag{3.16}$$

where f_i is the gravity force per unit volume, $\frac{\partial p}{\partial x_i}$ is the pressure force per unit volume, $\frac{\partial \tau_{ij}}{\partial x_j}$ is the viscous force per unit volume and $\frac{du_i}{dt}$ is the density acceleration per unit volume. Therefore in the x_1, x_2 and x_3 directions respectively yields

$$f_1 - \frac{\partial p}{\partial x_1} + \frac{\partial \tau_{11}}{\partial x_1} + \frac{\partial \tau_{21}}{\partial x_2} + \frac{\partial \tau_{31}}{\partial x_3} = \rho \left[\frac{\partial u_1}{\partial t} + u_1 \frac{\partial u_1}{\partial x_1} + u_2 \frac{\partial u_1}{\partial x_2} + u_3 \frac{\partial u_1}{\partial x_3} \right], \tag{3.17a}$$

$$f_2 - \frac{\partial p}{\partial x_2} + \frac{\partial \tau_{12}}{\partial x_1} + \frac{\partial \tau_{22}}{\partial x_2} + \frac{\partial \tau_{32}}{\partial x_3} = \rho \left[\frac{\partial u_2}{\partial t} + u_1 \frac{\partial u_2}{\partial x_1} + u_2 \frac{\partial u_2}{\partial x_2} + u_3 \frac{\partial u_2}{\partial x_3} \right], \tag{3.17b}$$

$$f_3 - \frac{\partial p}{\partial x_3} + \frac{\partial \tau_{13}}{\partial x_1} + \frac{\partial \tau_{23}}{\partial x_2} + \frac{\partial \tau_{33}}{\partial x_3} = \rho \left[\frac{\partial u_3}{\partial t} + u_1 \frac{\partial u_3}{\partial x_1} + u_2 \frac{\partial u_3}{\partial x_2} + u_3 \frac{\partial u_3}{\partial x_3} \right]. \tag{3.17c}$$

3.2.3 Navier-Stokes Equation

The type of fluid that will be considered here is Newtonian; where the shear stress is directly proportional to the strain rate for an incompressible flow. Hence, from (3.17) will give

$$\tau_{11} = 2\mu \frac{\partial u_1}{\partial x_1},$$

$$\tau_{22} = 2\mu \frac{\partial u_2}{\partial x_2},$$

$$\tau_{33} = 2\mu \frac{\partial u_3}{\partial x_3},$$

$$\tau_{12} = \tau_{21} = \mu \left(\frac{\partial u_1}{\partial x_2} + \frac{\partial u_2}{\partial x_1} \right),$$

$$\tau_{13} = \tau_{31} = \mu \left(\frac{\partial u_3}{\partial x_1} + \frac{\partial u_1}{\partial x_3} \right),$$

and

$$\tau_{23} = \tau_{32} = \mu\left(\frac{\partial u_2}{\partial x_3} + \frac{\partial u_3}{\partial x_2}\right).$$

where μ is the dynamic viscosity. As a result,

$$f_1 - \frac{\partial p}{\partial x_1} + \mu\left[\frac{\partial^2 u_1}{\partial x_1^2} + \frac{\partial^2 u_1}{\partial x_2^2} + \frac{\partial^2 u_1}{\partial x_3^2}\right] = \rho\left[\frac{\partial u_1}{\partial t} + u_1\frac{\partial u_1}{\partial x_1} + u_2\frac{\partial u_1}{\partial x_2} + u_3\frac{\partial u_1}{\partial x_3}\right],$$

$$f_2 - \frac{\partial p}{\partial x_2} + \mu\left[\frac{\partial^2 u_2}{\partial x_1^2} + \frac{\partial^2 u_2}{\partial x_2^2} + \frac{\partial^2 u_2}{\partial x_3^2}\right] = \rho\left[\frac{\partial u_2}{\partial t} + u_1\frac{\partial u_2}{\partial x_1} + u_2\frac{\partial u_2}{\partial x_2} + u_3\frac{\partial u_2}{\partial x_3}\right],$$

$$f_3 - \frac{\partial p}{\partial x_3} + \mu\left[\frac{\partial^2 u_3}{\partial x_1^2} + \frac{\partial^2 u_3}{\partial x_2^2} + \frac{\partial^2 u_3}{\partial x_3^2}\right] = \rho\left[\frac{\partial u_3}{\partial t} + u_1\frac{\partial u_3}{\partial x_1} + u_2\frac{\partial u_3}{\partial x_2} + u_3\frac{\partial u_3}{\partial x_3}\right],$$

and putting the above equations into index notation, the Navier-Stokes equation is obtained as

$$\rho\frac{Du_i}{Dt} = -\frac{\partial p}{\partial x_i} + \mu\frac{\partial^2 u_i}{\partial x_j \partial x_j} + f_i, \tag{3.18}$$

where the left hand side of (3.18) is the net force density which ρ is the density and $\frac{D}{Dt}$ is the material derivative as defined in equation (2.5). Hence,

$$\rho\frac{\partial u_i}{\partial t} + \rho u_j\frac{\partial u_i}{\partial x_j} = -\frac{\partial p}{\partial x_i} + \mu\frac{\partial^2 u_i}{\partial x_j \partial x_j} + f_i. \tag{3.19}$$

The above equation (3.19) is the Navier-Stokes equation for Newtonian fluid with constant density, constant viscosity and for an incompressible fluid.

From (3.19), the time independent Navier Stokes equation is given in dimensional form as

$$\rho u_j\frac{\partial u_i}{\partial x_j} = -\frac{\partial p}{\partial x_i} + \mu\frac{\partial^2 u_i}{\partial x_j \partial x_j} + f_i. \tag{3.20}$$

Non-dimensionalisation can be carried out in two different approaches: one method is to use the Bernoulli pressure $p = \rho U^2 p^*$, and the second is to use Stokes pressure $p = \frac{\mu U}{L}p^*$ where U is the uniform stream velocity, L is the body length, and p^* is the dimensionless pressure. The advantage of using Bernoulli pressure is that it allows the matching of the far-field to describe Oseen equation, while the Stokes pressure only describes the near-field behaviour of the fluid flow.

3.2.4 Bernoulli Pressure

To scale the Navier-Stokes equation using the Bernoulli pressure, the dimensionless variables for the velocity, pressure, force, time, and length scale used are

$$u_i = U u_i^* \ ,$$

$$p = \rho U^2 p^*,$$

$$f_i = |f_i| f_i^*,$$

$$t = T t^*,$$

and

$$x_i = L x_i^*.$$

Substituting the above dimensionless variables into equation (3.19) and simplifying yields

$$\rho \frac{\partial (U u_i^*)}{\partial T t^*} + \rho U u_j^* \frac{\partial (U u_i^*)}{\partial L x_j^*} = -\frac{\partial (\rho U^2 p^*)}{\partial L x_i^*} + \mu \frac{\partial^2 (U u_i^*)}{\partial x_j^* L \partial x_j^* L} + |f_i| f_i^* \ , \tag{3.21}$$

which further simplifies to

$$\frac{\rho U}{T} \frac{\partial u_i^*}{\partial t^*} + \frac{\rho U^2}{L} u_j^* \frac{\partial u_i^*}{\partial x_j^*} = -\frac{\rho U^2}{L} \frac{\partial p^*}{\partial x_i^*} + \frac{\mu U}{L^2} \frac{\partial^2 u_i^*}{\partial x_j^* \partial x_j^*} + |f_i| f_i^*. \tag{3.22}$$

Multiplying the above through with $\frac{L^2}{\mu U}$ yields

$$\frac{\rho L^2}{\mu T} \frac{\partial u_i^*}{\partial t^*} + \frac{\rho U L}{\mu} u_j^* \frac{\partial u_i^*}{\partial x_j^*} = -\frac{\rho U L}{\mu} \frac{\partial p^*}{\partial x_i^*} + \frac{\partial^2 u_i^*}{\partial x_j^* \partial x_j^*} + \frac{\rho L^2}{\mu U} |f_i| f_i^*, \tag{3.23}$$

to get

$$\beta \frac{\partial u_i^*}{\partial t^*} + Re u_j^* \frac{\partial u_i^*}{\partial x_j^*} = -Re \frac{\partial p^*}{\partial x_i^*} + \frac{\partial^2 u_i^*}{\partial x_j^* \partial x_j^*} + \frac{Re}{Fr^2} f_i^*, \tag{3.24}$$

where $\beta = \frac{\rho L^2}{\mu T}$, $Re = \frac{\rho L U}{\mu}$, and $Fr = \frac{U}{\sqrt{L|f_i|}}$.

The Froude number Fr, is a non-dimensional term that describes the ratio of inertial and gravitational forces. Fluid flows in which gravity is important include flow in an open channel where there is a free surface. External body forces are important as well as viscous surface forces.

Multiplying the immediate above equation through by $\frac{1}{Re}$ to obtained

$$\frac{\beta}{Re} \frac{\partial u_i^*}{\partial t^*} + u_j^* \frac{\partial u_i^*}{\partial x_j^*} = -\frac{\partial p^*}{\partial x_i^*} + \frac{1}{Re} \frac{\partial^2 u_i^*}{\partial x_j^* \partial x_j^*} + \frac{1}{Fr^2} f_i^*.$$

As $Re \to \infty$ and $Fr \to \infty$ gives the far-field which describes the Euler equation by making the second order term go to zero. The first two terms become of the same order to give

$$u_j^* \frac{\partial u_i^*}{\partial x_j^*} = -\frac{\partial p^*}{\partial x_i^*}. \tag{3.25}$$

Equation (3.25) above is known as the *Euler Equation*. This result is most often used in aerodynamics for different kinds of high Reynolds number flow models, but in this thesis focus will only be on low Reynolds number flow.

3.3 Stokes Equation

Using the Stokes pressure $p = \frac{\mu U}{L} p^*$, Stokes equation for a low Reynolds number flow is derive. Assuming that inertial terms are so small that they can be neglected in the Navier-Stokes equation (3.19) mentioned earlier, viscous forces will dominate the flow, and therefore the fluid will experience a very slow flow. Examples of fluids with such properties include honey, mucus, mayonnaise, etc. This kind of flow is generally referred to as creeping or viscous flow. Creeping flow is characterised with Reynolds number sufficiently less than unity (Pozrikidis, 2002).

Consider a flow of an incompressible fluid past an arbitrary fixed point in a reference domain with pressure p and velocity vectors: $u_i = (u_1, u_2)$ for two-dimensions and $u_i = (u_1, u_2, u_3)$ in three dimensions. The Stokes equation can be derived from the Navier-Stokes equation (3.19). To do so, consider a creeping flow with stream velocity U, and a body of length L; the pressure cannot be scaled with the "dynamic" or "inertial" term ρU^2, but rather must depend on a viscous scale $\frac{\mu U}{L}$ (White, 1991). Thus, the Stokes equation is obtained by non-dimensionalising the Navier-Stokes equation (3.19). To do so, consider L to be the characteristic length that represents body size, U to be the characteristic velocity which describes the intensity of the flow, and T to be the characteristic time. In this formulation, U, L and T are the scaling terms for the velocity, length, and time respectively.

The following operations can be used for the scaling. Starting with velocity term,

$$u_i^* \equiv \frac{u_i}{U} \tag{3.26}$$
$$\Rightarrow u_i = U u_i^*.$$

The pressure term, and in this case the Stokes pressure,

$$p^* \equiv \frac{pL}{\mu U} \tag{3.27}$$
$$\Rightarrow p = \frac{\mu U}{L} p^* \ .$$

The time and length parameters given by

$$t^* \equiv \frac{t}{T} \ , \tag{3.28}$$

$$\Rightarrow t = Tt^* \ ,$$

and

$$x_i^* \equiv \frac{x_i}{L} \ , \tag{3.29}$$
$$\Rightarrow x_i = Lx_i^*,$$

while the force is

$$f_i^* \equiv \frac{f_i}{|f_i|} \ , \tag{3.30}$$
$$\Rightarrow f_i = |f_i| f_i^*,$$

respectively. By substituting the above scaled variables into the Navier-Stokes equation (3.19) and solving for the dimensional variables, yields

$$\rho \left(\frac{\partial U u_i^*}{\partial T t^*} + U u_j^* \frac{\partial U u_i^*}{\partial L x_j^*} \right) = -\frac{\partial \mu U p^*}{\partial L^2 x_i^*} + \mu \frac{\partial^2 U u_i^*}{\partial x_j^* L \partial x_j^* L} + |f_i| f_i^*, \tag{3.31}$$

which simplifies to

$$\frac{\rho L^2}{\mu T} \frac{\partial u_i^*}{\partial t^*} + \frac{\rho L U}{\mu} u_j^* \frac{\partial u_i^*}{\partial x_j^*} = -\frac{\partial p^*}{\partial x_i^*} + \frac{\partial^2 u_i^*}{\partial x_j^* \partial x_j^*} + \frac{\rho L^2}{\mu U} |f_i| f_i^*. \tag{3.32}$$

The first and second terms on the left hand side of the above equation represent the accelerative and convective terms of the flow. The dimensionless coefficients of these two terms can be represented by $Re \cdot St = \frac{\rho L^2}{\mu T}$ where the Strouhal number $St = \frac{fL}{U}$, frequency $f = \frac{1}{T}$, and the Reynolds number $Re = \frac{\rho L U}{\mu}$ respectively. After substitution of these quantities, equation (3.32) becomes

$$Re \cdot St \frac{\partial u_i^*}{\partial t^*} + Re u_j^* \frac{\partial u_i^*}{\partial x_j^*} = -\frac{\partial p^*}{\partial x_i^*} + \frac{\partial^2 u_i^*}{\partial x_j^* \partial x_j^*} + \frac{Re}{Fr^2} f_i^* \ . \tag{3.33}$$

It can be seen that when there is no external force, the velocity of body motion is similar to the forward velocity, and so the Strouhal number is of order one ($St = \mathcal{O}(1)$). This makes the first term on the left hand side of (3.33) become the same as the Reynold's number: thus the dimensionless equation of motion (3.33) becomes

$$Re \left(\frac{\partial u_i^*}{\partial t^*} + u_j^* \frac{\partial u_i^*}{\partial x_j^*} \right) = -\frac{\partial p^*}{\partial x_i^*} + \frac{\partial^2 u_i^*}{\partial x_j^* \partial x_j^*} + \frac{Re}{Fr^2} f_i^* \ . \tag{3.34}$$

When $Re \ll \mathcal{O}(1)$, the accelerative and convective terms on the left side of (3.34) are small compared to the terms on the right hand side, and so they can be neglected.

Reverting to the physical variables, it is seen that the flow is governed by the steady state Stokes equation (Pozrikidis, 2002) giving by

$$0 = -\frac{\partial p}{\partial x_i} + \mu \frac{\partial^2 u_i}{\partial x_j \partial x_j} + f_i. \tag{3.35}$$

Equation (3.35) is called *steady Stokes* equation, where $u_i = (u_1, u_2, u_3)$ are in the $x_i = (x_1, x_2, x_3)$ direction. This is a linear differential equation for which a representation can be found using Green's integral theorem.

Suppose on the contrary, that there is an external force. Then, the time parameter is not simply equal to the ratio of length and velocity ($T \neq \frac{L}{U}$). For $Re << 1$, the second term on the left hand side of (3.33) is very small compared to the remaining terms, and so it can thus be neglected. The result is the *unsteady Stokes* equation:

$$\frac{\partial u_i}{\partial t} = -\frac{\partial p}{\partial x_i} + \mu \frac{\partial^2 u_i}{\partial x_j \partial x_j} + f_i. \tag{3.36}$$

Physically, equation (3.36) describes flows characterised by sudden acceleration or deceleration (Pozrikidis, 2002).

It can also be shown that pressure is a harmonic function when the Laplacian of the Stokes equation is considered together with the continuity equation.
Take the divergence of the Stokes equation

$$\frac{\partial}{\partial x_i}\left(-\frac{\partial p}{\partial x_i} + \mu \frac{\partial^2 u_i}{\partial x_j \partial x_j}\right) = 0, \tag{3.37}$$

$$\frac{\partial^2 p}{\partial x_i \partial x_i} + \mu \frac{\partial^2}{\partial x_j \partial x_j}\left(\frac{\partial u_i}{\partial x_i}\right) = 0, \tag{3.38}$$

but it was known from continuity equation that

$$\frac{\partial u_i}{\partial x_i} = 0, \tag{3.39}$$

hence the second term in (3.38) vanished to obtain the

$$\frac{\partial^2 p}{\partial x_i \partial x_i} = 0. \tag{3.40}$$

From (3.40), it shows that pressure is a harmonic function. The Stokes equation (3.35) is linear hence there are different mathematical approaches to solve it. One which will be considered in this thesis is BIM, which uses Green's functions, and thereafter the BEM to discretise it. Again, the Stokes equation is completely reversible and the instantaneous structure of the flow depends solely on the present configuration rather than on the history of the motion.

3.3.1 Green's Integral Representation of the Stokes Velocity

By representing the velocity in the Stokes equation as a surface integral, (3.35) can be equated to a surface integral in the far-field obtained for uniform Oseen flow past a body. Consider a volume V of fluid in Stokes flow (Chadwick, 2014). From Stokes equation (3.35),

$$\int_V \left(\frac{\partial p}{\partial x_i} - \mu \frac{\partial^2 u_i}{\partial x_j \partial x_j} + f_i \right) dV = 0. \tag{3.41}$$

From 3.41, $+f_i$ implies force exerted by point $\mathbf{x} = 0$ on fluid, while $-f_i$ implies force exerted by fluid on point $\mathbf{x} = 0$. Let us construct a Green's integral such that a result in $u_i(\underline{x})$ may be found. To this end, consider the variable $\underline{z} = \underline{x} - \underline{y}$ (here $\underline{x}$ is the coordinate of point of fluid while $\underline{y}$ is the point of integration V_y) and the volume integral $dV_y = dy_1 dy_2 dy_3$ in order to obtain a term that gives us $u_i(\underline{x})$. Multiplying the above integral by $u_i(\underline{y})$, for the point source solution where $f_i^{(k)} = \delta_{ik}\delta(\underline{z})$, where $\delta(\underline{z})$ is the Dirac delta function gives

$$\int_{V_y} \left(\frac{\partial p^{(k)}(\underline{z})}{\partial x_i} - \mu \frac{\partial^2 u_i^{(k)}(\underline{z})}{\partial x_j \partial x_j} + f_i^{(k)}(\underline{z}) \right) u_i(\underline{y}) dV_y = 0. \tag{3.42}$$

The terms in (3.42) except the force term, give a volume integral, however, we require a reformulation so we can apply the divergence theorem to obtain a surface integral. Lets therefore consider including further volume integral terms such that

$$\begin{aligned} \int_{V_y} \Bigg[& \left(\frac{\partial p^{(k)}(\underline{z})}{\partial x_i} - \mu \frac{\partial^2 u_i^{(k)}(\underline{z})}{\partial x_j \partial x_j} + f_i^{(k)}(\underline{z}) \right) u_i(\underline{y}) \\ & - \left(\frac{\partial p(\underline{y})}{\partial y_i} - \mu \frac{\partial^2 u_i(\underline{y})}{\partial y_j \partial y_j} + f_i(\underline{y}) \right) u_i^{(k)}(\underline{z}) \Bigg] dV_y = 0 \end{aligned} \tag{3.43}$$

However, as stated above, (3.43) can be simplified using the fact that

$$\begin{aligned}\frac{\partial}{\partial x_i} f(\underline{z}) &= \frac{\partial z_j}{\partial x_i}\frac{\partial}{\partial z_j} f(\underline{z}) \\ &= \delta_{ij}\frac{\partial}{\partial z_j} f(\underline{z}) \\ &= \frac{\partial}{\partial z_i} f(\underline{z}), \end{aligned} \tag{3.44}$$

and

$$\frac{\partial}{\partial y_i} f(\underline{z}) = \frac{\partial z_j}{\partial y_i}\frac{\partial}{\partial z_j} f(\underline{z}) \tag{3.45}$$

$$\begin{aligned} &= -\delta_{ij}\frac{\partial}{\partial z_j} f(\underline{z}) \\ &= -\frac{\partial}{\partial z_i} f(\underline{z}), \end{aligned} \tag{3.46}$$

that is

$$\frac{\partial}{\partial x_i} f(\underline{z}) = -\frac{\partial}{\partial y_i} f(\underline{z}). \tag{3.47}$$

to get

$$\begin{aligned}\int_{V_y} \Bigg[&\left(-\frac{\partial p^{(k)}(\underline{z})}{\partial y_i} - \mu\frac{\partial^2 u_i^{(k)}(\underline{z})}{\partial y_j \partial y_j} + f_i^{(k)}(\underline{z}) \right) u_i(\underline{y}) \\ &- \left(\frac{\partial p(\underline{y})}{\partial y_i} - \mu\frac{\partial^2 u_i(\underline{y})}{\partial y_j \partial y_j} + f_i(y) \right) u_i^{k)}(\underline{z}) \Bigg] dV_y = 0 \end{aligned} \tag{3.48}$$

However, simplifying (3.48) with the fact that

$$\frac{\partial u_i(y)}{\partial y_i} = 0$$

and

$$\begin{aligned}\frac{\partial}{\partial y_i} u_i^{(k)}(\underline{z}) &= \frac{\partial z_j}{\partial y_i}\frac{\partial u_i^{(k)}(\underline{z})}{\partial z_j} \\ &= -\delta_{ij}\frac{\partial}{\partial z_j} u_i^{(k)}(\underline{z}) \\ &= -\frac{\partial u_i^{(k)}(\underline{z})}{\partial z_i} \\ &= 0. \end{aligned} \tag{3.49}$$

Combining these results gives

$$\int_{V_y}\Bigg[-\frac{\partial}{\partial y_i}\left(p^{(k)}(\underline{z})u_i(\underline{y})+p(\underline{y})u_i^{(k)}(\underline{z})\right)-\mu\frac{\partial}{\partial y_j}\left(\frac{\partial u_i^{(k)}(\underline{z})}{\partial y_j}u_i(\underline{y})\right)$$
$$+\mu\frac{\partial u_i^{(k)}(\underline{z})}{\partial y_j}\frac{\partial u_i(\underline{y})}{\partial y_j}+\mu\frac{\partial}{\partial y_j}\left(\frac{\partial u_i}{\partial y_j}u_i^{(k)}(\underline{z})\right)-\mu\frac{\partial u_i}{\partial y_j}\frac{\partial u_i^{(k)}(\underline{z})}{\partial y_j}$$
$$-f_i^{(k)}(\underline{z})u_i(\underline{y})-f_i(\underline{y})u_i^{(k)}(\underline{z})\Bigg]dV_y=0. \tag{3.50}$$

This implies

$$\int_{V_y}\Bigg[-\frac{\partial}{\partial y_i}\left(p^{(k)}(\underline{z})u_i(\underline{y})+p(\underline{y})u_i^{(k)}(\underline{z})\right)-\mu\frac{\partial}{\partial y_j}\left(\frac{\partial u_i^{(k)}(\underline{z})}{\partial y_j}u_i(\underline{y})-\frac{\partial u_i(\underline{y})}{\partial y_j}u_i^{(k)}(\underline{z})\right)$$
$$+f_i^{(k)}(\underline{z})u_i(\underline{y})-f_i(\underline{y})u_i^{(k)}(\underline{z})\Bigg]dV_y=0.$$

The point source was defined to be

$$f_i^{(k)}(\underline{z})=\delta_{ik}\delta(\underline{z}), \tag{3.51}$$

where δ_{ik} is Kronecker delta and $\delta(\underline{z})$ is Dirac delta function, resulting in

$$\int_{V_y}f_i^{(k)}(\underline{z})u_i(\underline{y})dV_y=\int_{V_y}\delta_{ik}\delta(\underline{z})u_i(\underline{y})dV_y$$
$$=\int_{V_y}\delta(\underline{z})u_k(\underline{y})dV_y.$$

Since $\delta(\underline{z})\neq 0$ for $\underline{z}=\underline{0}$,

$$\int_{V_y}f_i^{(k)}(\underline{z})u_i(\underline{y})dV_y=u_k(\underline{x}). \tag{3.52}$$

Continuing with the evaluation as

$$u_k(\underline{x})=\int_{V_y}\Bigg[\frac{\partial}{\partial y_i}\left(p^{(k)}(\underline{z})u_i(\underline{y})+p(\underline{y})u_i^{(k)}(\underline{z})\right)$$
$$+\mu\frac{\partial}{\partial y_j}\left(\frac{\partial u_i^{(k)}(\underline{z})}{\partial y_j}u_i(\underline{y})-\frac{\partial u_i(\underline{y})}{\partial y_j}u_i^{(k)}(\underline{z})\right)$$
$$+f_i(\underline{y})u_i^{(k)}(\underline{z})\Bigg]dV_y$$
$$=\int_{s_y}\Bigg[\left(p^{(k)}(\underline{z})u_i(\underline{y})+p(\underline{y})u_i^{(k)}(\underline{z})\right)n_i^v$$
$$+\mu\left(\frac{\partial u_i^{(k)}(\underline{z})}{\partial y_j}u_i(\underline{y})-\frac{\partial u_i(\underline{y})}{\partial y_j}u_i^{(k)}(\underline{z})\right)n_i^v\Bigg]dS_y$$
$$+\int_{V_y}f_i(\underline{y})u_i^{(k)}(\underline{z})dV_y \tag{3.53}$$

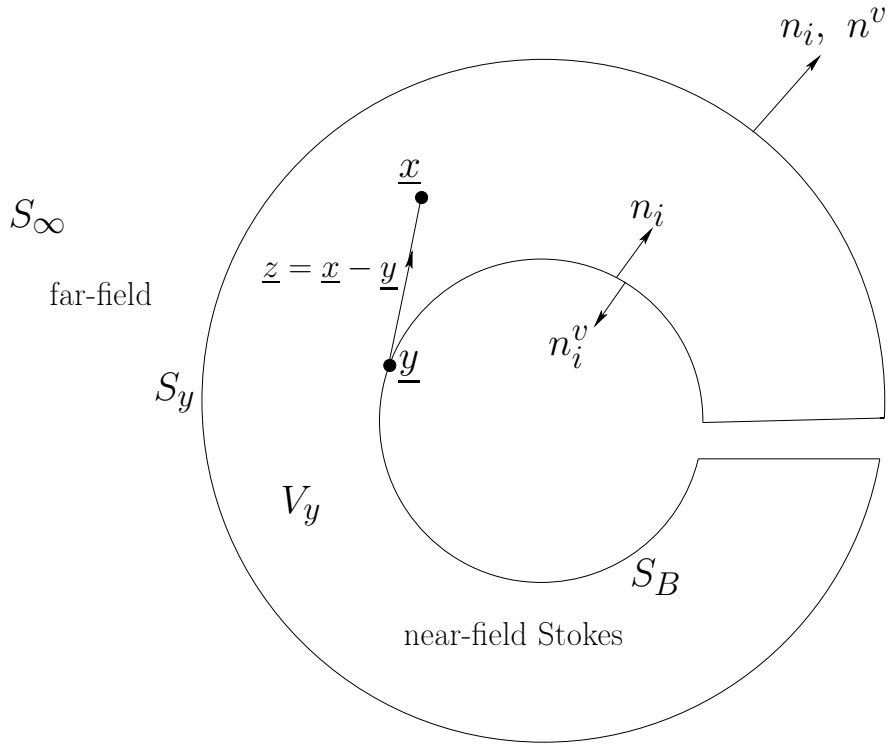

Figure 3.3: A volume representing near-field Stokes region and far-field Oseen region

Consider a volume V_y enclosed by the boundary S_y (see figure 3.3), where S_y includes both S_∞ and S_B with

$$n_i^v = \begin{cases} n_i & \text{on } S_\infty \\ -n_i & \text{on } S_B \ . \end{cases}$$

Combining these boundary conditions with equation (3.53) yields

$$\begin{aligned} u_k(\underline{x}) = -\int_{S_B} \Bigg[& \left(p^{(k)}(\underline{z}) u_i(\underline{y}) + p(\underline{y}) u_i^{(k)}(\underline{z}) \right) n_i \\ & + \mu \left(\frac{\partial u_i^{(k)}(\underline{z})}{\partial y_j} u_i(\underline{y}) - \frac{\partial u_i(\underline{y})}{\partial y_j} u_i^{(k)}(\underline{z}) \right) n_i \Bigg] dS_y \\ & + \int_{S_\infty} \Bigg[\left(p^{(k)}(\underline{z}) u_i(\underline{y}) + p(\underline{y}) u_i^{(k)}(\underline{z}) \right) n_i \\ & + \mu \left(\frac{\partial u_i^{(k)}(\underline{z})}{\partial y_j} u_i(\underline{y}) - \frac{\partial u_i(\underline{y})}{\partial y_j} u_i^{(k)}(\underline{z}) \right) n_i \Bigg] dS_y \\ & + \int_{V_y} f_i(\underline{y}) u_i^{(k)}(\underline{z}) dV_y \end{aligned} \tag{3.54}$$

where the surface integral over S_∞ touches the far-field. In the far-field, for uniform flow U past the body, Oseen flow holds.

Next, it will be shown that this Stokes flow is matched to the far-field integral

in Oseen flow, which is zero. The two-dimensional unit force solution of Stokes equation can be obtained from oseenlet solutions in the limit as $kr \to 0$, and $k = \frac{\rho U}{2\mu}$ for length dimension $r = L$ with

$$\begin{aligned} kr &= \frac{\rho U L}{2\mu} \\ &= \frac{1}{2} Re \end{aligned} \tag{3.55}$$

where Re is the Reynolds number. As the Reynolds number approaches zero, $Re \to 0$, yields Stokes equation.

To get the drag and lift stokeslet, consider the drag oseenlet given as

$$u_i^{(1)} = \frac{1}{2\pi\rho U}\left(\frac{\partial}{\partial x_i}\left(\ln r + e^{kx_1} K_0(kr)\right) - 2k e^{kx_1} K_0(kr)\delta_{i1}\right) , \tag{3.56}$$

where K_0 is the modified Bessel function of order zero and as $kr \to 0$,

$$e^{kx_1} = 1 + kx_1 + \mathcal{O}(r^2) \tag{3.57}$$

where "$\mathcal{O}$" means "of order" and

$$K_0(kr) = -\ln r + \mathcal{O}(r^2 \ln r) \ . \tag{3.58}$$

Therefore,

$$\begin{aligned} u_i^{(1)} &= \frac{1}{2\pi\rho U}\left(\frac{\partial}{\partial x_i}\left(\ln r + (1 + kx_1)(-\ln r)\right) - 2k(-\ln r)\delta_{i1}\right)[1 + \mathcal{O}(r)] \\ &= \frac{1}{2\pi\rho U}\left(\frac{x_i}{r^2} - \frac{x_i}{r^2} - k\delta_{i1}\ln r - \frac{kx_1x_i}{r^2} + 2k\ln r\delta_{i1}\right)[1 + \mathcal{O}(r)] \\ &= \frac{1}{2\pi\rho U}\left(k\delta_{i1}\ln r - \frac{kx_1x_i}{r^2}\right)[1 + \mathcal{O}(r)] . \end{aligned} \tag{3.59}$$

This gives the two dimensional drag oseenlet as

$$u_i^{(1)} = \frac{1}{4\pi\mu}\left(\delta_{i1}\ln r - \frac{x_1x_1}{r^2}\right)[1 + \mathcal{O}(r)] \tag{3.60}$$

with pressure $p^{(1)}$ as

$$p^{(1)} = -\frac{1}{2\pi}\frac{x_1}{r^2}. \tag{3.61}$$

Similarly the lift oseenlet is obtained as follows:

$$\begin{aligned} u_i^{(2)} &= \frac{1}{2\pi\rho U}\varepsilon_{ij3}\frac{\partial}{\partial x_j}\left(\ln r + e^{kx_1}K_0(kr)\right) \\ &= \frac{1}{2\pi\rho U}\varepsilon_{ij3}\left(\frac{\partial}{\partial x_j}\left(\ln r + (1 + kx_1)(-\ln r)\right)\right)[1 + \mathcal{O}(r)] \\ &= \frac{1}{2\pi\rho U}\varepsilon_{ij3}\frac{\partial}{\partial x_j}\left(-kx_1\ln r\right)[1 + \mathcal{O}(r)] \\ &= -\frac{1}{4\pi\mu}\varepsilon_{ij3}\left(\delta_{i2}\ln r + \frac{x_1x_j}{r^2}\right)[1 + \mathcal{O}(r)] . \end{aligned} \tag{3.62}$$

where r is the radius of the two dimensional circular cylinder. Also, $\varepsilon_{ijk} = 1$ for $(i,j,k) = (1,2,3),\ (2,3,1),\ (3,1,2)$, $\varepsilon_{ijk} = -1$ for $(i,j,k) = (1,3,2),\ (2,1,3),\ (3,2,1)$, and $\varepsilon_{ijk} = 0$ otherwise.

So for $i = 1$

$$u_1^{(2)} = -\frac{1}{4\pi\mu}\frac{x_1 x_2}{r^2}\left[1 + \mathcal{O}(r)\right], \tag{3.63}$$

and for $i = 2$

$$u_2^{(2)} = -\frac{1}{4\pi\mu}(-1)\left(\ln r + \frac{x_1 x_1}{r^2}\right)\left[1 + \mathcal{O}(r)\right] \tag{3.64}$$

$$= \frac{1}{4\pi\mu}\left(\ln r - \frac{x_2 x_2}{r^2}\right)\left[1 + O(r)\right] + \frac{1}{4\pi\mu}, \tag{3.65}$$

so that it yields

$$u_i^{(2)} = \frac{1}{4\pi\mu}\left(\delta_{i2}\ln r - \frac{x_1 x_2}{r^2}\right)\left[1 + \mathcal{O}(r)\right] + C_i \tag{3.66}$$

with

$$p^{(2)} = -\frac{1}{2\pi}\frac{x_2}{r^2}. \tag{3.67}$$

where $C_i = \frac{\delta_{i2}}{4\pi\mu}$ and $r^2 = x_1 x_1 + x_2 x_2$: hence the lift oseenlet is given by

$$u_i^{(m)} = \frac{1}{4\pi\mu}\left(\delta_{im}\ln r - \frac{x_i x_m}{r^2}\right)\left[1 + \mathcal{O}(r)\right] + C_i^{(m)}, \tag{3.68}$$

and

$$p^{(m)} = -\frac{1}{2\pi}\frac{x_m}{r^2}. \tag{3.69}$$

Therefore the **drag and lift stokeslets** are then given as

$$u_i^{(m)} = \frac{1}{4\pi\mu}\left(\delta_{im}\ln r - \frac{x_i x_m}{r^2}\right), \tag{3.70}$$

with

$$p^{(m)} = -\frac{1}{2\pi}\frac{x_m}{r^2}. \tag{3.71}$$

It can be shown that the drag and lift stokeslet satisfy Stokes equation (3.35), as follows:

$$0 = -\frac{\partial p}{\partial x_i} + \mu\frac{\partial^2 u_i}{\partial x_j \partial x_j} \tag{3.72}$$

$$\begin{aligned}
\frac{\partial u_i^{(m)}}{\partial x_j} &= \frac{1}{4\pi\mu}\left(\delta_{im}\frac{x_j}{r^2} - \left(\frac{r^2(x_i\delta_{mj} + \delta_{ij}x_m) - x_i x_m 2r}{r^4}\right)\frac{x_j}{r}\right) \\
&= \frac{1}{4\pi\mu}\left(\delta_{im}\frac{x_j}{r^2} - \left(\frac{x_i\delta_{mj}}{r^2} + \frac{x_m\delta_{ij}}{r^2} - \frac{2x_i x_j x_m}{r^4}\right)\right) \\
&= \frac{1}{4\pi\mu}\left(\frac{x_j\delta_{im}}{r^2} - \frac{x_i\delta_{mj}}{r^2} - \frac{x_m\delta_{ij}}{r^2} + \frac{2x_i x_j x_m}{r^4}\right),
\end{aligned} \tag{3.73}$$

$$\begin{aligned}
\frac{\partial^2 u_i^{(m)}}{\partial x_j \partial x_j} &= \frac{1}{4\pi\mu}\left(\frac{r^2 2\delta_{im} - x_j\delta_{im}2x_j}{r^4} - \frac{r^2\delta_{mj} - x_i\delta_{mj}2x_j}{r^4}\right. \\
&\left. - \frac{r^2\delta_{mj}\delta_{ij} - x_m\delta_{ij}2x_j}{r^4} + \frac{r^4\left(x_i(2x_m + x_j\delta_{mj}) + \delta_{ij}x_j x_m - x_i x_j x_m 4r^3 x_j/r\right)}{r^8}\right) \\
&= \frac{1}{4\pi\mu}\left[\frac{2\delta_{im}}{r^2} - \frac{2\delta_{im}}{r^2} - \frac{\delta_{im}}{r^2} + \frac{2x_i x_m}{r^4} - \frac{\delta_{im}}{r^2} + \frac{2x_i x_m}{r^4}\right. \\
&\left. + \frac{1}{r^4}\left(2x_i x_m + x_i x_m + x_i x_m\right) - \frac{1}{r^8}\left(4r^2 x_i x_m r^2\right)\right] \\
&= \frac{1}{4\pi\mu}\left(\frac{4x_i x_m}{r^4} - \frac{2\delta_{im}}{r^2}\right). \qquad (3.74)
\end{aligned}$$

Pressure was earlier given as

$$p^{(m)} = -\frac{1}{2\pi}\frac{x_m}{r^2}, \qquad (3.75)$$

therefore differentiating yields

$$\begin{aligned}
\frac{\partial p^{(m)}}{\partial x_i} &= -\frac{1}{2\pi}\left(\frac{r^2\delta_{im} - x_m 2x_i}{r^4}\right) \\
&= -\frac{1}{2\pi}\left(\frac{\delta_{im}}{r^2} - \frac{2x_i x_m}{r^4}\right). \qquad (3.76)
\end{aligned}$$

Substituting this in the Stokes equation (3.35) yields

$$-\frac{\partial p^{(m)}}{\partial x_i} + \mu\frac{\partial^2 u_i^{(m)}}{\partial x_j \partial x_j} = -\frac{1}{2\pi}\left(\frac{\delta_{im}}{r^2} - \frac{2x_i x_m}{r^4}\right) + \frac{1}{4\pi\mu}\left(\frac{4x_i x_m}{r^4} - \frac{2\delta_{im}}{r^2}\right) = 0 \qquad (3.77)$$

for $r > 0$ which satisfies Stokes equation. This shows that the velocity and pressure chosen for the Oseen equation also satisfy Stokes equation.

The force calculation is similar to that of Oseen, but in this thesis focus will be on the Oseen equation-hence the need for force calculations in Stokes equation will be omitted.

3.4 Oseen Equation

Oseen's equation arises from the fact that the assumptions made for low Reynold's number ($Re \ll \mathcal{O}(1)$) describe a viscous fluid. Recall that Reynold's number was define as the ratio of the inertia terms to the viscous terms

$$Re = \frac{Inertia\ Terms}{Viscous\ Terms}.$$

When $Re \ll \mathcal{O}(1)$, the viscous term will dominate over the inertia term and as a result, the viscous terms dominate the entire flow. However, Oseen felt it was not a good approximation to ignore the entire inertia term. He showed that the inertia terms are first order spatial derivatives while the viscous terms are second order spatial derivatives. In certain cases, these derivatives are comparable in magnitude and ignoring the inertia term is not justified (Pozrikidis, 2002). Consider the inertia term

$$\begin{aligned} u_j \frac{\partial u_i}{\partial x_j} =& (U\delta_{i1} + u_j^*)\frac{\partial u_i^*}{\partial x_j} \\ =& U\frac{\partial u_i^*}{\partial x_1} + u_j^*\frac{\partial u_i^*}{\partial x_j} \end{aligned} \tag{3.78}$$

As one gets further and further away from the body, (i.e. as $r \to \infty$), the fluid velocity tends to the undisturbed free stream velocity U and the term $U\frac{\partial u_i}{\partial x_1}$ becomes the dominant term. Using this result, Oseen's proposal was to include the free stream velocity term only as he showed that this was the principal inaccuracy of the original assumption when the inertia term is ignored altogether. Thus, as one gets further away from the body, the magnitude of term $U\frac{\partial u_i}{\partial x_1}$ approaches that of the viscous term.

We have seen that the incompressible Newtonian fluid flow is governed by the Navier-Stokes equation (3.19) and the continuity equation (3.7). The Oseen equations are equations of motion for viscous fluids. These equations are valid for a steady and uniform flow past a fixed body or, equivalently, a body moving with uniform, steady speed through a fluid that is otherwise undisturbed. Thus, the Oseen equation is a linearisation of the Navier-Stokes equation in the far-field region (Oseen, 1927). To derive the Oseen equation, let U to be a uniform flow velocity which is parallel to the x_1-axis with a body of arbitrary shape fixed in the stream. It is expected that far from the body, the velocity should be nearly the same as the uniform flow velocity $U\underline{\hat{x}}_1$. Oseen therefore decomposes both the velocity and the pressure as

$$u_i = U\delta_{i1} + u_i^* + \mathcal{O}(\epsilon^2) \tag{3.79}$$

and

$$p = p_o + p^* + \mathcal{O}(\epsilon^2), \tag{3.80}$$

where U is the free stream velocity, u_i^* is the perturbation velocity, and δ_{ij} is the Kronecker delta function (Strauss, 1992). In the Oseen approximation, $\epsilon \ll \mathcal{O}(1)$, so $\epsilon = \mathcal{O}\left(|\frac{u^*}{U}|\right)$: which is to say the perturbation velocity is small compared to the free stream velocity, so $|\frac{u^*}{U}|$ and $|\frac{p^*}{p_0}| = \mathcal{O}(\epsilon)$ hold. The perturbation velocity u_i^* and the pressure p^* depend on position and, in the unsteady case, on time. Oseen approximation assume that the velocity u_i is approximately equal to the uniform flow velocity U. Thus the Oseen approximation is valid only on the condition $|\frac{u^*}{U}| \ll \mathcal{O}(1)$.

The non-linear term in the Navier-Stokes equation can be linearise to get the Oseen equation. For convenience, the Navier-Stokes equation is restate:

$$\rho\frac{\partial u_i}{\partial t} + \rho u_j\frac{\partial u_i}{\partial x_j} = -\frac{\partial p}{\partial x_i} + \mu\frac{\partial^2 u_i}{\partial x_j \partial x_j} - f_i \tag{3.81}$$

with

$$\frac{\partial u_i}{\partial x_i} = 0. \tag{3.82}$$

The *time independent* Navier-Stokes equation (where $\rho\frac{\partial u}{\partial t} = 0$) in (3.81) is given by

$$\rho u_j\frac{\partial u_i}{\partial x_j} = -\frac{\partial p}{\partial x_i} + \mu\frac{\partial^2 u_i}{\partial x_j \partial x_j} - f_i, \tag{3.83}$$

with

$$\frac{\partial u_i}{\partial x_i} = 0. \tag{3.84}$$

Substituting the Oseen approximation for the velocity (3.79) and pressure (3.80) gives the following:

$$\rho\left[U\delta_{i1} + u_i^* + \mathcal{O}(\epsilon^2)\right]\frac{\partial}{\partial x_j}\left[U\delta_{i1} + u_i^* + \mathcal{O}(\epsilon^2)\right] = -\frac{\partial}{\partial x_i}\left[p_o + p^* + \mathcal{O}(\epsilon^2)\right] + \mu\frac{\partial^2}{\partial x_j \partial x_j}\left[U\delta_{i1} + u_i^* + \mathcal{O}(\epsilon^2)\right] - f_i. \tag{3.85}$$

The brackets on the left hand side become

$$\rho U\delta_{i1}\frac{\partial u_i^*}{\partial x_j} = \rho U\frac{\partial u_i^*}{\partial x_1}, \tag{3.86}$$

and the right hand side becomes

$$-\frac{\partial p^*}{\partial x_i} + \mu\frac{\partial^2 u_i^*}{\partial x_j \partial x_j} - f_i, \tag{3.87}$$

where

$$\delta_{ij} = \begin{cases} 0 & \text{if } i \neq j \\ 1 & \text{if } i = j \end{cases}.$$

This is the Oseen equation

$$\rho U \frac{\partial u_i^*}{\partial x_1} = -\frac{\partial p^*}{\partial x_i} + \mu \frac{\partial^2 u_i^*}{\partial x_j \partial x_j} - f_i \tag{3.88}$$

with the continuity equation

$$\frac{\partial u_i}{\partial x_i} = 0.$$

Dropping the suffix "*" for brevity gives

$$\rho U \frac{\partial u_i}{\partial x_1} = -\frac{\partial p}{\partial x_i} + \mu \frac{\partial^2 u_i}{\partial x_j \partial x_j} - f_i \tag{3.89}$$

with the continuity equation

$$\frac{\partial u_i}{\partial x_i} = 0 \tag{3.90}$$

Far from the body, the fluid velocity approaches that of the constant free stream velocity U, meaning that the perturbation velocity components are indeed much smaller than the free stream velocity and the Oseen equation is valid. On the other hand, the Oseen equation is not necessarily physical for the flow close to the body. The Oseen equation is invalid for a body whose normal vector is almost parallel to the free stream. Mathematically, it has been shown that if the normal vector is approximately parallel to the free stream then on applying the no-slip condition for the viscous fluid flow it is found that the modulus of the velocity vector, $|u_i|$, is of order U and the Oseen equation does not hold. Physically this means that the body is such that the perturbation potential is large (Oseen, 1927).

3.4.1 Green's Integral Representation of the Oseen Velocity

By taking equation (3.89) and representing the velocity with a surface integral, the Oseen equation can be equated to a surface integral in the near field obtained by solving the near field flow. Consider a volume of fluid V in Oseen flow (Chadwick, 2014), from the Oseen equation (3.89) above gives

$$\int_V \left(\rho U \frac{\partial u_i}{\partial x_1} + \frac{\partial p}{\partial x_i} - \mu \frac{\partial^2 u_i}{\partial x_j \partial x_j} + f_i \right) dV = 0. \tag{3.91}$$

We want a term that gives the result $u_i(\underline{x})$. This may be achieved by setting the variable $\underline{z} = \underline{x} - \underline{y}$ (here $\underline{x}$ is the coordinate of point of fluid and $\underline{y}$ is the coordinate of point of integration V_y) and the volume integral $dV_y = dy_1 dy_2 dy_3$ and multiplying the above integral by $u_i(\underline{y})$. For the point force solution

$$f_i^{(j)} = \delta_{ij}\delta(\underline{z}), \tag{3.92}$$

where $\delta(\underline{z})$ is the Dirac delta function, this gives

$$\int_{V_y} \left(\rho U \frac{\partial u_i^{(k)}(\underline{z})}{\partial x_1} + \frac{\partial p^{(k)}(\underline{z})}{\partial x_i} - \mu \frac{\partial^2 u_i^{(k)}(\underline{z})}{\partial x_j \partial x_j} + f_i^{(k)}(\underline{z}) \right) u_i(\underline{y}) dV_y = 0. \tag{3.93}$$

The terms in (3.93) except the force term, give a volume integral whereas we require a surface integral. We can obtain the surface integrals using the divergence theorem. Consider the first term in (3.93)

$$\int_{V_y} \rho U \frac{\partial u_i^{(k)} \underline{z}}{\partial x_1} u_i(\underline{y}) dV_y. \tag{3.94}$$

In order to use the divergence theorem, we require a volume integral of the type

$$\int_{V_y} \rho U \frac{\partial}{\partial x_1} \left(u_i^{(k)}(\underline{z}) u_i(\underline{y}) \right) dV_y. \tag{3.95}$$

Therefore let us consider including further volume integral terms such that

$$\begin{aligned} \int_{V_y} \Bigg[& \left(\rho U \frac{\partial u_i^{(k)}(\underline{z})}{\partial x_1} + \frac{\partial p^{(k)}(\underline{z})}{\partial x_i} - \mu \frac{\partial^2 u_i^{(k)}(\underline{z})}{\partial x_j \partial x_j} + f_i^{(k)}(\underline{z}) \right) u_i(\underline{y}) \\ & - \left(\rho U \frac{\partial u_i(\underline{y})}{\partial y_1} + \frac{\partial p(\underline{y})}{\partial y_i} - \mu \frac{\partial^2 u_i(\underline{y})}{\partial y_j \partial y_j} + f_i(y) \right) u_i^{(k)}(z) \Bigg] dV_y = 0. \end{aligned} \tag{3.96}$$

To make the above equation more soluble, the following formulae help in the simplification. It is established that

$$\begin{aligned} \frac{\partial}{\partial x_i} f(\underline{z}) &= \frac{\partial z_j}{\partial x_i} \frac{\partial}{\partial z_j} f(\underline{z}) \\ &= \delta_{ij} \frac{\partial}{\partial z_j} f(\underline{z}) \\ &= \frac{\partial}{\partial z_i} f(\underline{z}), \end{aligned} \tag{3.97}$$

and also that

$$\begin{aligned} \frac{\partial}{\partial y_i} f(\underline{z}) &= \frac{\partial z_j}{\partial y_i} \frac{\partial}{\partial z_j} f(\underline{z}) \\ &= -\delta_{ij} \frac{\partial}{\partial z_j} f(\underline{z}) \\ &= -\frac{\partial}{\partial z_i} f(\underline{z}), \end{aligned} \tag{3.98}$$

which shows that

$$\frac{\partial}{\partial x_i} f(\underline{z}) = -\frac{\partial}{\partial y_i} f(\underline{z}). \tag{3.99}$$

Hence, (3.96) becomes

$$\begin{aligned} \int_{V_y} \Bigg[\left(-\rho U \frac{\partial u_i^{(k)}(\underline{z})}{\partial y_1} - \frac{\partial p^{(k)}(\underline{z})}{\partial y_i} - \mu \frac{\partial^2 u_i^{(k)}(\underline{z})}{\partial y_j \partial y_j} + f_i^{(k)}(\underline{z}) \right) u_i(\underline{y}) \\ + \left(-\rho U \frac{\partial u_i(\underline{y})}{\partial y_1} - \frac{\partial p(\underline{y})}{\partial y_i} + \mu \frac{\partial^2 u_i(\underline{y})}{\partial y_j \partial y_j} - f_i(y) \right) u_i^{(k)}(\underline{z}) \Bigg] dV_y = 0 \ . \end{aligned} \tag{3.100}$$

equation (3.100) now simplifies because it has now been transformed to have common coordinate ($y - coordinate$) to yield

$$\begin{aligned} \int_{V_y} \Bigg[& - \rho U \frac{\partial}{\partial y_1} u_i^{(k)}(\underline{z}) u_i(\underline{y}) - \frac{\partial}{\partial y_i} \left(p^{(k)}(\underline{z}) u_i(\underline{y}) + p(\underline{y}) u_i^{(k)}(\underline{z}) \right) \\ & - \mu \frac{\partial}{\partial y_j} \left(\frac{u_i^{(k)}(\underline{z})}{\partial y_j} u_i(\underline{y}) \right) + \mu \frac{\partial}{\partial y_j} \left(\frac{\partial u_i(\underline{y})}{\partial y_j} u_i^{(k)}(\underline{z}) \right) \Bigg] dV_y \\ & = \int_{V_y} \left(-f_i^{(k)}(\underline{z}) u_(\underline{y}) + f_i(\underline{y}) u_i^{(k)}(\underline{z}) \right) dV_y. \end{aligned} \tag{3.101}$$

Simplifying the equation above with the fact that

$$\frac{\partial u_i(\underline{y})}{\partial y_i} = 0 \tag{3.102}$$

and

$$\frac{\partial u_i^{(k)}(\underline{z})}{\partial y_i} = \frac{\partial u_i^{(k)}(\underline{z})}{\partial z_i} = 0 \ , \tag{3.103}$$

the terms

$$\mu \frac{\partial u_i^{(k)}(\underline{z})}{\partial y_j} \frac{\partial u_i(\underline{y})}{\partial y_j}$$

in equation (3.101) cancel out. On the right hand side,

$$\int_{V_y} f_i^{(k)}(\underline{z}) u_i(\underline{y}) dV_y = \int_{V_y} \delta_{ij} \delta(\underline{z}) u_i(\underline{y}) dV_y = u_j(\underline{x}) \tag{3.104}$$

and so

$$\begin{aligned} u_j(\underline{x}) = \int_{V_y} \Bigg[& - \rho U \frac{\partial}{\partial y_1} \left(u_i^{(k)}(\underline{z}) u_i(\underline{y}) \right) + \frac{\partial}{\partial y_i} \left(p^{(k)}(\underline{z}) u_i(\underline{y}) + p(\underline{y}) u_i^{(k)}(\underline{z}) \right) \\ & + \mu \frac{\partial}{\partial y_j} \left(\frac{\partial}{\partial y_j} u_i^{(k)}(\underline{z}) u_i(\underline{y}) \right) - \mu \frac{\partial}{\partial y_j} \left(\frac{\partial u_i(\underline{y})}{\partial y_j} u_i^{(k)}(\underline{z}) \right) \Bigg] dV_y \\ & + \int_{V_y} f_i(\underline{y}) u_i^{(k)}(\underline{z}) dV_y \ , \end{aligned} \tag{3.105}$$

Using the divergence theorem we can see that we are now left with

$$u_j(\underline{x}) = -\int_{s_m} \left(\left[\rho U u_i^{(k)}(\underline{z}) u_i(\underline{y}) \right] n_1 + \left[p^{(k)}(\underline{z}) u_i(\underline{y}) + p(\underline{y}) u_i^{(k)}(\underline{z}) \right] n_i \right.$$
$$\left. + \left[\mu \frac{\partial u_i^{(k)}(\underline{z})}{\partial y_j} u_i(\underline{y}) - \mu \frac{\partial u_i^{(k)}(\underline{y})}{\partial y_j} u_i^{(k)}(\underline{z}) \right] n_j \right) dS_y$$
$$+ \int_{V_y} f_i(\underline{y}) u_i^{(k)}(\underline{z}) dV_y \ . \tag{3.106}$$

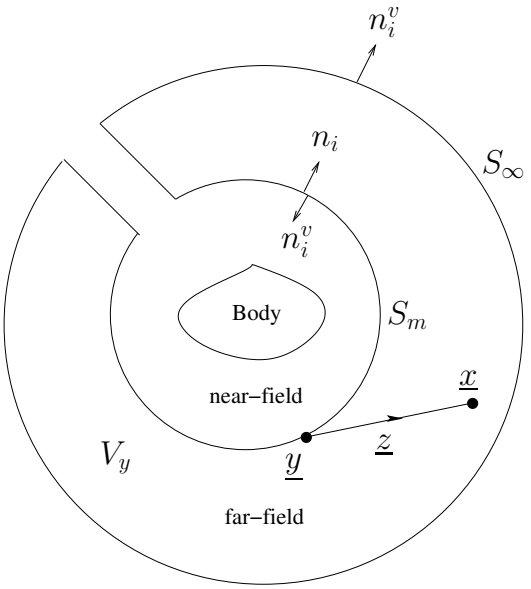

Figure 3.4: A volume representing far-field Oseen flow with normal pointing outward and inward to the body.

From figure 3.4 and equation (3.106), we can see that n_i is the outward pointing normal to S_m but the inward pointing normal to S_y. n_i^v is the outward pointing normal to $S_y = S_\infty + S_m$, the enclosing volume V_y. On the boundary S_m, we have that $n_i^v = -n_i$. To clarify: Representing the velocity by a surface integral at point $\underline{x}$, the velocity is $\underline{u}(\underline{x})$ and the pressure is $p(\underline{x})$.

In order to obtain the oseenlet, we distribute Green's functions $\underline{u}^{(k)}(\underline{z})$, and $p^{(k)}(\underline{z})$ over surface S_y (see figure 3.3). Assuming no body forces in the far-field,

$$\int_{V_y} f_i(\underline{y}) u_i^{(k)}(\underline{z}) dV_y = 0 \ . \tag{3.107}$$

We shall find that integration of S_∞ into the near field everywhere such that $S_m = 0$

then gives

$$u_j(\underline{x}) = \int_{V_m} f_i(\underline{y}) u_i^{(k)}(\underline{z}) dV_y \ , \tag{3.108}$$

which is a distribution of volume forces in V_m bounded by the surface S_m.

3.5 Summary of Chapter

In this chapter, equations that govern the fluid flow under consideration are derived. It began by deriving the Navier-Stokes equation from cauchy equation, the Navier-Stokes equation was linearised to Stokes equation as the Reynolds number tends to zero. The Oseen equation is linearised from the Navier-Stokes equation using the assumption that far from the body surface, the velocity becomes the uniform stream velocity. Furthermore, the Green's integral representation for the Stokes and Oseen velocity are given here, which is what will be use for the matched asymptotic expansion in the next chapter.

Chapter 4

Model Formulation With Boundary Element Method

4.1 Introduction

The numerical method that will be utilised for the simulation in this reseach is BEM. The mathematical formulation of the Boundary Element Method is presented in this chapter. This will cover the formulation for the Laplace equation, Stokes equation, and Oseen equation using BEM. Because of the presence of singularities, we are not able to integrate around a Green's function directly. Analytic removal of the Green's function singularity is therefore undertaken here. A further discretisation of the integral equation is obtained for the equations listed above. It is this discretisation that will be used for the computer program develop for the simulation.

4.2 Boundary Integral Formulation for the Laplace Equation

We begin by considering the two-dimensional Laplace equation and its derived Boundary Integral representation. Consider a point x_i in a fluid and point y_i as

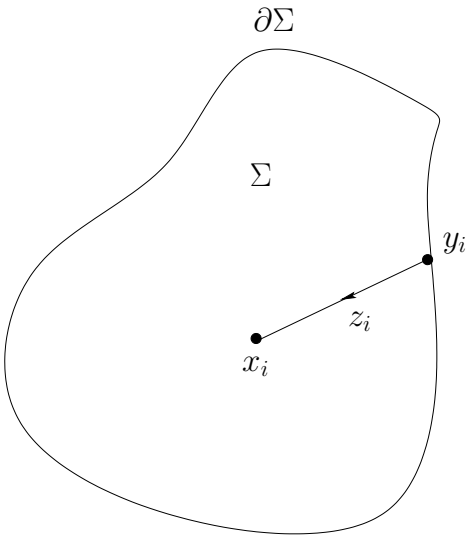

Figure 4.1: A point x_i in a domain Σ

a point of integration such that $z_i = x_i - y_i$ (see figure 4.1). BEM is subsequently applied on the integral representation obtained in Chapter 2 through the method that follows. For notational purposes, we shall use comma "," as subscript for derivatives with respect to x_i and semi colon ";" as subscript for derivatives with respect to y_i. Additionally, Σ represents the domain of the fluid and $\partial\Sigma$ represents the boundary of said domain Σ.

The Laplace equation and Laplace Green's function are respectively given by

$$\phi_{,ii} = 0 \tag{4.1}$$

and

$$G_{,ii} = \delta \tag{4.2}$$

such that

$$\int_{\Sigma} \delta d\Sigma = a, \tag{4.3}$$

where a is a fraction of the domain at the origin subtended by angle $\theta = 2\pi a$ (see figure 4.2) such that if the domain encompasses the origin $a = 1$, $\theta = 2\pi$: otherwise $a = 0$ and so $\theta = 0$. Evaluating the Green's function assuming no domain restriction (that is $a = 1$) yields

$$\int_{\Sigma} G_{,ii} d\Sigma = \int_{\Sigma} \delta d\Sigma = 1.$$

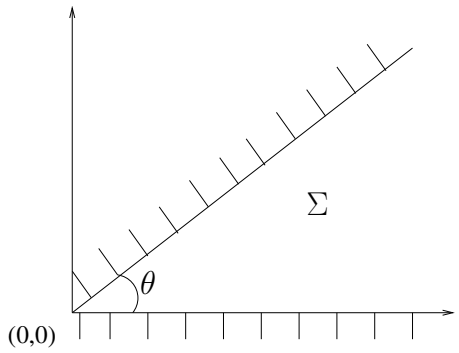

Figure 4.2: Angle subtended at the origin showing domain region

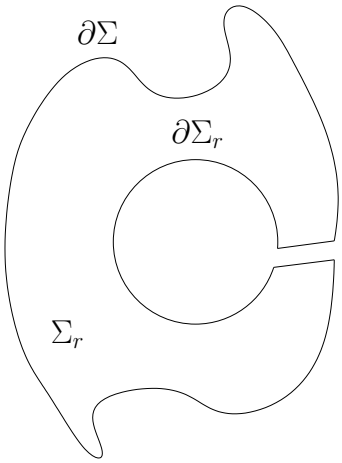

Figure 4.3: Two boundaries enclosing a domain Σ_r

From divergence theorem,

$$\int_{\Sigma} G_{,ii} d\Sigma = \int_{\partial\Sigma} G_{,i} n_i^{\Sigma} d\partial\Sigma = 1.$$

where $n_i^{\Sigma_r}$ is the outward pointing normal to $\partial\Sigma_r$. When the origin is not in Σ_r (see figure 4.3) we get

$$\int_{\Sigma_r} G_{,ii} d\Sigma = \int_{\partial\Sigma} G_{,i} n_i^{\Sigma_r} d\partial\Sigma + \int_{\partial\Sigma_r} G_{,i} n_i^{\Sigma_r} d\partial\Sigma = 0. \tag{4.4}$$

When n_i is outward pointing normal to $\partial\Sigma_r$, then $n_i = -n_i^{\Sigma}$ and the above becomes

$$\int_{\Sigma_r} G_{,ii} d\Sigma = \int_{\partial\Sigma} G_{,i} n_i^{\Sigma} d\partial\Sigma - \int_{\partial\Sigma_r} G_{,i} n_i d\partial\Sigma, \tag{4.5}$$

and so

$$\begin{aligned} \int_{\Sigma} G_{,ii} d\Sigma &= \int_{\partial\Sigma} G_{,i} n_i^{\Sigma} d\partial\Sigma \\ &= \int_{\partial\Sigma_r} G_{,i} n_i d\partial\Sigma \ . \end{aligned} \tag{4.6}$$

Note that $\frac{\partial r}{\partial x_i} = \frac{x_i}{r}$, $n_i = \frac{x_i}{r}$, $x_i x_i = r^2$, and the Green's function in 2D is $G = \frac{1}{2\pi} \ln r$ while in 3D Green's function is $G = -\frac{1}{4\pi R^2}$.

So in two dimensions,

$$\begin{aligned}\int_0^{2\pi} \frac{1}{2\pi} (\ln r)_{,i} n_i r d\theta =& \frac{1}{2\pi} \int_0^{2\pi} \frac{1}{r} \frac{x_i}{r} \frac{x_i}{r} r d\theta \\ =& \frac{1}{2\pi} 2\pi \\ =& 1.\end{aligned}$$

Similarly in three dimensions

$$\begin{aligned}\int_{\partial\Sigma_R} G_{,i} n_i d\partial\Sigma &= \iint_{S_R} -\left(\frac{1}{4\pi R}\right)_{,i} n_i dS \\ &= \iint_{S_R} -\frac{1}{4\pi} \left(-\frac{1}{R^2}\right) \frac{x_i}{R} \frac{x_i}{R} dS \\ &= \frac{1}{4\pi R^2} \iint_{S_R} dS \\ &= \frac{4\pi R^2}{4\pi R^2} \\ &= 1.\end{aligned}$$

The above formula derives from the fact that $\frac{\partial R}{\partial x_i} = \frac{x_i}{R}$, $n_i = \frac{x_i}{R}$, and the area of a sphere is $4\pi R^2$ that is

$$\int_{\alpha=0}^{2\pi} \int_{\theta=0}^{\pi} R \sin\theta d\alpha R d\theta = 2\pi R^2 \left[-\cos\theta\right]_0^{\pi} = 4\pi R^2 \tag{4.7}$$

To compute the solution to the Laplace equation (4.1) above in a particular domain of interest, we need to know either the Dirichlet boundary condition for the unknown function ϕ or the Neumann boundary condition, or in some cases a mixture of both Dirichlet and Neumann boundary conditions in areas of overlapping portions of the boundaries (Pozrikidis, 2002). The Dirichlet boundary condition specifies the values that a solution needs to take along the boundary of the domain. The Neumann boundary condition specifies the values in which the derivative of a solution is applied within the boundary of the domain (Cheng & Cheng, 2005).

4.2.1 Construction of Green's Function for the 2D Laplace Equation

The Green's function of a differential equation is the impulse response of an inhomogeneous linear differential equation defined on a given domain when boundary conditions and initial conditions are known. The Green's function of Laplace's equation in 2D constitutes a special class of harmonic functions that are singular at an arbitrary point $\mathbf{x}_0 = (x_0, y_0)$. Hence, the Green's function satisfies the singularity-forced Laplace equation

$$\nabla^2 G(\mathbf{x}, \mathbf{x}_0) - \delta(\mathbf{x} - \mathbf{x}_0) = 0 \tag{4.8}$$

where $\mathbf{x} = (x, y)$ is a point in the field, $\mathbf{x}_0 = (x_0, y_0)$ is the point of integration where the singular point is located, and $\delta(\mathbf{x} - \mathbf{x}_0)$ is the Dirac delta function in 2D.
We then define the Dirac delta function as

$$\int_\Sigma \delta(\mathbf{x} - \mathbf{x}_0) d\Sigma = \begin{cases} 1, & \text{if } \mathbf{x} \in \Sigma \\ 0, & \text{if } \mathbf{x} \notin \Sigma \\ \frac{1}{2}, & \text{if } \mathbf{x} \in \partial\Sigma \ . \end{cases} \tag{4.9}$$

4.2.2 Construction of Green's Integral

To construct the the Green's function, it will require applying Green's second identity for a non-singular harmonic function (4.1) and the Laplace Green's function (4.2). Multiply equation (4.1) by G, equation (4.2) by ϕ, subtract the two results together, and then integrate over the domain Σ bounded by the collection of closed contour, that is

$$\int_\Sigma \left(\phi G_{,ii} - G\phi_{;ii}\right) d\Sigma_y = \int_\Sigma \left(\phi\delta - 0\right) d\Sigma_y. \tag{4.10}$$

Considering only the left hand side of equation (4.10) and with the fact that symmetry holds for the Laplace Green's function, that is to say $G_{,ii} = G_{;ii}$, and applying

divergence theorem gives

$$\begin{aligned}\int_{\Sigma}\left(\phi G_{,ii}-G\phi_{;ii}\right)d\Sigma_y &= \int_{\Sigma}\left(\phi G_{;ii}-G\phi_{;ii}\right)d\Sigma_y \\ &= \int_{\Sigma}\Big((\phi G_{;i})_{;i}-\phi_{;i}G_{;i}-(G\phi_{;i})_{;i}-G_{;i}\phi_{;i}\Big)d\Sigma_y \\ &= \int_{\Sigma}\Big((\phi G_{;i})_{;i}-(G\phi_{;i})_{;i}\Big)d\Sigma_y \\ &= \int_{\partial\Sigma}\Big(\phi G_{;i}-G\phi_{;i}\Big)n_i^{\Sigma}d\partial\Sigma_y.\end{aligned}$$

The right hand side of equation (4.10) gives

$$\int_{\Sigma}(\phi\delta-0)\partial\Sigma_y = a\phi(\underline{x}), \tag{4.11}$$

where, as stated earlier a is a fraction of the domain at the origin subtended by an angle $\theta = 2\pi a$. Therefore,

$$a\phi(\underline{x}) = \int_{\partial\Sigma}\Big(\phi G_{;i}-G\phi_{;i}\Big)n_i^{\Sigma}d\partial\Sigma_y\ . \tag{4.12}$$

Equation (4.12) gives the boundary integral representation of a harmonic function. This integral representation is with respect to the boundary values for the given domain and also the boundary distribution of the normal derivative of the harmonic function. Therefore to find the value of $\phi(\underline{x})$ at any given point in the domain of reference $\partial\Sigma_y$, it is required that only the right hand side of (4.12) should be computed.

For the interior problem,

$$a\phi(\underline{x}) = \int_{\partial\Sigma}\Big(\phi G_{;i}n_i-G\phi_{;i}n_i\Big)d\partial\Sigma_y, \tag{4.13}$$

and for the exterior problem (see figure 4.4) we get

$$a\phi(\underline{x}) = \int_{\partial\Sigma_o+\partial\Sigma_1+\partial\Sigma_2+\partial\Sigma_\infty}\Big(\phi G_{;i}-G\phi_{;i}\Big)n_i^{\Sigma}d\partial\Sigma_y \tag{4.14}$$

All other terms on the boundary, that is $\int_{\partial\Sigma_1} = -\int_{\partial\Sigma_2}$, since n_i^{Σ} on $\partial\Sigma_1$ is the same as $-n_i^{\Sigma}$ on $\partial\Sigma_2$ therefore it cancel out, and assuming that the infinite part goes to zero, that is

$$\int_{\partial\Sigma_\infty}\left(G\phi_{;i}n_i-\phi G_{;i}n_i\right)d\partial\Sigma_y \longrightarrow 0,$$

we obtain

$$a\phi(\underline{x}) = \int_{\partial\Sigma_o}\Big(\phi G_{;i}-G\phi_{;i}\Big)n_i^{\Sigma}d\partial\Sigma_y. \tag{4.15}$$

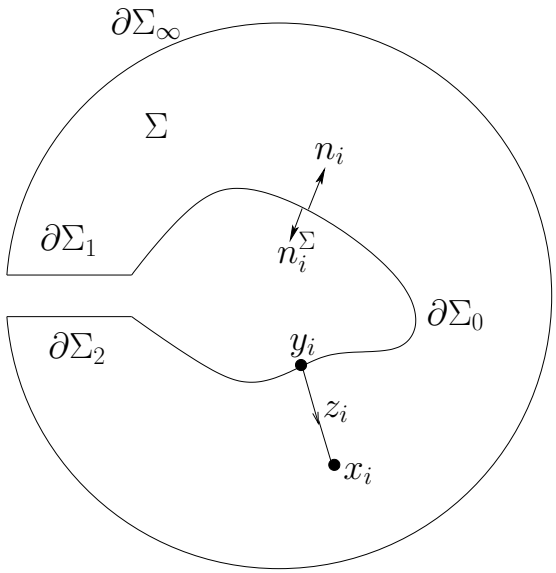

Figure 4.4: Four boundaries enclosing a domain

4.3 Boundary Element Formulation for the Laplace Equation

4.3.1 Model formulation using the Boundary Element Method

Let $F = \phi_{;i} n_i$. Substituting this into 4.15 we get,

$$a\phi(\underline{x}) = \int_{\partial\Sigma_o} (GF - \phi G_{;i} n_i)\, d\partial\Sigma_y. \tag{4.16}$$

If we take N_q as the shape function and W_q as the weighting function, then we can discretise (4.16) with $\phi = \phi_q N_q$, $F = f_q N_q$, W_q, and $1 \leq q, s, m \leq M$ using Dirichlet boundary condition. Multiply both sides of equation (4.16) by the weighting function W_q and integrate both sides over the domain $\partial\Sigma_y$, yielding

$$\int_{\partial\Sigma_o} W_m (a\phi_q N_q) d\partial\Sigma_x = \int_{\partial\Sigma_o} W_m \int_{\partial\Sigma_o} (G f_q N_q - \phi_q N_q G_{;i} n_i)\, d\partial\Sigma_y d\partial\Sigma_x, \tag{4.17}$$

$$\begin{aligned} a\phi_q \int_{\partial\Sigma_o} W_m N_q d\partial\Sigma_x =& f_q \int_{\partial\Sigma_o} W_m \int_{\partial\Sigma_o} G N_q d\partial\Sigma_y d\partial\Sigma_x \\ & - \phi_q \int_{\partial\Sigma_o} W_m \int_{\partial\Sigma_o} N_q G_{;i} n_i N_q d\partial\Sigma_y d\partial\Sigma_x, \end{aligned} \tag{4.18}$$

and

$$f_q\Big(\int_{\partial\Sigma_o} W_m \int_{\partial\Sigma_o} GN_q d\partial\Sigma_y d\partial\Sigma_x\Big) = a\phi_q \int_{\partial\Sigma_o} W_m N_q d\partial\Sigma_x + \phi_q\Big(\int_{\partial\Sigma_o} W_m \int_{\partial\Sigma_o} N_q G_{;i} n_i d\partial\Sigma_y d\partial\Sigma_x\Big), \tag{4.19}$$

which in matrix form, becomes

$$A_{mq} f_q = Y_m, \tag{4.20}$$

where

$$A_{mq} = \int_{\partial\Sigma_o} W_m \int_{\partial\Sigma_o} GN_q d\partial\Sigma_y d\partial\Sigma_x \tag{4.21}$$

and

$$Y_m = a\phi_q \int_{\partial\Sigma_o} W_m N_q d\partial\Sigma_x + \phi_q\Big(\int_{\partial\Sigma_o} W_m \int_{\partial\Sigma_o} N_q G_{;i} n_i d\partial\Sigma_y d\partial\Sigma_x\Big). \tag{4.22}$$

On a smooth boundary, $a = \frac{1}{2}$, while in a flow field, $a = 1$. We want to find

$$f_q = A^{-1}_{mq} Y_m \ . \tag{4.23}$$

Our next task is to find the unknown f_q on a smooth boundary. When this is done then the flow at any point in the fluid can be determined. To progress, consider the boundary points $\underline{x}_q$ and weighting function $W_m = \delta(\underline{x} - \underline{x}_{m+\frac{1}{2}})$ positioned at $\underline{x}_{m+\frac{1}{2}} = \frac{\underline{x}_{m+1} + \underline{x}_m}{2}$ (see figure 4.5).

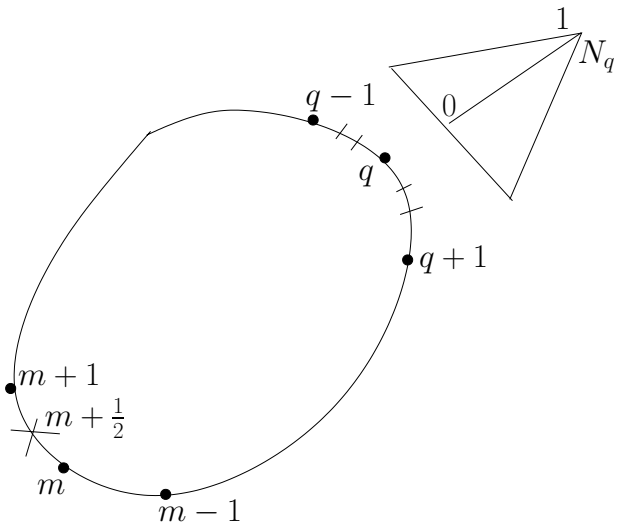

Figure 4.5: Shape function and positioning of weighting function

To interpolate the solution for the discrete values we use the linear shape function giving as

$$N_q = \begin{cases} \frac{|\underline{x}-\underline{x}_{q-1}|}{|\underline{x}_q-\underline{x}_{q-1}|} & \begin{cases} 0, & \text{if } \underline{x} = \underline{x}_{q-1} \\ 1, & \text{if } \underline{x} = \underline{x}_q \end{cases} \quad (\text{linear if } \underline{x}_{q-1} \leq \underline{x} \leq \underline{x}_q) \\ \frac{|\underline{x}-\underline{x}_{q+1}|}{|\underline{x}_q-\underline{x}_{q+1}|} & \begin{cases} 0, & \text{if } \underline{x} = \underline{x}_{q+1} \\ 1, & \text{if } \underline{x} = \underline{x}_q \end{cases} \quad (\text{linear if } \underline{x}_q \leq \underline{x} \leq \underline{x}_{q+1}) \\ 0, & \text{otherwise .} \end{cases} \tag{4.24}$$

Making necessary substitutions and simplification from the values defined above, we find that A_{mq} from equation (4.20) becomes

$$\begin{aligned} A_{mq} &= \int_{\partial\Sigma_o} \delta\left(\underline{x} - \underline{x}_{m+\frac{1}{2}}\right) \left(\int_{\partial\Sigma_o} G N_q d\partial\Sigma_x\right) d\partial\Sigma_y \\ &= \int_{\partial\Sigma_o} G_{m+\frac{1}{2}} N_q d\partial\Sigma_y \end{aligned} \tag{4.25}$$

where $G_{m+\frac{1}{2}} = G\left(\underline{x}_{m+\frac{1}{2}} - \underline{y}\right)$ and

$$\begin{aligned} Y_m &= a\phi_q \int_{\partial\Sigma_o} \delta\left(\underline{x} - \underline{x}_{m+\frac{1}{2}}\right) N_q d\partial\Sigma_x + \phi_q \int_{\partial\Sigma_o} \delta\left(\underline{x} - \underline{x}_{m+\frac{1}{2}}\right) \int_{\partial\Sigma_o} N_q G_{;i} n_i d\partial\Sigma_y d\partial\Sigma_x \\ &= a\phi_q N_q(\underline{x}_{m+\frac{1}{2}}) + \phi_q \int_{\partial\Sigma_o} G_{m+\frac{1}{2};i} n_i N_q d\partial\Sigma_y \\ &= a\phi_{m+\frac{1}{2}} + \phi_q \int_{\partial\Sigma_o} G_{m+\frac{1}{2};i} n_i N_q d\partial\Sigma_y. \end{aligned} \tag{4.26}$$

Equation (4.26) is the discretised form of the boundary element formulation for the Laplace equation. Next we shall define the Gaussian points and also remove singularities that exist as a result of the logarithmic function in the two dimensional Laplace Green's function.

4.3.2 Two Point Gaussian Quadrature

Using a quadratic functional $f(x)$ we integrate to get the Gaussian point:

$$\begin{aligned} \int_{-1}^{1} f(x)dx &= \int_{-1}^{1} \left(a_o + a_1 x + a_2 x^2\right) dx \\ &= 2a_0 + \frac{2a_2}{3} \end{aligned} \tag{4.27}$$

with $F(-\xi) = a_0 - a_1\xi + a_2\xi^2$ and $F(\xi) = a_0 + a_1\xi + a_2\xi^2$ so that

$$\begin{aligned} F(\xi) + F(-\xi) &= 2a_0 + 2a_2\xi^2 \\ &= 2a_0 + \frac{2a_2}{3}. \end{aligned}$$

for $\xi^2 = \frac{1}{3}$ we have

$$\int_{-1}^{1} f(x)dx = f\left(-\frac{1}{\sqrt{3}}\right) + f\left(\frac{1}{\sqrt{3}}\right)$$

at $x^* = ax$, which implies that

$$\begin{aligned} \int_{-a}^{a} f\left(\frac{x^*}{a}\right)\frac{1}{a}dx^* =& \frac{1}{a}\int_{-a}^{a} g(x^*)dx^* \\ =& g\left(-\frac{a}{\sqrt{3}}\right) + g\left(\frac{a}{\sqrt{3}}\right), \end{aligned}$$

where $f\left(\frac{x^*}{a}\right) = g(x^*)$ and $f(x) = g(xa)$.

At $x = x^* + a + b$, it becomes

$$\begin{aligned} \frac{1}{a}\int_{b}^{2a+b} g(x-a-b)dx &= \frac{1}{a}\int_{b}^{2a+b} h(x)dx \\ &= h\left(a+b-\frac{a}{\sqrt{3}}\right) + h\left(a+b+\frac{a}{\sqrt{3}}\right) \end{aligned}$$

where $h(x) = g(x-a-b)$ and $h(x^* + a + b) = g(x^*)$.

Let $c = 2a + b$ and $a = \frac{c-b}{2}$, so that

$$\frac{1}{a}\int_{b}^{c} h(x)dx = h\left(\frac{b+c}{2} - \frac{\frac{c-b}{2}}{\sqrt{3}}\right) + h\left(\frac{b+c}{2} + \frac{\frac{c-b}{2}}{\sqrt{3}}\right)$$

$$\int_{b}^{c} h(x)dx = W\left(h\left(x^{GP1}\right) + h\left(x^{GP2}\right)\right), \tag{4.28}$$

where $GP1$ refers to the Gaussian point one, and so on, $W = \frac{c-b}{2}$, and $x^{GP1/GP2} = \frac{b+c}{2} \pm \frac{\frac{c-b}{2}}{\sqrt{3}}$. To obtain the third and fourth Gaussian points we repeat the same procedure as above, but this time with $\xi = -\frac{1}{\sqrt{3}}$.

Therefore, the matrix A_{mq} can be written as

$$\begin{aligned} A_{mq} &= \int_{\partial\Sigma_o} G_{m+\frac{1}{2}} N_q d\partial\Sigma_y \\ &= \int_{q-1}^{q} G_{m+\frac{1}{2}} N_q d\partial\Sigma_y + \int_{q}^{q+1} G_{m+\frac{1}{2}} N_q d\partial\Sigma_y \\ &= \frac{2}{l^{q-}}\left[G\left(x_{m+\frac{1}{2}} - y_q^{GP1}\right) N_q(y_q^{GP1}) + G\left(x_{m+\frac{1}{2}} - y_q^{GP2}\right) N_q(y_q^{GP2})\right] \\ &+ \frac{2}{l^{q+}}\left[G\left(x_{m+\frac{1}{2}} - y_q^{GP3}\right) N_q(y_q^{GP3}) + G\left(x_{m+\frac{1}{2}} - y_q^{GP4}\right) N_q(y_q^{GP4})\right], \end{aligned} \tag{4.29}$$

where $l^{q-} = |y_q - y_{q-1}|$, $l^{q+} = |y_{q+1} - y_q|$,

$$\underline{y}_q^{GP1/GP2} = \frac{\underline{y}_{q-1} + \underline{y}_q}{2} \mp \frac{\frac{\underline{y}_q + \underline{y}_{q-1}}{2}}{\sqrt{3}},$$

$$\underline{y}_q^{GP3/GP4} = \frac{\underline{y}_{q+1} + \underline{y}_q}{2} \mp \frac{\frac{\underline{y}_{q+1} + \underline{y}_q}{2}}{\sqrt{3}},$$

and

$$\begin{aligned} N_q\left(\underline{y}_q^{GP1/GP2}\right) =& \left| \frac{\frac{\underline{y}_{q-1} + \underline{y}_q}{2} \mp \frac{\frac{\underline{y}_q + \underline{y}_{q-1}}{2}}{-} \underline{y}_{q-1}}{\underline{y}_q + \underline{y}_{q-1}} \right| \\ =& \frac{1}{2}\left(1 \mp \frac{1}{\sqrt{3}}\right). \end{aligned}$$

Similarly, for the remaining Gaussian points

$$N_q\left(\underline{y}_q^{GP3/GP4}\right) = \frac{1}{2}\left(1 \pm \frac{1}{\sqrt{3}}\right).$$

Therefore,

$$\begin{aligned} A_{mq} = \frac{l^{q-}}{2}\left[\frac{1}{2\pi}\ln r\mid_{(GP1)}\left(\frac{1-\frac{1}{\sqrt{3}}}{2}\right) + \frac{1}{2\pi}\ln r\mid_{(GP2)}\left(\frac{1+\frac{1}{\sqrt{3}}}{2}\right)\right] \\ + \frac{l^{q+}}{2}\left[\frac{1}{2\pi}\ln r\mid_{(GP3)}\left(\frac{1+\frac{1}{\sqrt{3}}}{2}\right) + \frac{1}{2\pi}\ln r\mid_{(GP4)}\left(\frac{1-\frac{1}{\sqrt{3}}}{2}\right)\right] \end{aligned} \quad (4.30)$$

where $r\mid_{(GP1)} = |\underline{x}_{m+\frac{1}{2}} - \underline{y}_q^{GP1}|$, and similarly for the remaining Gaussian points.

4.3.3 Analytical Removal of the Green's Function Singularity

The two points of singularities in the two dimensional Laplace Green's function are when $m = q - 1$ and when $m = q$.

For $m = q-1$,

$$\begin{aligned}\int_{q-1}^{q} G_{m+\frac{1}{2}} N_q d\partial\Sigma_y =& \frac{1}{2\pi}\int_{q-1}^{q} \ln r N_q d\partial\Sigma_y \\ =& \frac{1}{2\pi}\int_{-1}^{1} \ln|\xi k^-| N_q d\xi, \text{ where } 2k^- = |\underline{y}_q - \underline{y}_{q-1}| \\ =& \frac{k^-}{2\pi}\int_{-1}^{1} \ln|\xi k^-| \frac{\xi+1}{2} d\xi \\ =& \frac{k^-}{2\pi}\int_{-1}^{1} \ln|\xi k^-| \frac{1}{2} d\xi \\ =& \frac{k^-}{2\pi}\int_{0}^{1} \ln \xi k^- \xi d\xi \\ =& \frac{k^-}{2\pi}\left[\xi \ln k^- + \xi \ln \xi - \xi\right]_0^1 \\ =& \frac{k^-}{2\pi}(\ln k^- - 1), \quad \text{where } k^- = \frac{l^{q-}}{2} \end{aligned} \tag{4.31}$$

Thus,

$$\begin{aligned} A_{mq} = \frac{l^{q-}}{4\pi}(\ln l^{q-} - \ln 2 - 1) + \frac{2}{l^{q+}}\Bigg[& \frac{1}{2\pi} \ln r \,|_{(GP3)} \left(\frac{1+\frac{1}{\sqrt{3}}}{2}\right) \\ & + \frac{1}{2\pi} \ln r \,|_{(GP4)} \left(\frac{1-\frac{1}{\sqrt{3}}}{2}\right)\Bigg]. \end{aligned} \tag{4.32}$$

For $m = q$,

$$\begin{aligned}\int_{q}^{q+1} G_{m+\frac{1}{2}} N_q d\partial\Sigma_y =& \frac{1}{2\pi}\int_{q}^{q+1} \ln r N_q d\partial\Sigma_y \\ =& \frac{1}{2\pi}\int_{-1}^{1} \ln|\xi k^+| N_q k^+ d\xi, \quad \text{where } 2k^+ = |\underline{y}_{q+1} - \underline{y}_q| \\ =& \frac{k^+}{2\pi}\int_{-1}^{1} \ln|\xi k^+| \left(\frac{-\xi+1}{2}\right) d\xi \\ =& \frac{k^+}{2\pi}\int_{-1}^{1} \ln|\xi k^+| \frac{1}{2} d\xi \\ =& \frac{k^+}{2\pi}\int_{0}^{1} \ln \xi k^+ d\xi \\ =& \frac{k^+}{2\pi}(\ln k^+ - 1), \end{aligned} \tag{4.33}$$

and so

$$\begin{aligned} A_{mq} = \frac{l^{q+}}{4\pi}(\ln l^{q+} - \ln 2 - 1) + \frac{2}{l^{q-}}\Bigg[& \frac{1}{2\pi} \ln r \,|_{(GP1)} \left(\frac{1-\frac{1}{\sqrt{3}}}{2}\right) \\ & + \frac{1}{2\pi} \ln r \,|_{(GP2)} \left(\frac{1+\frac{1}{\sqrt{3}}}{2}\right)\Bigg]. \end{aligned} \tag{4.34}$$

The equation (4.34) above is the final discretisation for the left hand side of the equation (4.20) which will be used in the implementation of the computation that will be used later in this work. Note that removing the singularity at the point $m = q + 1$ is not necessary because there is no singularity at that point since the point of integration is on the left hand side. Also notice that the left hand side includes single layer potential which does not contain singularity, while the double layer potential on the right hand side contains singularity.

For the right hand side of (4.20), the following simplification applies:

$$\begin{aligned}
Y_m =& a\phi_{m+\frac{1}{2}} + \phi_q \int_{\partial\Sigma} G_{m+\frac{1}{2};i} n_i N_q d\partial\Sigma_y \\
=& a\phi_{m+\frac{1}{2}} + \phi_q \int_{q-1}^{q} G_{m+\frac{1}{2};i} n_i N_q d\partial\Sigma_y + \phi_q \int_{q}^{q+1} G_{m+\frac{1}{2};i} n_i N_q d\partial\Sigma_y \\
=& a\phi_{m+\frac{1}{2}} + \phi_q \Bigg[\frac{l^{q-}}{2} \Bigg(G\left(\underline{x}_{m+\frac{1}{2}} - \underline{y}_q^{GP1}\right)_{;i} n_i^{GP1} N_q\left(\underline{y}_q^{GP1}\right) \\
&+ G\left(\underline{x}_{m+\frac{1}{2}} - \underline{y}_q^{GP1}\right)_{i} n_i^{GP1} N_q\left(\underline{y}_q^{GP1}\right) \Bigg) + \frac{l^{q+}}{2} \Bigg(G\left(\underline{x}_{m+\frac{1}{2}} - \underline{y}_q^{GP3}\right); in_i^{GP3} N_q\left(\underline{y}_q^{GP3}\right) \\
&+ G\left(\underline{x}_{m+\frac{1}{2}} - \underline{y}_q^{GP4}\right)_{i} n_i^{GP4} N_q\left(\underline{y}_q^{GP4}\right) \Bigg) \Bigg],
\end{aligned}$$

where

$$\begin{aligned}
G_{;i} =& -\frac{dG}{dz_i} \\
=& -\frac{dG}{dr}\frac{dr}{dz_i} \\
=& -\frac{d}{dr}\left(\frac{1}{2\pi}\ln r\right)\frac{z_i}{r} \\
=& -\frac{1}{2\pi}\left(\frac{x_i - y_i}{r^2}\right),
\end{aligned}$$

so that

$$G\left(\underline{x}_{m+\frac{1}{2}} - \underline{y}_q^{GP1}\right)_{;i} = -\frac{1}{2\pi}\left(\frac{\underline{x}_{m+\frac{1}{2}i} - \underline{y}_{qi}^{GP1}}{r^2\mid_{(GP1)}}\right) \tag{4.35}$$

for $\left(\underline{x}_{m+\frac{1}{2}}\right)_i = \underline{x}_{m+\frac{1}{2}i}$, $(y_q)_i = y_{qi}$, and $r\mid_{(GP1)} = |\underline{x}_{m+\frac{1}{2}} - \underline{y}_q^{GP1}|$. A similar procedure can be done to obtain the remaining Gaussian points, and hence the right hand side

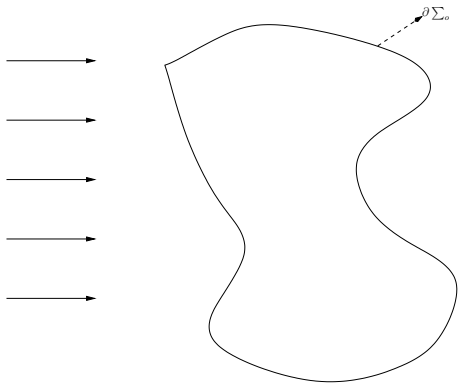

Figure 4.6: Flow past a boundary of a solid body, given by $\partial\Sigma_0$

of (4.20) becomes

$$\begin{aligned} Y_m = a\phi_{m+\frac{1}{2}} + \phi_q \Bigg[& \frac{l^{q-}}{2} \Bigg(\left(-\frac{1}{2\pi}\right) \left(\frac{\underline{x}_{m+\frac{1}{2}i} - \underline{y}_{qi}^{GP1}}{r^2(GP1)} \right) n_i^{GP1} \left(\frac{1-\frac{1}{\sqrt{3}}}{2} \right) \\ & + \left(-\frac{1}{2\pi}\right) \left(\frac{\underline{x}_{m+\frac{1}{2}i} - \underline{y}_{qi}^{GP2}}{r^2(GP2)} \right) n_i^{GP2} \left(\frac{1+\frac{1}{\sqrt{3}}}{2} \right) \\ & + \frac{l^{q+}}{2} \Bigg(\left(-\frac{1}{2\pi}\right) \left(\frac{\underline{x}_{m+\frac{1}{2}i} - \underline{y}_{qi}^{GP3}}{r^2(GP3)} \right) n_i^{GP3} \left(\frac{1-\frac{1}{\sqrt{3}}}{2} \right) \\ & + \left(-\frac{1}{2\pi}\right) \left(\frac{\underline{x}_{m+\frac{1}{2}i} - \underline{y}_{qi}^{GP4}}{r^2(GP4)} \right) n_i^{GP4} \left(\frac{1-\frac{1}{\sqrt{3}}}{2} \right) \Bigg] \end{aligned} \tag{4.36}$$

4.4 Boundary Element Formulation for Exterior Problems Using the Stokes and Oseen Equations

Consider a body fixed in a flow field with steady uniform fluid flow (see figure 4.6). We shall use the Boundary Element Method to model the boundary of the fixed body in Stokes flow. To discretise the Stokes equation given in (3.35) and using (4.16) for the boundary integral representation of the Laplace equation we can write

$$\begin{aligned} au_i &= \int_{\partial\Sigma_0} f_j u_{ij} dl' \\ &= \int_{\partial\Sigma_0} N_\beta f_{\beta j} u_{ij} dl' \end{aligned} \tag{4.37}$$

where $N_\beta(\underline{x}^{'})$ is the shape function, $u_{ij}(\underline{x}-\underline{x}^{'})$ is the Green's function evaluated at $\underline{x}^{'}$, $\underline{x}^{'}$ is a position on the domain $\partial\Sigma_0$, $dl^{'}$ is an element of the length integration variable. $1 \leq i, j \leq m$, where m is the size of the dimensional space and $1 \leq \beta \leq n$ represents the descritisation points.

On the boundary,

$$\int_{\partial\Sigma_0} W_\alpha u_i dl = \int_{\partial\Sigma_0} W_\alpha \int_{\partial\Sigma_0} N_\beta f_{\beta j} u_{ij} dl^{'} dl$$

where $1 \leq \alpha \leq n$, $W_\alpha(\underline{x})$ is the weighting function at node α integrated over $\underline{x}$ position on Σ element of length dl.

As a result,

$$u_{\alpha i} = u_{\alpha\beta ij} f_{\beta j} \tag{4.38}$$

where

$$u_{\alpha i} = \int_{\partial\Sigma_0} W_\alpha u_i dl$$

$$u_{\alpha\beta ij} = \int_{\partial\Sigma_0} W_\alpha \int_{\partial\Sigma_0} N_\beta u_{ij} dl^{'} dl \ .$$

We need to renumber (4.38) so that we can put it into a matrix form in order to solve it in a matrix solver.

Hence, we renumber to $\alpha^* = \alpha + (i-1)n$, and $\alpha = \alpha^* - (i-1)n$,

with $\beta^* = \beta + (j-1)n$, and $\beta = \beta^* - (j-1)n$, where $1 \leq \alpha^*, \beta^* \leq m \times n$, $i = 1 + \left(\frac{\alpha^*}{n+1}\right)_{\text{integer division}}$, and $j = 1 + \left(\frac{\beta^*}{n+1}\right)_{\text{integer division}}$.

In renumbered form, (4.38) becomes

$$u_{\alpha^*} = u_{\alpha^*\beta^*} f_{\beta^*}, \tag{4.39}$$

and the matrix we require is

$$f_{\beta^*} = u^{-1}_{\alpha^*\beta^*} u_{\alpha^*}. \tag{4.40}$$

Consider a uniform flow δ_{i1} past a two dimensional ($m = 2$) circular cylinder of radius 1 (see figure 4.4), given that the weighting function is the collocation point and the shape function is a linear two-point Gaussian, we want to evaluate u_{α^*} $[u_{\alpha i}]$

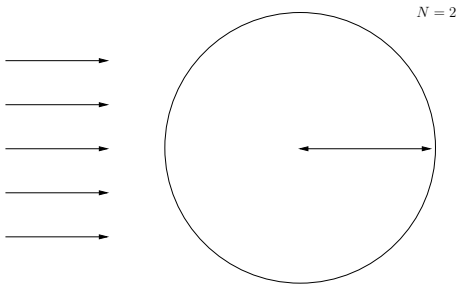

Figure 4.7: Uniform flow past a circular cylinder.

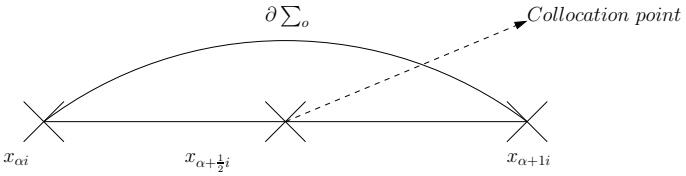

Figure 4.8: Collocation points

$$
\begin{aligned}
u_{\alpha i} &= \int_{\partial\Sigma_0} W_\alpha u_i dl \\
&= \int_{\partial\Sigma_0} \delta(\underline{x}_{\alpha+\frac{1}{2}}) u_i dl \\
&= u_i(\underline{x}_{\alpha+\frac{1}{2}})
\end{aligned}
$$

The last term on the above equation is the mid point shown in figure 4.8 .

For clarity purposes, $\underline{x}_\alpha / x_{\alpha i}$ is a position vector x_i of node α and $\underline{x}_{\alpha+\frac{1}{2}} / x_{\alpha+\frac{1}{2}i}$ is the position vector x_i of the mid-point between nodes α and $\alpha+1$. $x_{\alpha+\frac{1}{2}i} = \frac{1}{2}(x_{\alpha i} + x_{\alpha+1i})$ is the mid-point with the boundary condition $u_i|_{\partial\Sigma_0} = -\delta_{i1}$, which means that $u_{\alpha i} = u_{\alpha+\frac{1}{2}i} = -\delta_{i1}$. We also want to evaluate the Non-degenerative singularity case, first, for $\alpha \neq \beta - 1, \beta$ which gives

$$
\begin{aligned}
u_{\alpha\beta ij} &= \int_{\partial\Sigma_0} W_\alpha \int_{\partial\Sigma_0} N_\beta u_{ij} dl^{'} dl \\
&= \int_{\partial\Sigma_0} N_\beta u_{ij} (\underline{x}_{\alpha+\frac{1}{2}} - \underline{x}) dl^{'} \\
&= N_{\beta I} gpw_I u_{ij}(\underline{y}), \qquad (4.41)
\end{aligned}
$$

where $y_i = x_{\alpha+\frac{1}{2}i} - x_{\beta iI}$, $N_{\beta I}$ is the shape function at Gaussian points I, $N_{\beta I} = \left(\frac{1}{2} - \frac{1}{2\sqrt{3}}, \frac{1}{2} + \frac{1}{2\sqrt{3}}, \frac{1}{2} + \frac{1}{2\sqrt{3}}, \frac{1}{2} - \frac{1}{2\sqrt{3}}\right)$, gpw_I is the Gaussian point weight at point I with $gpw_I = \left(\frac{l^-}{2}, \frac{l^-}{2}, \frac{l^+}{2}, \frac{l^+}{2}\right)$ where the length between nodes is given as $l^- = \mid x_{\beta i} - x_{\beta+1i} \mid$, and $l^+ = \mid x_{\beta+1i} - x_{\beta i} \mid$. The four different Gaussian points are

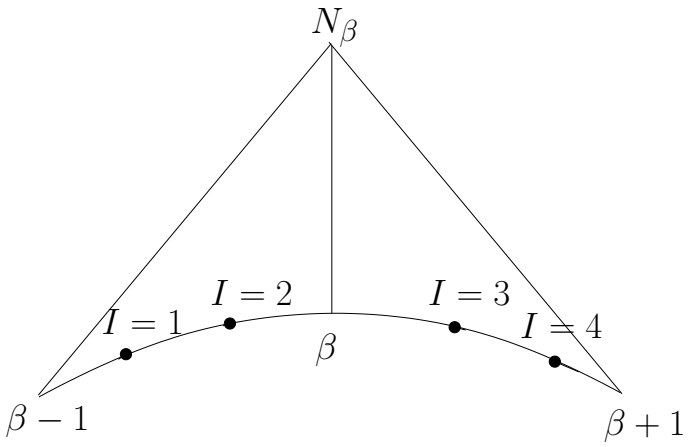

Figure 4.9: Four Gaussian points

illustrated in figure 4.9, $x_{\beta iI}$ is the position x_i of Gaussian point I of node β such that

$$\begin{aligned} x_{\beta iI} =& \frac{x_{\beta-1i}+x_{\beta i}}{2} - \frac{x_{\beta i}-x_{\beta-1i}}{2\sqrt{3}}, \\ & \frac{x_{\beta-1i}+x_{\beta i}}{2} + \frac{x_{\beta i}-x_{\beta-1i}}{2\sqrt{3}}, \\ & \frac{x_{\beta+1i}+x_{\beta i}}{2} - \frac{x_{\beta+1i}-x_{\beta i}}{2\sqrt{3}}, \\ & \frac{x_{\beta+1i}+x_{\beta i}}{2} + \frac{x_{\beta+1i}-x_{\beta i}}{2\sqrt{3}} \end{aligned}$$

$u_{ij}(y)$ is the stokeslet given by

$$u_{ij}(y) = \frac{Re}{4\pi}\left(\delta_{ij}\ln r - \frac{y_i y_j}{r^2}\right), \tag{4.42}$$

and where $r = +\sqrt{y_i y_j}$.

We also wish to evaluate the regenerate case with singularities for $i=j$, $\alpha=\beta$. In this case, the singularity needs to be removed

$$\begin{aligned} u_{\alpha\beta ij} =& \int_{\partial\Sigma_0} N_\beta u_{ij} dl' \\ =& \int_{l^-} N_\beta u_{ij} dl' + \int_{l^+} N_\beta \left(u_{ij} - u_{ij}^{s^*}\right) dl' + \int_{l^+} N_\beta u_{ij}^{s^*} dl' \\ =& N_{\beta 1} u_{ij}(\underline{y}) gpw_1 + N_{\beta 2} u_{ij}(\underline{y}) gpw_2 + N_{\beta 3}\left(u_{ij} - u_{ij}^{s^*}\right) gpw_3 \\ & + N_{\beta 4}\left(u_{ij} - u_{ij}^{s^*}\right) + \int_{l^+} N_\beta u_{ij}^{s^*} dl', \end{aligned}$$

where s^* denotes a singularity, and when the singularity is solved analytically, it becomes

$$u_{ij} = \frac{Re}{4\pi}\delta_{ij}\ln r. \tag{4.43}$$

Thus,

$$\begin{aligned}\int_{l^+} N_\beta u_{ij}^{s^*} dl' =& \frac{Re}{4\pi} \int_{l^+} N_\beta \ln r dl' \\ =& \frac{Re}{4\pi} \delta_{ij} \left(\frac{l^+}{2} \left(\ln \left(\frac{l^+}{2} \right) - 1 \right) \right), \end{aligned} \tag{4.44}$$

and when $i = j$ and $\alpha = \beta - 1$, then

$$\begin{aligned} u_{\alpha\beta ij} =& \int_{\partial\Sigma_0} N_\beta u_{ij} dl' \\ =& \int_{l^-} N_\beta \left(u_{ij} - u_{ij}^{s^*} \right) dl' + \int_{l^-} N_\beta u_{ij}^{s^*} dl' + \int_{l^+} N_\beta u_{ij} dl' \\ =& N_{\beta 1} \left(u_{ij} - u_{ij}^{s^*} \right) gpw_1 + N_{\beta 2} \left(u_{ij} - u_{ij}^{s^*} \right) gpw_2 \\ &+ \int_{l^-} N_\beta u_{ij}^{s^*} dl' + N_{\beta 3} u_{ij} gpw_3 + N_{\beta 4} u_{ij} gpw_4 \end{aligned} \tag{4.45}$$

so that we have

$$\begin{aligned}\int_{l^-} N_\beta u_{ij}^{s^*} dl' =& \frac{Re}{4\pi} \delta_{ij} \int_{l^-} N_\beta \ln r dl' \\ =& \frac{Re}{4\pi} \delta_{ij} \left(\frac{l^-}{2} \left(\ln \left(\frac{l^-}{2} \right) - 1 \right) \right). \end{aligned} \tag{4.46}$$

To find the solution to (4.45), we shall find the velocity in the domain, pressure coefficient on the cylinder, as well as the drag coefficient.

In the fluid, $a = 1$, and the velocity becomes

$$\begin{aligned} u_i(\underline{x}) =& \int_{\partial\Sigma_0} N_\beta f_{\beta j} u_{ij} dl' \\ \approx& N_{\beta I} f_{\beta j} u_{ij} (\underline{x} - \underline{x}_{\beta I}) gpw_I. \end{aligned} \tag{4.47}$$

By linear superposition,

$$p(\underline{x}) \approx f_{\beta j} N_{\beta I} p_j (\underline{x} - \underline{x}_{\beta I}) gpw_I \tag{4.48}$$

where p_j is the Stokes pressure given by

$$p_j = \frac{-1}{2\pi} \frac{y_j}{r^2} \tag{4.49}$$

On the cylinder, the pressure at node β is

$$p_\beta = -f_{\beta j} n_j|_\beta \tag{4.50}$$

where $n_j|_\beta = x_{\beta j}$.

The force coefficient:

$$\begin{aligned} C_i =& \int_{\partial\Sigma_0} f_i dl \\ \approx& \int_{\partial\Sigma_0} N_\beta f_{\beta i} dl \\ \approx& f_{\beta i} N_{\beta i} gpw_I \qquad (4.51) \\ =& f_{\beta i}\left(s_\beta\left(\frac{l^+ + l^-}{2}\right)\right) \\ =& f_{\beta i} s_\beta L \qquad (4.52) \end{aligned}$$

where $s_\beta = 1$ is the summation vector and $l = \frac{l^+ + l^-}{2}$ for n nodes. When $l^- = l^+ = l$, then $l = \frac{2\pi}{n}$, and

$$\begin{aligned} C_i =& \frac{2\pi}{n} f_{\beta i} s_\beta \\ =& \frac{2\pi}{n} \sum_{\beta=1}^{n} f_{\beta i}. \qquad (4.53) \end{aligned}$$

Where $i = 1$, equation (4.53) describes the drag coefficient, while for $i = 2$, it describes the lift coefficient.

These numerical results must be tested against known analytical solutions. The analytical solutions are

$$u_i = \frac{8\pi}{Re} u_{i1} + \frac{2\pi}{Re} u_{i1,jj}$$

and

$$p = \frac{8\pi}{Re} p_1 + \frac{2\pi}{Re} p_{1,jj},$$

so the analytical solution is represented by a drag stokeslet of strength $\frac{8\pi}{Re}$ plus a quadrupole giving drag, such that

$$C_D = \frac{8\pi}{Re}\ . \qquad (4.54)$$

Recall that the stokeslet velocity and pressure are given earlier in (3.70) as

$$u_{ij} = \frac{Re}{4\pi}\left(\delta_{ij} \ln r - \frac{y_i y_j}{r^2}\right),$$

$$p_j = -\frac{1}{2\pi}\frac{y_j}{r^2},$$

and as per equation (3.35) we know that Stokes equation is given by

$$0 = -p_{,i} + \frac{1}{Re} u_{i,jj}$$

Therefore, the velocity is shown to be a uniform stream, given by

$$\begin{aligned}
u_i|_{r=1} &= \left[\frac{8\pi}{Re}u_{i1} + 2\pi p_{1,i}\right]_{r=1} \\
&= \left[\frac{8\pi}{Re}\left(\frac{Re}{4\pi}\left(\delta_{ij}\ln r - \frac{y_i y_j}{r^2}\right)\right) + 2\pi\left(-\frac{1}{2\pi}\frac{y_j}{r^2}\right)_{,i}\right]_{r=1} \\
&= \left[2\delta_{i1}\ln r - \frac{2y_i y_1}{r^2} - \frac{r^2\delta_{i1} - y_i 2r y_i/r}{r^4}\right]_{r=1} \\
&= \left[2\delta_{i1}\ln r - \frac{2y_i y_1}{r^2} - \frac{\delta_{i1}}{r^2} + \frac{2y_i y_1}{r^4}\right]_{r=1} \\
&= -\delta_{i1}.
\end{aligned}$$

4.5 Development of BEM Codes

The Numerical method considered here is for size $2n \times 2n$, where $n = 100$, and in this particular problem the CPU timing is about 1.358 seconds for each simulation. The codes are developed in `Fortran 95`. Major steps (see flow chat in figure 4.10) for the numerical implementation of the matched asymptotic expansion using Boundary Element Method described in chapter 3 are summarised as follows:

Step 1: Read input file

The input file is read at beginning of the programme. These are files that contain all the initial data, the dimension of the problem is specified at this stage. All the constant terms to be use, this include values of the Reynolds number (Re) and pi (π) are given at this stage.

Step 2: Generate data

Go to a function file and generate data for either circular cylinder, elliptical cylinder, or the tail-like body shape. Define the no slip boundary condition at this stage.

Step 3: Allocate memory

Allocate memory for all the variables that will be used for the numerical simulation.

Step 4: Build the system of matrix

Generate mesh of model and collocation points. This will result into a system of equations that will be solved using a linear solver.

Step 5: Check for singularity

Go round and select the collocation points and the integration elements using the oseenlets.

- If the collocation point is located in the integral element then it is singular, hence remove the singularities analytically.
- But if the collocation point is not inside the integration element, then it is not singular.

Step 6: Add all submatrix

Put all matrix together, now the matrix is without any singularity because they are removed at step 5, this now form the matrix $\mathbf{A}$.

Step 7: Call matrix solver

Call a Gaussian matrix solver, apply boundary condition and calculate the solution.

Step 8: Calculate drag coefficient

Calculate the drag coefficient for different Reynolds number in the range $0.001 < Re < 4$.

Step 9: Postprocess

Postprocess and visualise different results of interest for flow past a circular cylinder, flow past an elliptical cylinder, and flow past a tail-like body shape.

Step 10: Print results

Print results and End the programme.

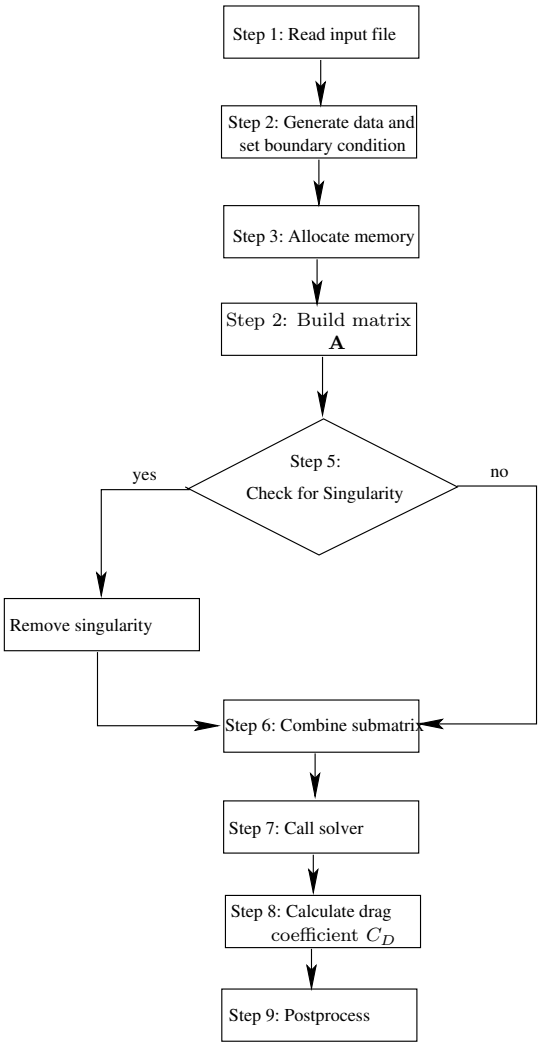

Figure 4.10: Flow chart showing code

4.6 Summary of Chapter

This chapter presents Boundary Element Method formulation of the equations that will be discretised and validated in the subsequent chapter. The chapter introduces Boundary element formulation for Laplace's equation and its Green's integral representation. The same procedure has been used for the BEM formulation of Oseen's equation. The discretisation procedure for BEM is presented in this chapter, where we show analytical removal of the Green's function singularity. This chapter now sets the path for the computer programme that will be use for the simulation.

Chapter 5

Validation of New Results and Matched Asymptotic Integration

5.1 Introduction

We have provided the formulation of BEM for Stokes and Oseen equation. In this chapter, we shall use the method of matched asymptotic expansion to match the near-field Stokes flow and far-field Oseen flow. The matched asymptotic expansion will answer the question that arises from Stokes' paradox for flow in two dimension, hence this formulation will not be a problem as the Oseen flow approximates to the Stokes flow. As a way of validation, this match asymptotic formulation will be tested against existing experiment for flow past a circular cylinder in two dimension in an unbounded domain. It will also be compared with some other analytical work of Lamb, Kaplun, Proudman and Pearson, and the numerical work of Lee and Leal, Yano and Kieda, and Tamotika.

5.2 Validation of the Boundary Element Code Using Stokes equation

The total velocity is the combination of the uniform stream velocity of unit size in the x_1 direction added to the perturbation velocity, resulting in

$$u_i^{\dagger} = \delta_{i1} + u_i. \tag{5.1}$$

In this study, the perturbation velocity is the stokeslet. Later when the Oseen equation will be considered, the perturbation velocity will then take the form of the oseenlet. These changes will enable comparison between near-field and far-field studies. The no-slip boundary condition refers to a situation whereby the fluid assumes a zero velocity at a solid boundary (Day, 1990). With the no-slip boundary condition and uniform stream velocity in the x_1 direction, the total velocity becomes

$$0 = \delta_{i1} + u_i,$$

$$\implies u_i = -\delta_{i1}, \tag{5.2}$$

that is the perturbation velocity now becomes the uniform stream velocity, which in the boundary element code developed, is set to unity.

Flow past a circular cylinder has been a benchmark problem in fluid mechanics for a long time. This will be used to test the BEM developed in `Fortran 95` for the Stokes equation and then modified for for the Oseen equation. For the purpose of visualisation only, the pressure plots, the vector plots, and the streamlines plots for both the analytical and the numerical studies are presented here.

5.2.1 Comparison of Analytical and Numerical Results

Analytical results of the Stokes equation are obtained for the velocity distribution, streamlines distribution, and pressure coefficient as follows. The analytic solution of the velocity $u_i = (u_1, u_2)$ at the point $x_i = (x_1, x_2)$ is given by

$$u_1 = 1 + 2\ln r - \frac{2x_1x_1}{r^2} - \frac{1}{r^2} + \frac{2x_1x_1}{r^2r^2} \tag{5.3}$$

and

$$u_2 = \frac{-2x_2x_1}{r^2} + \frac{x_2x_1}{r^2r^2}, \tag{5.4}$$

where r is the distance from the origin.

It should be noted here in (5.3) and (5.4) that the velocity is unbounded in the far-field which contradicts the far-field boundary condition and is known as the Stokes' paradox. Figure 5.1 shows the velocity distribution of $u_i = (u_1, u_2)$ at the point $x_i = (x_1, x_2)$. Figure 5.1a shows the numerical velocity profile for flow past a circular cylinder in two dimensional space within an unbounded domain. The boundary of the cylinder is divided into n parts. We truncate the x_1 values within the interval -2 to 7 while the x_2 values were truncated to between -2.5 to 2.5. Similarly, figure 5.1b is the analytical velocity profile with the same intervals as in figure 5.1a. The two subplots in figure 5.1, are similar, which shows that the analytical results agree well with the computed numerical results.

5.2.2 Streamline plots

The streamlines plot here is not for comparison of analytical and numerical results, but for illustrative purposes only. Figure 5.2 shows the streamline plots for our circular cylinder. The time step of the simulation is set to 100 far from the body, increasing to 200 near the body in order to model rapid changes in the flow. To obtain a very smooth curve, we divide the cylinder into n discrete regions. At $n = 100$ convergence is achieved. Lower values of n can be seen in the velocity distribution plots in figure 5.1 and the pressure coefficient plot in figure 5.3.

5.2.3 Convergence Studies

The numerical method developed converges and is stable as the number of interpolation points (collocation points) increases. As seen in figure 5.3, when there are only 10 nodal points, the analytical results do not matched exactly with the numerical results. As the nodal points increase, the numerical results closely match the analytical results. It is important to note that at $n = 100$ the convergence is good

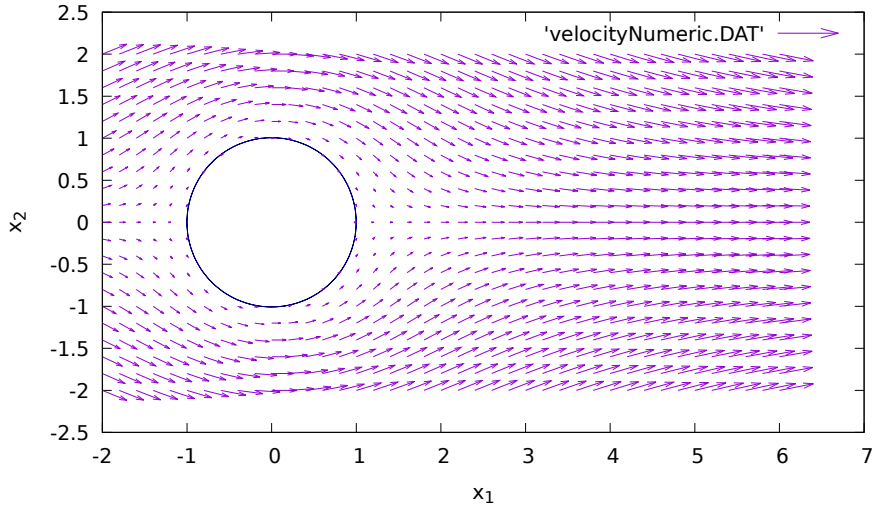

(a) Numerical result of Velocity profile

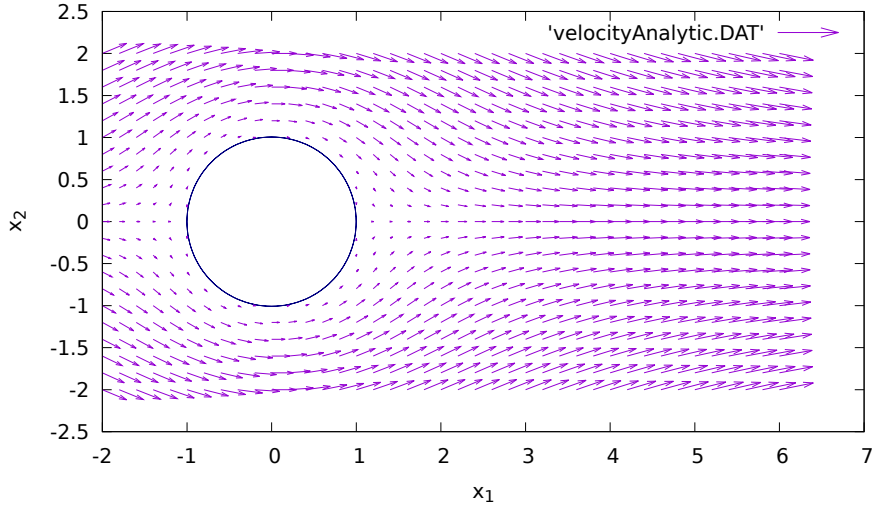

(b) Analytical result of Velocity distribution

Figure 5.1: Velocity distribution of flow past a circular cylinder in two dimensions for low Reynolds number ($Re = 0.1$).

and the model is stable. The numerical and analytical results match.

The Stokes equation is symmetrical. This can be seen with the results of the Boundary Element code developed here for the pressure coefficient, velocities vector and streamlines (see figure 5.3). This results taken together show that the boundary element code is working as expected.

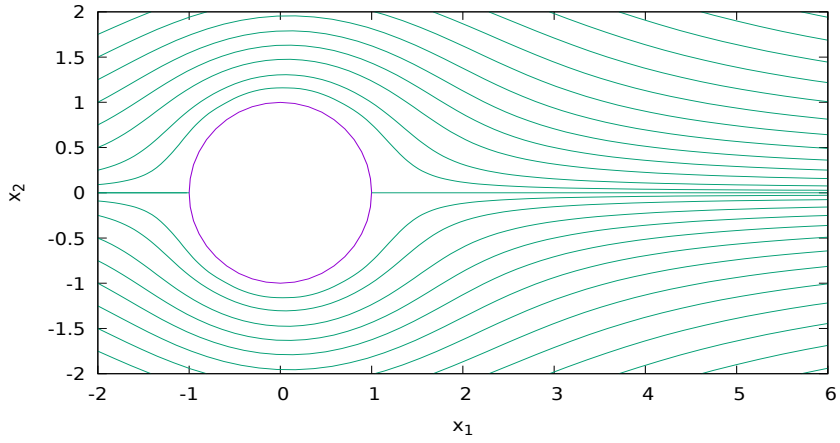

(a) Streamlines showing the analytical distribution

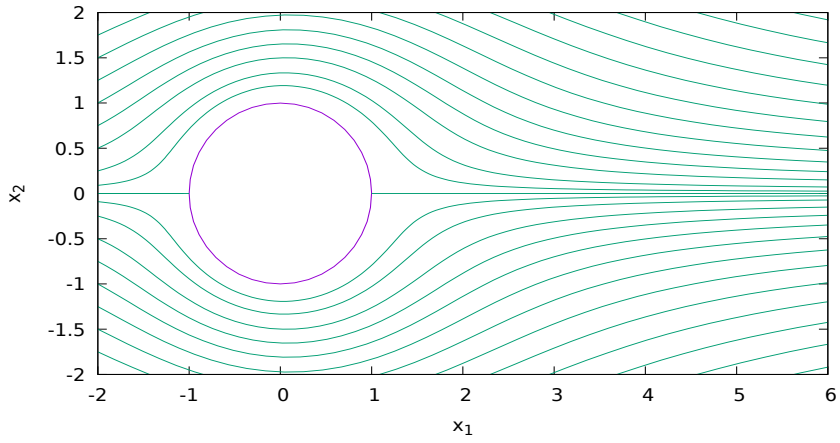

(b) Streamlines showing for the numerical distribution

Figure 5.2: Streamline distribution of flow past circular cylinder in two dimensions for low Reynold's number of $Re = 0.1$

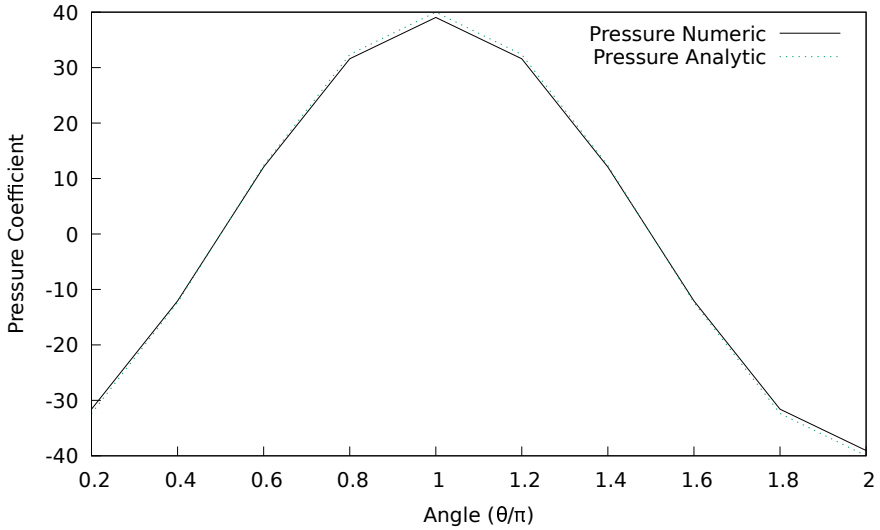

(a) pressure coefficient for few number of points, $n = 10$.

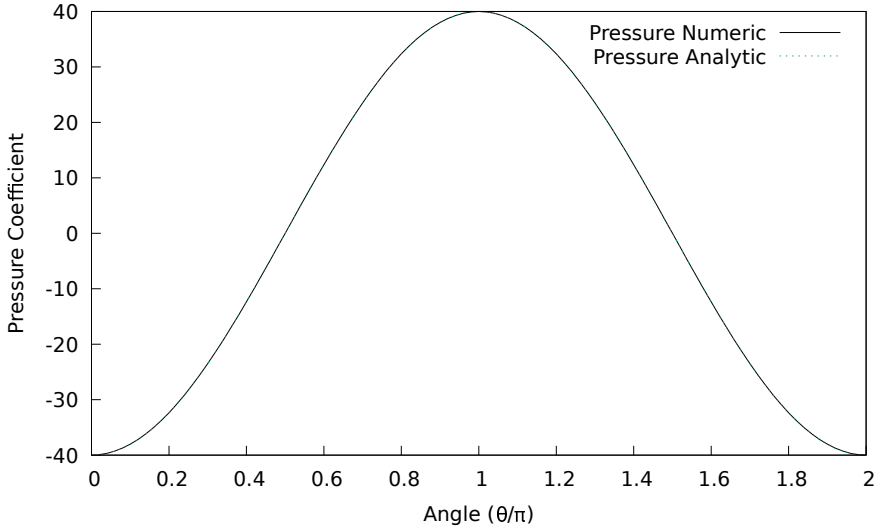

(b) pressure coefficient for a higher number of points, $n = 100$.

Figure 5.3: Pressure coefficient for analytic and numeric results for low Reynolds number $Re = 0.1$

5.2.4 Error Calculation

Calculation of the error size will enable comparison of the accuracy of the boundary element code developed here. This will further confirm the difference between the analytical and the numerical results obtained in this study. Often, it is useful to consider the size of an error relative to the true quantity. This quantity is sometimes multiplied by 100 and expressed as a percentage. The analytical solution is υ_{ext} and the numerical solution computed using BEM is denoted as υ_{apx}, (where υ_{ext} is the

exact velocity while υ_{apx} is the approximate velocity). The relative error (ε) can be calculated using the idea of infinity norm ($\| \ \|_\infty$), defined as

$$\varepsilon = \frac{\|\upsilon_{apx} - \upsilon_{ext}\|}{\|\upsilon_{ext}\|} \times 100. \tag{5.5}$$

To demonstrate the error calculation using 5.5 above, error for the pressure coefficient is shown in figure 5.4. It can be seen that as the number of node increases from $n = 10$ to $n = 100$, the error decreases significantly as the value of the error when $n = 100$ is less than when $n = 10$.

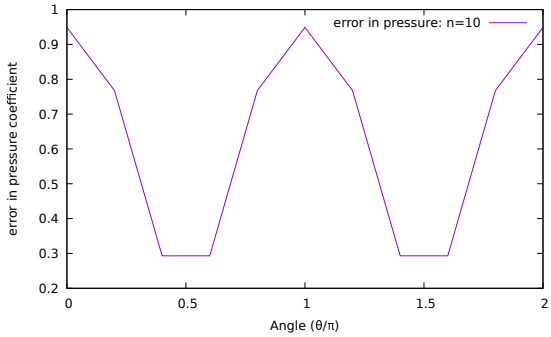

(a) pressure error coefficient for $n = 10$

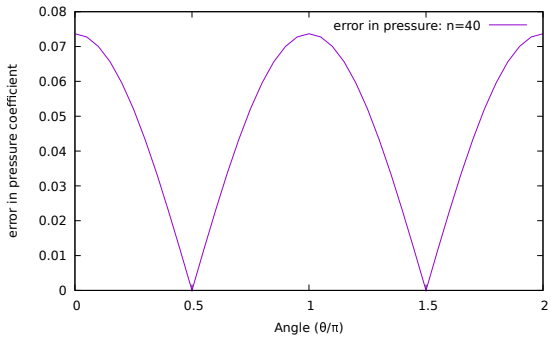

(b) pressure error coefficient for $n = 40$

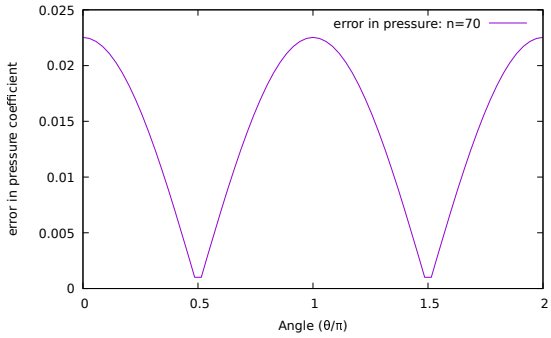

(c) pressure error coefficient for $n = 70$

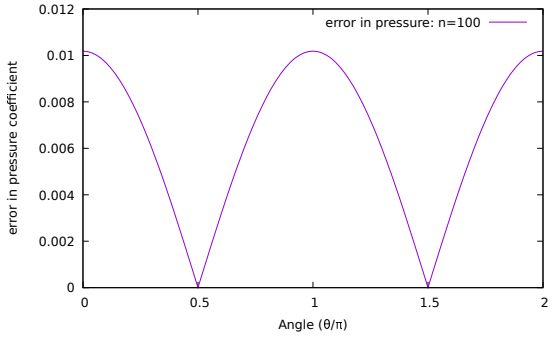

(d) pressure error coefficient for $n = 100$

Figure 5.4: Pressure error coefficient for analytic and numeric results for low Reynolds number $Re = 0.1$

5.3 Method of Matched Asymptotic Expansion

The work of Chadwick (Chadwick, 2013) matches the near-field region using Stokes flow with the far-field using Oseen flow. The common boundary, where the matching takes effect, has L as the length dimension of the matched region and it is seen that $Re\frac{L}{l}$ is the error, where l is the body length. The error is therefore reduced by choosing $L = l$, and Oseen flow assumed everywhere in the flow field (see section 5.3.1 below).

5.3.1 Green's Integral Formulation for Outer Region

Consider the space Σ enclosed by the boundary and approaching the point x_i. The body boundary is denoted by l_B, and the boundary on the far-field tends to an infinite distance away l_∞, (see figure 5.5). The Green's integral formulation for the Oseen flow (Oseen, 1927) can be found by considering the integral stated in (3.100), restated here:

$$\begin{aligned}\int_\Sigma \left(-\rho U\frac{\partial u_i^{(m)}(z)}{\partial y_1} - \frac{\partial p^{(m)}(z)}{\partial y_i} - \mu\frac{\partial^2 u_i^{(m)}(z)}{\partial y_j \partial y_j} + f_i^{(m)}(z)\right) u_i(y)d\Sigma \\ + \int_\Sigma \left(-\rho U\frac{\partial u_i(y)}{\partial y_1} - \frac{\partial p(y)}{\partial y_i} + \mu\frac{\partial^2 u_i(y)}{\partial y_j \partial y_j} - f_i(y)\right) u_i^{(m)}(z)d\Sigma = 0,\end{aligned} \tag{5.6}$$

where y_i is a vector position of the exterior domain integrated space Σ (and in this case an area integral), and $z_i = x_i - y_i$ such that the differential equation for the Green's functions satisfies the conjugate Oseen equation, since $\frac{\partial}{\partial y_j} = -\frac{\partial}{\partial x_j}$ and $f_i^{(m)}(z) = \delta(z)\delta_{im}$, where $\delta(z)$ is the Dirac delta function.

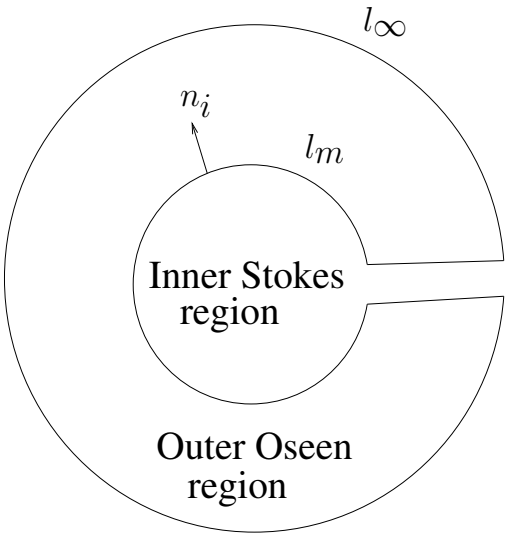

(a) Green's integral representation for outer Oseen flow

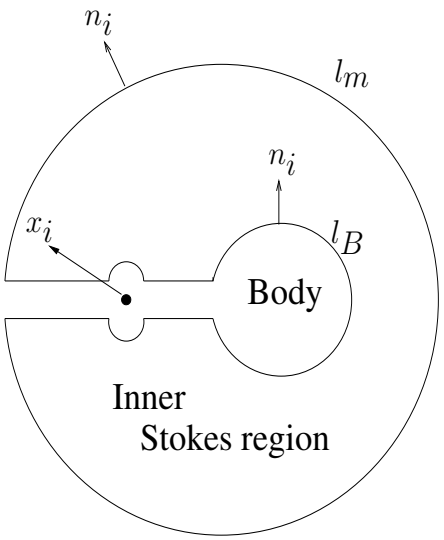

(b) Green's integral representation of inner St

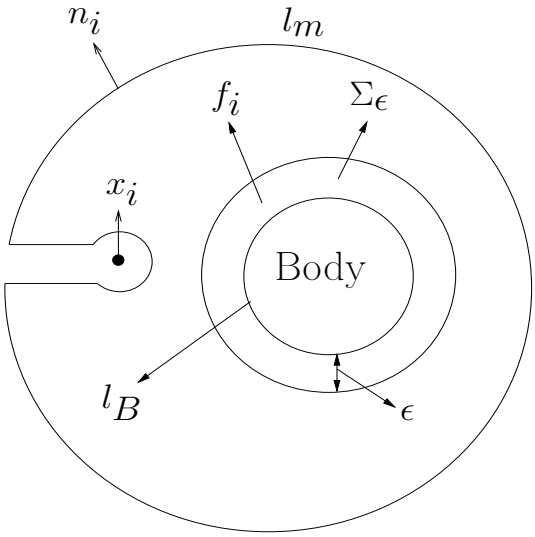

(c) Spatial distribution of point sources

Figure 5.5: Green's integral representation of a body in a near-field and far-field region.

In the outer region there is no body force, so $f_i = 0$. The point x_i is in the inner region, so there is no contribution $f_i^{(m)}(z)$ around the point x_i. Rearranging

(5.6) then gives

$$\int_{\Sigma} -\rho U \frac{\partial}{\partial y_1}\left(u_i^{(m)}(z)u_i(y)\right)d\Sigma - \int_{\Sigma}\frac{\partial}{\partial y_i}\left(p^{(m)}(z)u_i(y)+p(y)u^{(m)}(z)\right)d\Sigma$$
$$+\int_{\Sigma} -\left(\mu\frac{\partial}{\partial y_j}\left(\frac{\partial u_i^{(m)}(z)}{\partial y_j}u_i(y)\right)+\mu\frac{\partial}{\partial y_j}\left(\frac{\partial u_i(y)}{\partial y_j}u_i^{(m)}(z)\right)\right)d\Sigma \quad (5.7)$$
$$=\int_{\Sigma}\left(-f_i^{(m)}(z)u_i(y)+f_i^{(m)}(z)u_i(y)\right)d\Sigma.$$

From the continuity equation (3.84), it can be seen that $\mu\frac{\partial u_i^{(m)}}{\partial y_j}\frac{\partial u_i}{\partial y_j}$ cancel out in (5.7) on applying the divergence theorem. This then gives the Oseen integral representation as

$$u_m(x) = \int_{l_m}\left(\rho U u_i^{(m)}(z)u_i(y)n_1+\left(p^{(m)}(z)u_i(y)+p(y)u_i^{(m)}(z)\right)n_i\right)dl$$
$$+\int_{l_m}\mu\left(\frac{\partial u_i^{(m)}(z)}{\partial y_j}u_i(y)-\frac{\partial u_i(y)}{\partial y_j}u_i^{(m)}(z)\right)n_j dl, \quad (5.8)$$

where l_m is the matching boundary. From Fishwick and Chadwick (Fishwick & Chadwick, 2006), the far field integral bounding the exterior domain Σ in the Oseen representation is zero where the boundary of the domain in two-dimensions is a closed curve.

5.3.2 Green's Integral Formulation for the Inner Region

The same approach used in the preceding section can be applied to find the Green's integral representation for the inner Stokes flow over a different domain integral (see figure 5.5b). Again there is no body force, so $f_i = 0$, but there is a contribution around the point x_i. Evaluating the Green's function force term in (5.6), which is same as (3.104), gives

$$-\int_{\Sigma} f_i^{(m)}(z)u_i(y)d\Sigma = -\int_{\Sigma}\delta(z)\delta_{im}u_i(y)d\Sigma = -u_m(x). \quad (5.9)$$

Rearranging and simplifying (5.6) then gives

$$-u_m(x) = \int_{\Sigma} -\rho U\frac{\partial}{\partial y_1}\left(u_i^{(m)}(z)u_i(y)\frac{\partial}{\partial y_i}\left(p^{(m)}(z)u_i(y)+p(y)u^{(m)}(z)\right)\right)d\Sigma$$
$$+\int_{\Sigma} -\mu\frac{\partial}{\partial y_j}\left(\left(\frac{\partial u_i^{(m)}(z)}{\partial y_j}u_i(y)\right)+\left(\frac{\partial u_i(y)}{\partial y_j}u_i^{(m)}(z)\right)\right)d\Sigma. \quad (5.10)$$

Finally, applying the divergence theorem to the space in figure 5.5b gives the boundary integral representation

$$\begin{aligned} u_m^s(x) = &- \int_{l_B} \left(p^{(m)s}(z) u_i^s(y) + p^s(y) u_i^{(m)s}(z) \right) n_i dl \\ &- \int_{l_B} \mu \left(\frac{\partial u_i^{(m)s}(z)}{\partial y_j} u_i^s(y) - \frac{\partial u_i^s(y)}{\partial y_j} u_i^{(m)s}(z) \right) n_j dl \\ &+ \int_{l_m} \left(p^{(m)s}(z) u_i^s(y) + p^s(y) u_i^{(m)s}(z) \right) n_i dl \\ &+ \int_{l_m} \mu \left(\frac{\partial u_i^{(m)s}(z)}{\partial y_j} u_i^s(y) - \frac{\partial u_i^s(y)}{\partial y_j} u_i^{(m)s}(z) \right) n_j dl. \end{aligned} \tag{5.11}$$

5.3.3 Matching the Inner and Outer regions

Here, the inner and outer region are matched using equations (5.11) and (5.8). An error introduced as a result of the matching is identified. In two-dimensions, the constant term $C_i^{(m)}$ gives the leading order approximation to the velocity oseenlet

$$\left[1 + \mathcal{O}\left(\frac{1}{\ln kr} \right) \right] = \left[1 + \mathcal{O}\left(\frac{1}{\ln Re\frac{L}{l}} \right) \right]$$

on the matching boundary where $\frac{r}{L} = \mathcal{O}(1)$. Hence, the matching integral in (5.11) is

$$\begin{aligned} &\int_{l_m} \left(p^{(m)s}(z) u_i^s(y) + p^s(y) u_i^{(m)s}(z) \right) n_i dl + \int_{l_m} \mu \left(\frac{\partial u_i^{(m)s}(z)}{\partial y_j} u_i^s(y) - \frac{\partial u_i^s(y)}{\partial y_j} u_i^{(m)s}(z) \right) n_j dl \\ &\quad \times \left[1 + \mathcal{O}\left(\frac{1}{\ln Re\frac{L}{l}} \right) \right] = - \int_{l_m} \left(\rho U u_i^{(m)}(z) u_i(y) n_1 + \left(p^{(m)}(z) u_i(y) + p(y) u_i^{(m)}(z) \right) n_i \right) dl \\ &\quad + \int_{l_m} \mu \left(\frac{\partial u_i^{(m)}(z)}{\partial y_j} u_i(y) - \frac{\partial u_i(y)}{\partial y_j} u_i^{(m)}(z) \right) n_j dl = 0. \end{aligned} \tag{5.12}$$

In order, to make the error as small as possible, the matching boundary can be taken to be of order $L = l$, where l is the body dimension. The error in the approximations then becomes $\mathcal{O}\left(\frac{1}{\ln Re}\right)$ for two dimensional flow. From the mathematical approximation above matching the outer and inner regions in Oseen flow approximates to Stokes flow. This explains why Oseen flow can be used throughout the domain for a low Reynolds number flow since near the body Oseen flow breaks down. Hence, the Oseen equation approximates to the Stokes equation at the body boundary and can be use to model low Reynolds number flow.

5.4 Green's Integral for the Boundary Element Method

Now consider the space Σ enclosed by the boundary around the body boundary, l_B, and the boundary on the far-field an infinite distance away l_∞. The body is represented by a distribution of forces f_i in the region Σ_ϵ which is a distance ϵ away from the body boundary l_B (see figure 5.5). Equation (5.8) then becomes (up to the error in the matching (5.12))

$$\begin{aligned}\int_\Sigma \Big(- f_i^{(m)}(z)u_i(y) + f_i(y)u_i^{(m)}(z)\Big)d\Sigma &= \int_\Sigma -\rho U \frac{\partial}{\partial y_1}\left(u_i^{(m)}(z)u_i(y)\right)d\Sigma \\ &- \int_\Sigma \frac{\partial}{\partial y_i}\left(p^{(m)}(z)u_i(y) + p(y)u^{(m)}(z)\right)d\Sigma \\ &- \int_\Sigma \left(\mu\frac{\partial}{\partial y_j}\left(\frac{\partial u^{(m)}(z)}{\partial y_j}u_i(y)\right) + \mu\frac{\partial}{\partial y_j}\left(\frac{\partial u_i(y)}{\partial y_j}u_i^{(m)}(z)\right)\right)d\Sigma \\ &= \int_{l_\infty}\left(\rho U u_i^{(m)}(z)u_i(y)n_1 + \left(p^{(m)}(z)u_i(y) + p(y)u_i^{(m)}(z)\right)n_i\right)dl \\ &- \int_{l_\infty}\mu\left(\frac{\partial u_i^{(m)}(z)}{\partial y_j}u_i(y) - \frac{\partial u_i(y)}{\partial y_j}u_i^{(m)}(z)\right)n_j dl = 0.\end{aligned} \tag{5.13}$$

We let

$$\int_{\Sigma_\epsilon} f_i(y)u_i^{(m)}(z)d\Sigma = \int_{l_B} F_i(y)u_i^{(m)}(z)dl \tag{5.14}$$

on the body boundary so that as $\epsilon \to 0$, it gives the force on the body as

$$F_i(y) = \lim_{\epsilon\to 0}\int_0^\epsilon f_i(y)d\epsilon \quad . \tag{5.15}$$

Therefore,

$$\begin{aligned}u_m &= \int_\Sigma \left(-f_i^{(m)}(z)u_i(y) + f_i(y)u_i^{(m)}(z)\right)d\Sigma \\ &= \int_{\Sigma_\epsilon} f_i(y)u_i^{(m)}(z)d\Sigma,\end{aligned} \tag{5.16}$$

and hence,

$$u_m(x) = \int_{l_B} F_i(y)u_m^{(i)}dl \ , \tag{5.17}$$

because by symmetry, $u_i^{(m)} = u_m^{(i)}$ from (see equation (3.56).

To proceed with the numerical method, (5.17) must be discretised in BEM.

5.5 Boundary Element Method for Low Reynolds Number Flow

In the preceding section, the oseenlet is derived and given in (5.17) for a two-dimensional flow satisfying the Oseen equation for the far-field region. It was also shown above that in the matched region the oseenlet becomes the stokeslet near the body boundary. Here we shall compute the drag experienced by a circular cylinder in a steady flow in an unbounded domain. To do this, we shall make reference to the Boundary Element Method developed in chapter three for the discretisation of the system of equations (4.20), and so (5.17) will be discretised using the Boundary Element Method with a point collocation weighting function as seen in figure 5.6a, where $x_{\alpha i}$ is the position x_i of node α. The two nodal points are given by $x_{\alpha i}$ and $x_{\alpha i+1}$, while the midpoint between them is the collocation point. We have chosen the collocation point to not lie on the nodes so that the Green's function singularity in the integral is more easily removed, since the singularity then lies wholly within the element integration rather than divided across two elements. For ease of numerical formulation, the boundary is approximated by a linear variation rather than a curved variation, but as the number of nodes are increased the collocation points will move closer to the boundary and so this is not expected to be a problem.

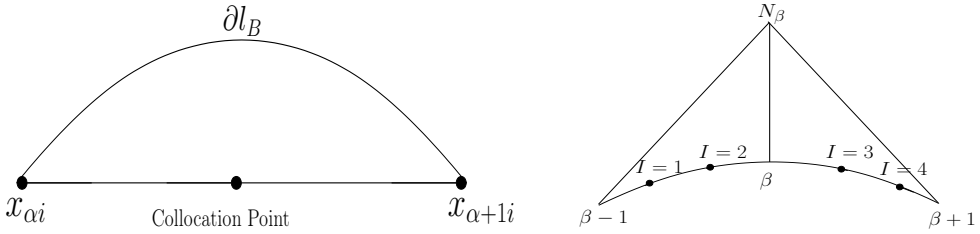

(a) Collocation points (b) Diagram showing Gaussian points

Figure 5.6: The nodal points and Gaussian points used for collocation

In figure 5.6b, a two-point Gaussian quadrature is shown with Gaussian points $I = 1, 2$ for the integral from node $\beta - 1$ to β, and $I = 3, 4$ for the integral from node β to $\beta + 1$. N_β is the linear shape function at node β and gpw_I is the Gaussian point weight at point I. Hence, from the Boundary Element formulation we made

in Chapter three for equation (4.37), and (5.17) now becomes

$$\begin{aligned} u_i(x) &= \int_{l_B} N_\beta f_{\beta j} u_i^{(j)} dl \\ &= f_{\beta j} N_{\beta j} u_{ijI} gpw_I \ , \end{aligned} \tag{5.18}$$

where there are implied summations over $1 \leq \beta \leq n$ (for n nodes), over $1 \leq I \leq 4$ for Gaussian points associated with node β (see figure 5.6), and over $1 \leq j \leq 2$ spatial dimensions. u_{ijI} is the value of the oseenlet Green's function $u_i^{(j)}$ positioned at the Gaussian point I of node β, and determined at the node α. Hence, this collocation point method transforms the integral equation into a linear system of algebraic equations with a no slip boundary condition in vector form, yielding

$$\mathbf{Af} = \mathbf{Y}, \tag{5.19}$$

where $\mathbf{A}$ is a $2n \times 2n$ matrix, $\mathbf{f}$ is the force coefficient and $\mathbf{Y}$ is an n dimensional vector given by applying the boundary condition as detailed in chapter three.

5.5.1 Comparison With Existing Methods

We compare the present method against existing methods for the drag coefficient. The drag coefficient C_D from the Boundary Element Method presented in this study is compared against the analytical results of Lamb (Lamb, 1932) (5.20), Tomotika (Tomotika & Aoi, 1951) (5.21), Kaplun (Kaplun & Lagerstrom, 1957) (5.22), the experimental results of Tritton (Tritton, 1959), and the numerical results of Yano and Kieda (Yano & Kieda, 1980), all for a Reynolds number Re ranging between 0 and 4 (see figure 5.7). The approximation of the drag coefficients for the various listed results are

$$\text{Lamb:} \quad C_D = \frac{4\pi}{ReT_1} \tag{5.20}$$

$$\text{Tomotika:} \quad C_D = \frac{4\pi}{ReT_1}\left(1 - T_2\right) \tag{5.21}$$

$$\text{Kaplun:} \quad C_D = \frac{4\pi}{ReT_1}\left(1 - 0.87T_1^{-2}\right) \tag{5.22}$$

where the Reynolds number Re is defined by $Re = \frac{aU}{\nu}$ with a as the cylinder radius, and $\nu = \frac{\mu}{\rho}$ as the kinematic viscosity with μ as the dynamic viscosity of the ambient

fluid. The parameter $T_1 = \left(\frac{1}{2} - \gamma - \log\frac{Re}{4}\right)^{-1}$, where $\gamma = 0.577216...$ is the Euler constant.

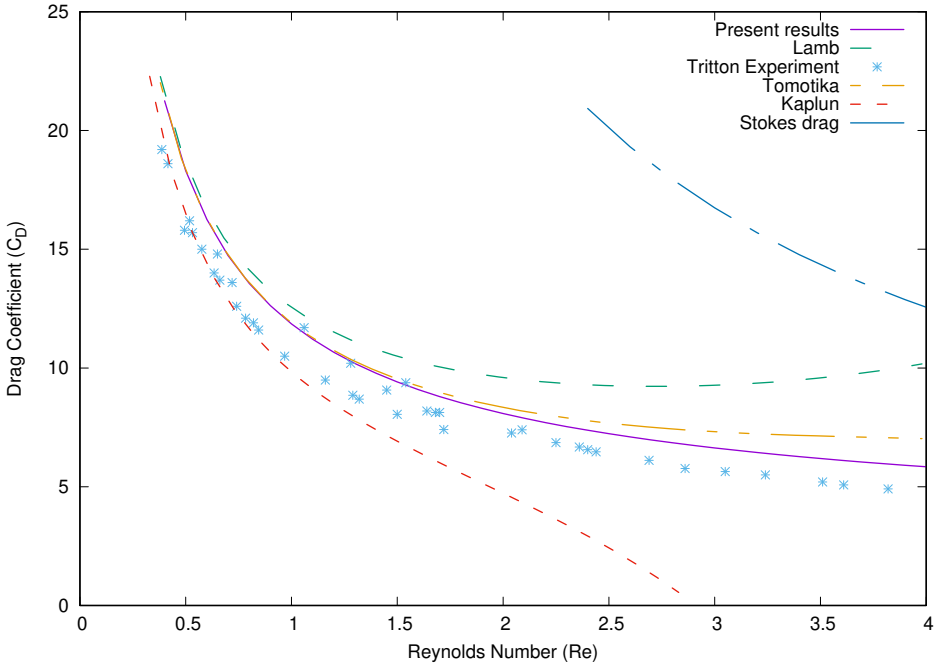

Figure 5.7: Drag coefficient C_D are plotted against the Reynolds number ($0 < Re < 4$)

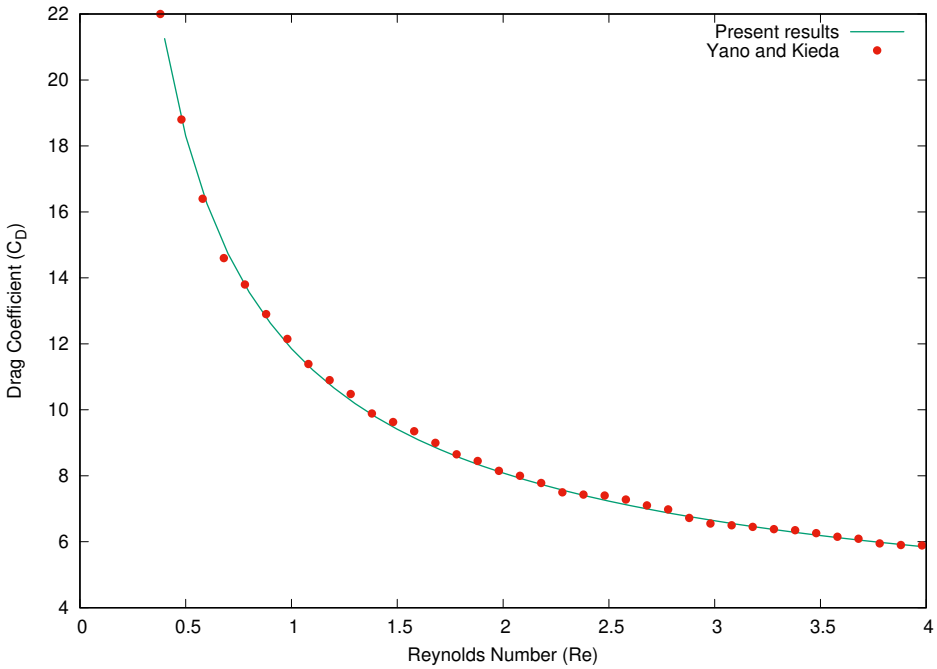

Figure 5.8: Comparing BEM result with Yano and Kieda

Figure 5.8 shows that our results are aligned almost exactly with the discrete

singularity numerical results of Yano and Kieda (Yano & Kieda, 1980).

In figure 5.7, the drag coefficient is plotted against the Reynolds number. Lamb's (Lamb, 1932) and Kaplun's (Kaplun & Lagerstrom, 1957) vary increasingly as the Reynolds number is increased beyond 1 ($Re > 1$) by showing more significant difference and the present results together with Yano and Kieda (Yano & Kieda, 1980) give the closest match to Tritton's experiment (Tritton, 1959). Tomotika also vary from Tritton's experiment as the Reynolds number increases, but the deviation is not as faster as those of Lamb's and Kaplun's. The Stokes drag shows clearly that the velocity diverges when considering a 2D flow past a circular cylinder in an unbounded domain as expected from Stokes paradox. Analytic result of Kaplun and Lagerstrom actually diverge to a negative value as the Reynolds number increase above 2.9 ($Re > 2.9$). On the other hand, when considering the Reynolds number below 1 ($Re < 1$), it can be seen that the difference in the results are not significant (see figure 5.7), they all aligned with experiment at very low Reynolds number. This means that if we were to consider very low Reynolds number of value like $Re < 0.01$, there will not be any significant difference.

Furthermore, the present result is compared with the discrete singularity result of Yano and Kieda (Yano & Kieda, 1980) at similar range of Reynolds number (see figure 5.8). In their formulation, Yano and Kieda choose a specific points within a body surface and distributed oseenlets, sink, and sources within a body. It is unclear on how to extend the work of Yano and Kieda (Yano & Kieda, 1980) to a general closed body as their method specifically tailored to the circular cylinder, whereas the method presented here is straightforward to apply for any closed body.

5.6 Proundman and Pearson Derived from Lamb's Result

In the paper presented by Lee and Leal, the drag coefficient used is that of Proudman and Pearson. We show below that this drag coefficient is the same as the drag coefficient presented by Lamb when evaluated at very low Reynolds number.

Therefore, what Lee and Leal and Proudman and Pearson did was simply using the approximation giving by Lamb. We have shown by leading order terms that such drag is simply Lamb drag.

The drag coefficient given in Lamb is

$$
\begin{aligned}
C_D &= \frac{-8\pi}{Re}\left(\frac{1}{2}-\gamma-\ln Re+\ln 8\right) \qquad (5.23)\\
&= \frac{-8\pi}{Re\times\ln Re}\frac{1}{\left(1-\frac{\frac{1}{2}-\gamma+\ln 8}{\ln Re}\right)}\\
&= \frac{-8\pi}{Re\times\ln Re}\left(1+\frac{\frac{1}{2}-\gamma+\ln 8}{\ln Re}\right)\\
&= \frac{-8\pi}{Re(\ln Re)^2}\left(\ln Re+\frac{1}{2}-\gamma+\ln 8\right)\\
&= \frac{-8\pi}{Re\ln Re}\left(1+\frac{1}{\ln Re}\left(\frac{1}{2}-\gamma+\ln 8\right)\right)\\
&= \frac{-4\pi}{Re(\ln Re+\ln 2)}\left(1+\frac{1}{\ln Re+\ln 2}\left(\frac{1}{2}-\gamma+\ln 8\right)\right)\\
&= \frac{-4\pi}{Re\ln Re}\left(1-\frac{\ln 2}{\ln Re}\right)\left(1+\frac{1}{\ln Re}\left(\frac{1}{2}-\gamma+\ln 8\right)\right)\\
&= \frac{-4\pi}{Re\ln Re}\left(1+\frac{1}{\ln Re}\left(\frac{1}{2}-\gamma+\ln 4\right)\right). \qquad (5.24)
\end{aligned}
$$

Hence, it can be seen from above that the Lamb's drag coefficient is simplified by leading order terms to arrived at Lee and Leal's drag coefficient given as

$$C_D = \frac{-4\pi}{Re\ln Re}\left(1+\frac{1}{\ln Re}\left(\frac{1}{2}-\gamma+\ln 4\right)\right) \qquad (5.25)$$

Drag coefficient of Lee and Leal was denoted by F_x in their paper, if F_x is divided by the Reynolds number, we will then obtain our present drag coefficient, that is

$$C_D = \frac{F_x}{Re} \qquad (5.26)$$

Figure 5.9 agrees with the above proof for Reynolds number between 0.01 and 0.1, but immediately above that range we see that Lee and Leal's result diverges. This is true because their approach is based on Lamb's approximation.

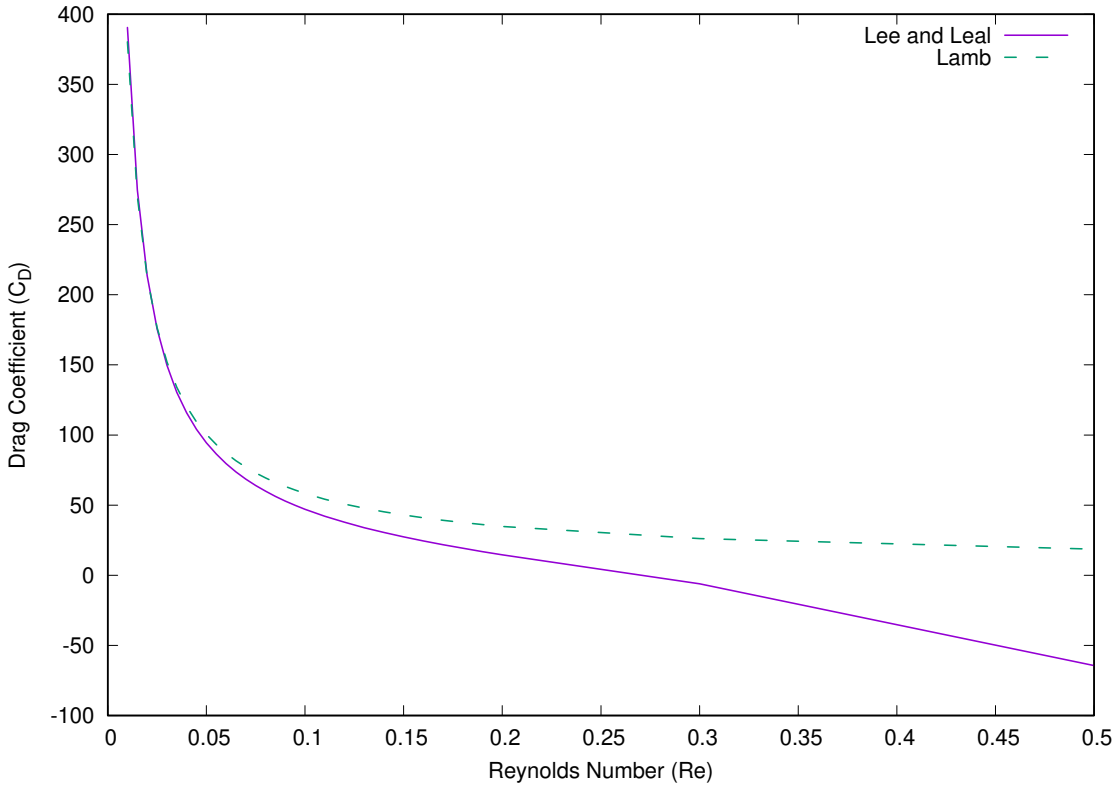

Figure 5.9: Comparison between Lee and Leal, and Lamb for very low Reynolds number

5.7 Summary of the Chapter

In this chapter, the matched asymptotic expansion has been discussed and it was followed by validation of BEM developed in this studies. The result was compared to experiment and some other analytical and numerical results for the drag coefficient at varying Reynolds number. The comparison shows that our result gives better approximation than all the other ones, the only result that near the present result is the one by Yano and Kieda. Despite Yano and Kieda being near to the present result in comparison, the present result accounts for any body shape while the former is only for a particular circular cylinder.

Chapter 6

Two Dimensional Flow Past a Stationary and Moving Body

6.1 Introduction

In this chapter, different flows past a body will be discussed and results will be presented for BEM that was developed in chapter 4 of this thesis. Different flows to be consider here include flow past a circular cylinder, flow past an elliptical cylinder, and flow past a body in motion. The goal is to end up with a model that can be used for micro-robotic and microscopic scale swimming in viscous fluid, especially for flagellated-propelled organisms.

6.2 Flow Past a Circular Cylinder

For illustration purposes, streamlines for flow past a circular cylinder of radius one in Oseen flow are shown in figures 6.1, 6.2, and 6.3 for the Reynolds number $Re = 0.01$, $Re = 1$, and $Re = 4$ respectively. When the Reynolds number is increased from 0.01 to 4, it can be seen that eddies begin to form in the wake of the circular cylinder for $Re = 4$ (see figure 6.3). On the other hand, when $Re = 0.01$, the streamlines move faster over the circular cylinder (see figure 6.1). This implies that the velocity for

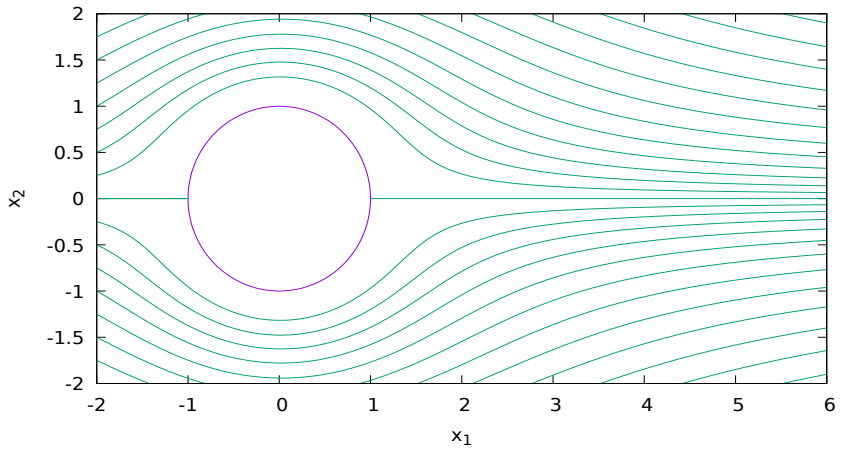

Figure 6.1: Streamlines of steady flow past a circular cylinder at $Re = 0.01$ in an unbounded domain

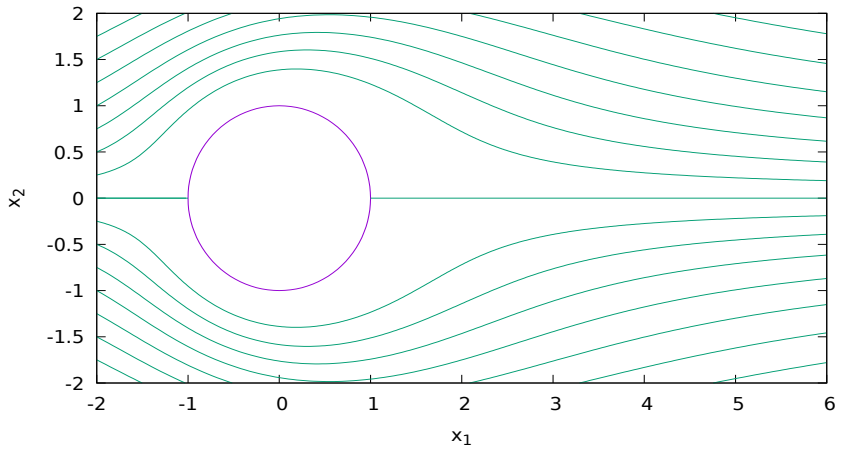

Figure 6.2: Streamlines of steady flow past a circular cylinder at $Re = 1$ in an unbounded domain

flow with $Re = 0.01$ needs to be faster than for $Re = 1$. When figures 6.1 and 6.2 are compared to the previous streamlines plotted in the last Chapter (see figure 5.2), similarities can be seen for flow at different low Reynolds number, even though the figures presented in this chapter are for Oseen flow while those in previous chapters are for Stokes flow yet they both give good representation of the flow.

As expected, it can be seen that the results predicted by the present BEM are very similar to the results of Lamb (Lamb, 1932) at very low Reynolds number between $0.01 < Re < 0.3$ (see figure 6.4). This means that provided the Reynolds number is very low, the analytical result of Lamb for the drag coefficient is the

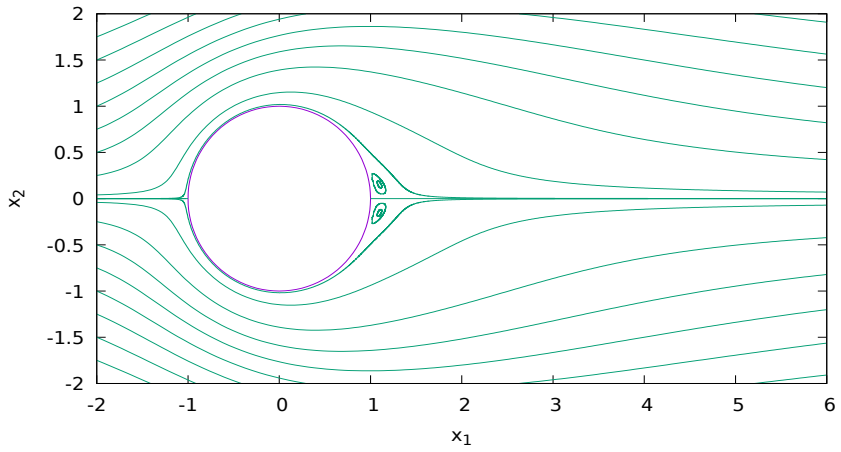

Figure 6.3: Streamlines of steady flow past a circular cylinder at $Re = 4$ in an unbounded domain which forms eddies

same with our present result and also the same with Proudman and Pearson as seen with analysis given in equation (5.23) shown in figure (6.4). These results are consistent with those of Lee and Leal (Lee & Leal, 1986) and Proudman and Pearson (Proudman & Pearson, 1957). On the one hand, when the Reynolds number is very low (about $Re = 0.01$) the results of Lamb, Lee and Leal, and present result appear the same for the drag coefficient (figure 6.5). On the other hand, as the Reynolds number increases ($Re > 0.1$), Lee and Leal drag coefficient begins to diverge away from the result of Lamb and the present result of BEM to negative values. This shows that when the Reynolds number is very low, all the three results are the same for both the analytic and numerical results, the difference began to show when Reynolds number increases. So the results of Lee and Leal (Lee & Leal, 1986) which were obtained through matched asymptotic expansion in terms of $\frac{1}{\log Re}$, are only valid for very small Reynolds number; even when $Re = 0.05$ the expansion is not very good because $\frac{1}{\log Re}$ is about 1/3 (see figure 6.5). This reveals our result gives better numerical approximation for a flow past a circular cylinder in 2D. As it was shown in the previous chapter when considering drag force, it can be seen that the present BEM provides good quality results in comparison to other existing methods.

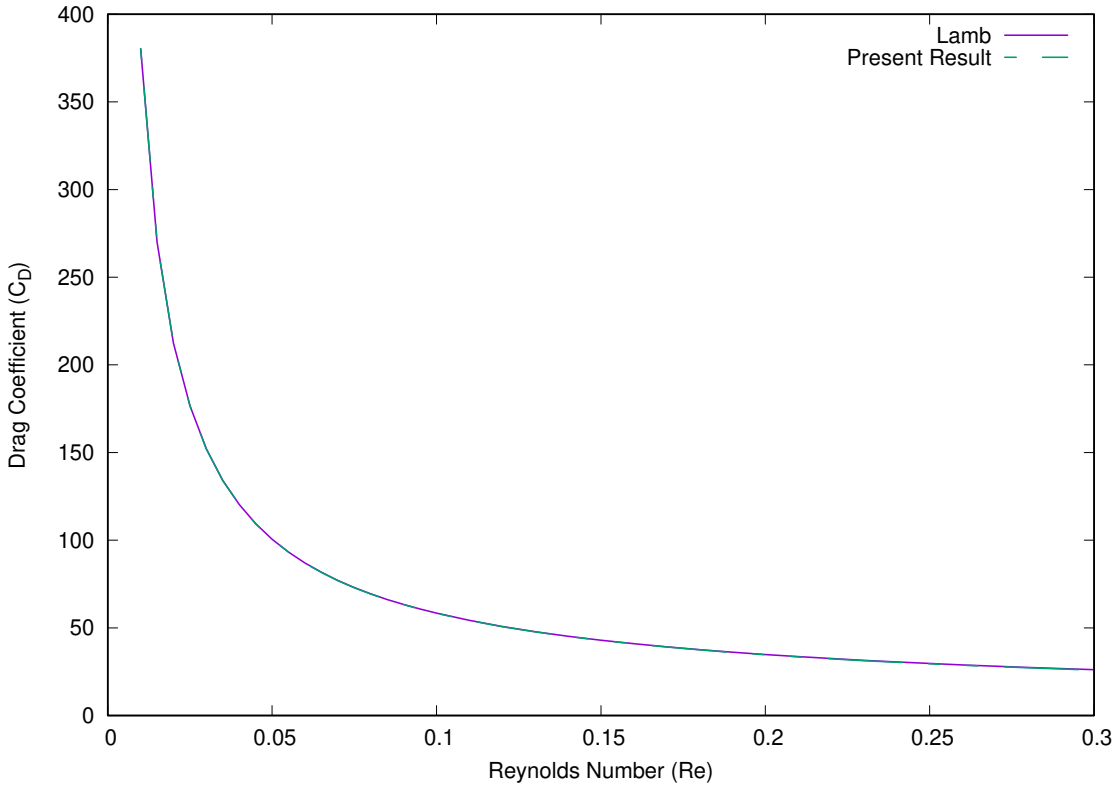

Figure 6.4: Comparison of drag coefficient with Reynolds number for $0 \leq Re \leq 0.3$ for Lamb's result and those predicted by BEM.

When $Re = 0.1$ and $Re = 1$, the result is not going to give an accurate representation (see figure 6.5). But if we are able to plot result for Reynolds number near zero (say $Re < 0.025$), then we will expect that Lee and Leal's result which is Proudman and Pearson will be identical to Lamb's result, since Lee and Leal was obtained from Lamb (see equation (5.23)). Hence, as soon as Re increases to a value of even around 0.1 (see figure 6.5) then the expansion is not valid and Lee and Leal's method is significantly different from Lamb's which is significantly different from the present results. In comparison to experiment (Tritton, 1959), the present results are most consistent (see figure 5.7 from previous chapter).

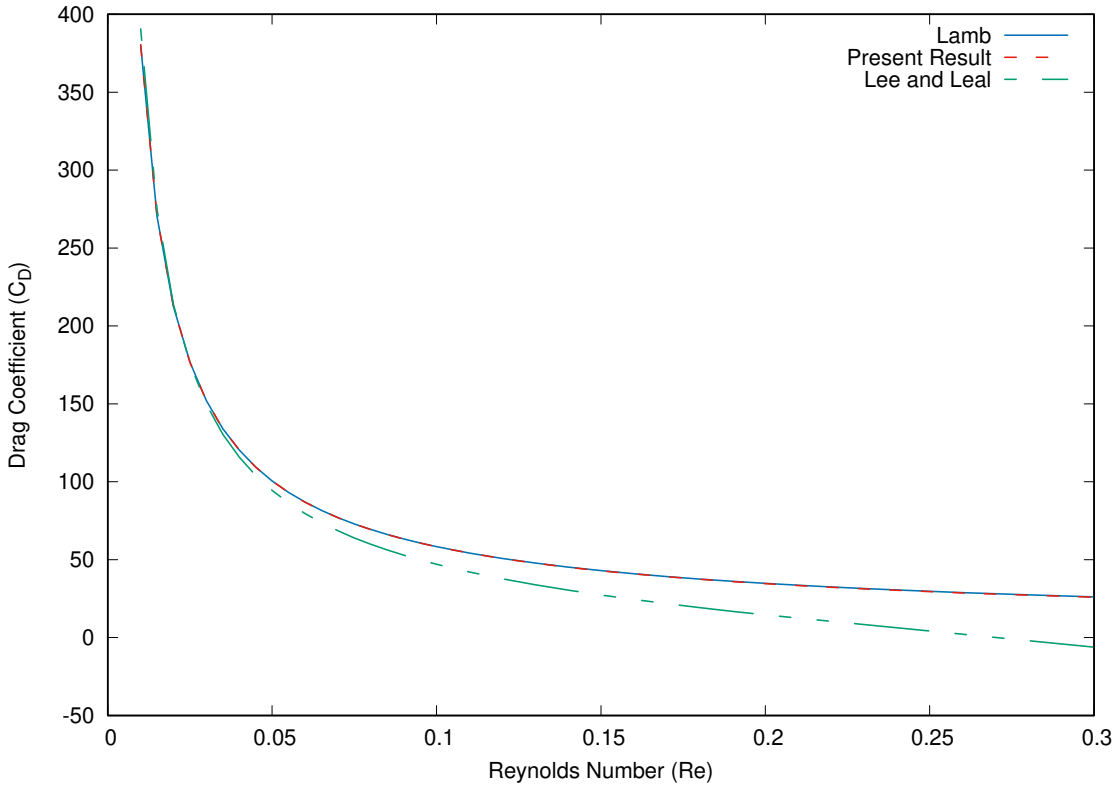

Figure 6.5: Comparisons of drag coefficient for very low Re in range $0.01 \leq Re \leq 0.3$ for Lamb, Lee and Leal/Proudman and Pearson, and our BEM

6.3 Flow Past an Elliptical Body

In this section, flow past an elliptical body is considered. Just like in the previous section (6.2) where for illustration purposes, the streamlines for the flow past a circular cylinder were presented. The streamlines for the elliptical cylinder will also first be presented at different angles for illustration with the present BEM, then it can be compared with other results. The ellipse is inclined to an angle of 45° and then to 90°. The present result for BEM is tested for the elliptical body and the results are compared to those of Proudman and Pearson (Proudman & Pearson, 1957), and Yano and Kieda (Yano & Kieda, 1980). To obtain results for an elliptical cylinder, consider carrying out the following rotation by changing the coordinates x and y to x' and y' (see figure 6.6). To rotate the point A around the origin with angle α, it is seen that $x = r$ and so

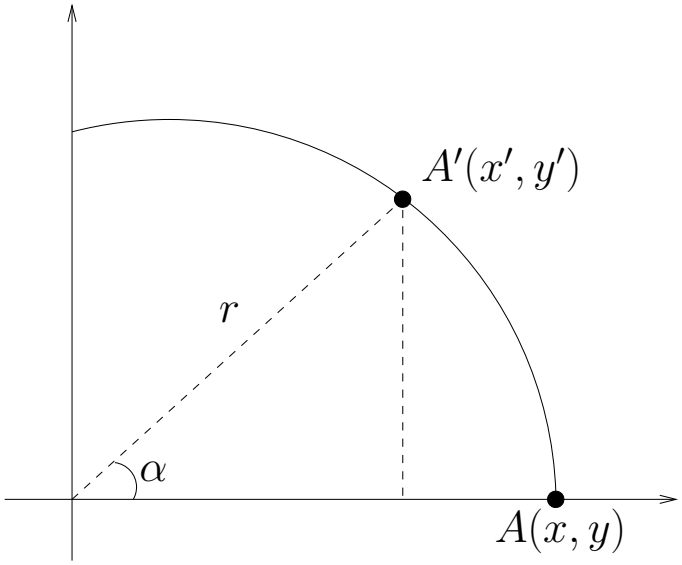

(a) Change of coordinates from point A to new point A' via one angle.

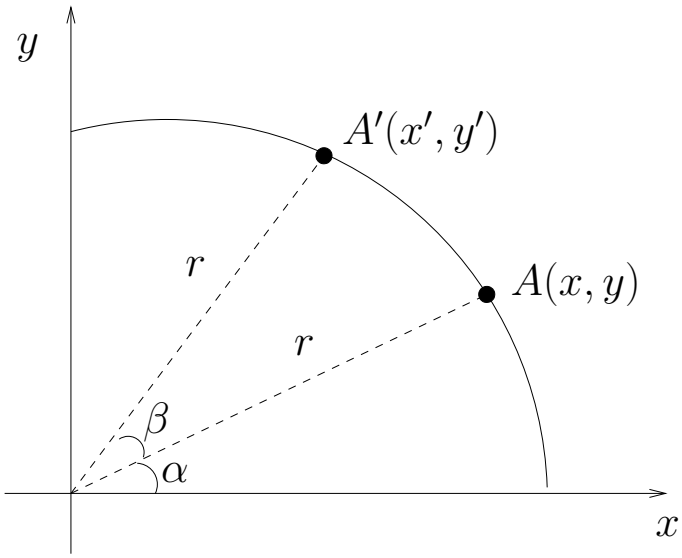

(b) Change of coordinates from point A to new point A' via two angles.

Figure 6.6: Rotating an angle to change coordinate from point A to point A'.

$$\cos\alpha = \frac{x'}{r} \tag{6.1}$$

and

$$\sin\alpha = \frac{y'}{r} \tag{6.2}$$

which yields $x' = r\cos\alpha = x\cos\alpha$ and $y' = r\sin\alpha = x\sin\alpha$, since $r = x$. It can be seen that to rotate point A around the origin to arbitrary angle so that $x' = r\cos(\alpha+\beta)$ and $y' = r\sin(\alpha+\beta)$.

$$\begin{aligned} x' &= r\cos(\alpha+\beta) \\ &= r\cos\alpha\cos\beta - r\sin\alpha\sin\beta \\ &= x\cos\beta - y\sin\beta \end{aligned} \tag{6.3}$$

and

$$\begin{aligned} y' &= r\sin(\alpha+\beta) \\ &= r\sin\alpha\cos\beta + r\cos\alpha\sin\beta \\ &= y\cos\beta + x\sin\beta \end{aligned} \tag{6.4}$$

We now have the coordinate (x, y) rotated to (x', y') and the new coordinate system is given as (6.3) and (6.4), which we can now use and run the simulation for the the ellipse.

The first case considered here is for the ellipse to be set at an angle 45° and then the Reynolds number is varied to visualise the flow. When the Reynolds number is set to $Re = 1$ (see figure 6.7), the flow velocity is high compared to when the Reynolds number is $Re = 0.1$ (see figure 6.8)and $Re = 0.01$ (see figure 6.9). The lowest Reynolds number has the least flow motion while the higher Reynolds number has the most flow motion just like in the case of circular cylinder when eddies began to form for $Re = 4$. Meanwhile the angle is now set to 90° and the Reynolds number is varied for same values as for when it was set to angle 45°. Similarly when the Reynolds number is $Re = 1$, the flow is faster (see figure 6.10) compared to when $Re = 0.1$ (see figure 6.11) and $Re = 0.01$ (see figure 6.12). Hence from figures 6.7 to 6.12, streamlines for flow past the elliptical body inclined at different angles and different Reynolds number are shown to represent the flow using the present method developed.

We know that analytical approximations exist for a circular cylinder and elliptical cylinder (Shintani et al 1983), but as the body geometry becomes complicated, it becomes difficult to get analytical solutions. However, BEM developed here can

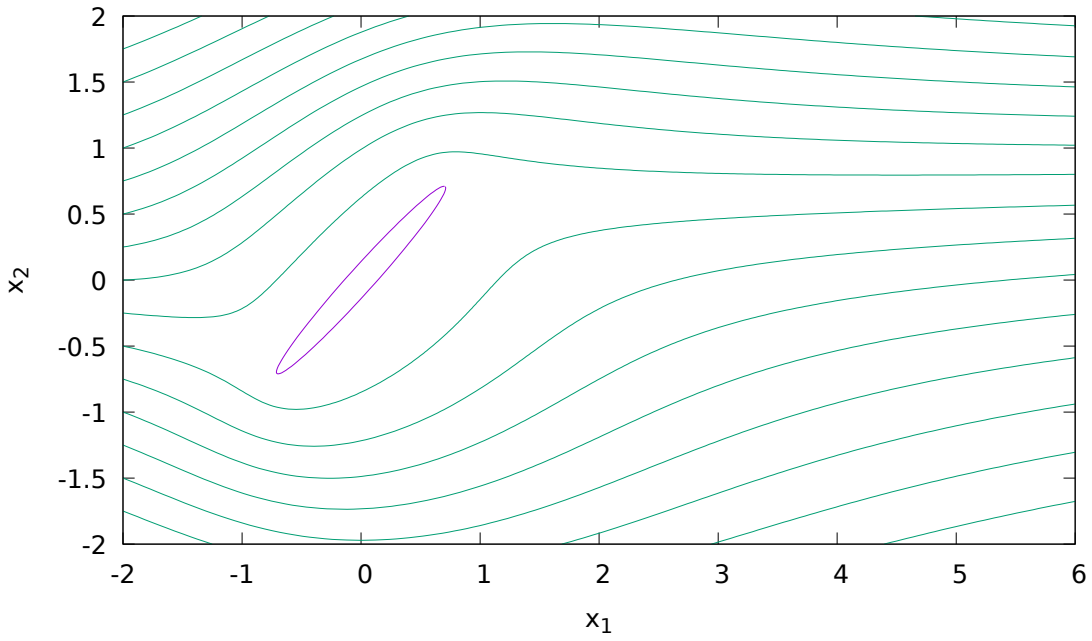

Figure 6.7: Streamlines past an elliptical cylinder with angle of inclination $\alpha = 45°$ and Reynolds number $Re = 1$.

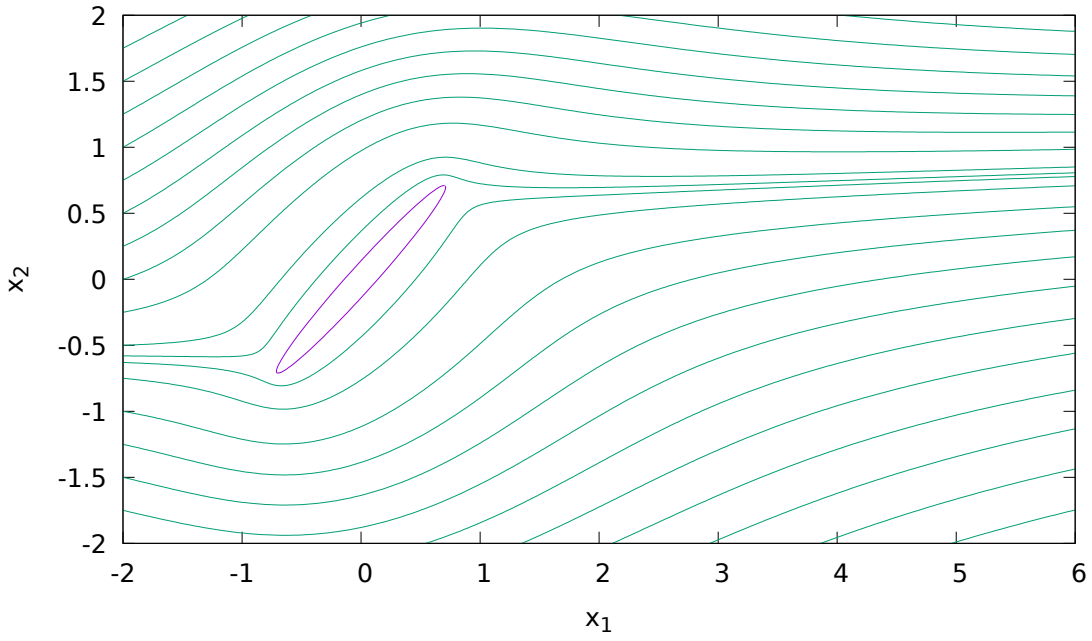

Figure 6.8: Streamlines past an elliptical cylinder with angle of inclination $\alpha = 45°$ and Reynolds number $Re = 0.1$.

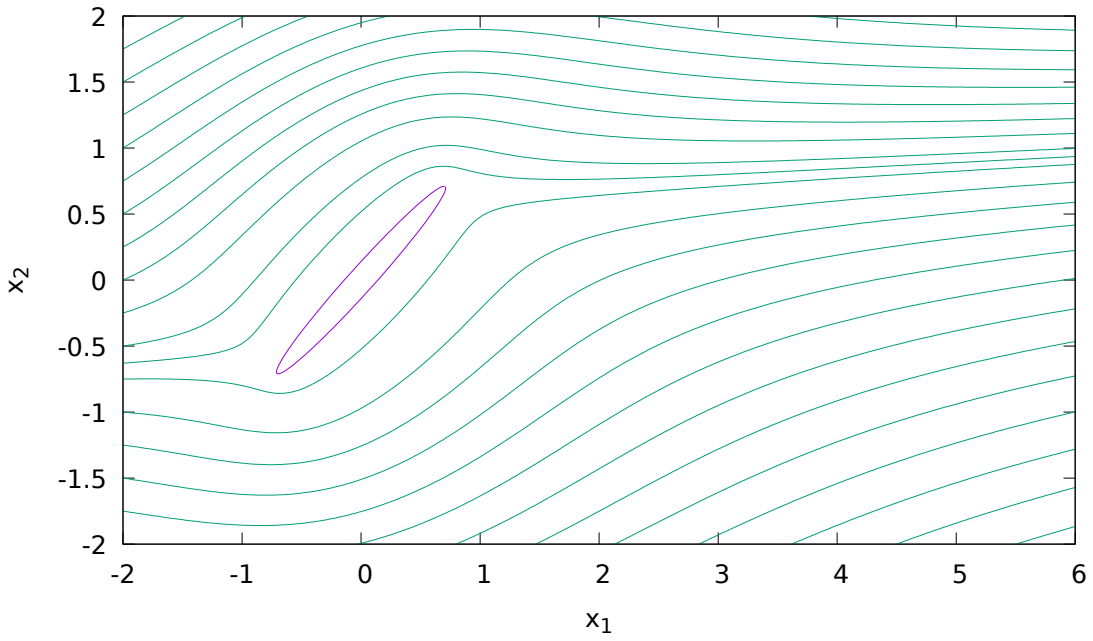

Figure 6.9: Streamlines past an elliptical cylinder with angle of inclination $\alpha = 45°$ and Reynolds number $Re = 0.01$.

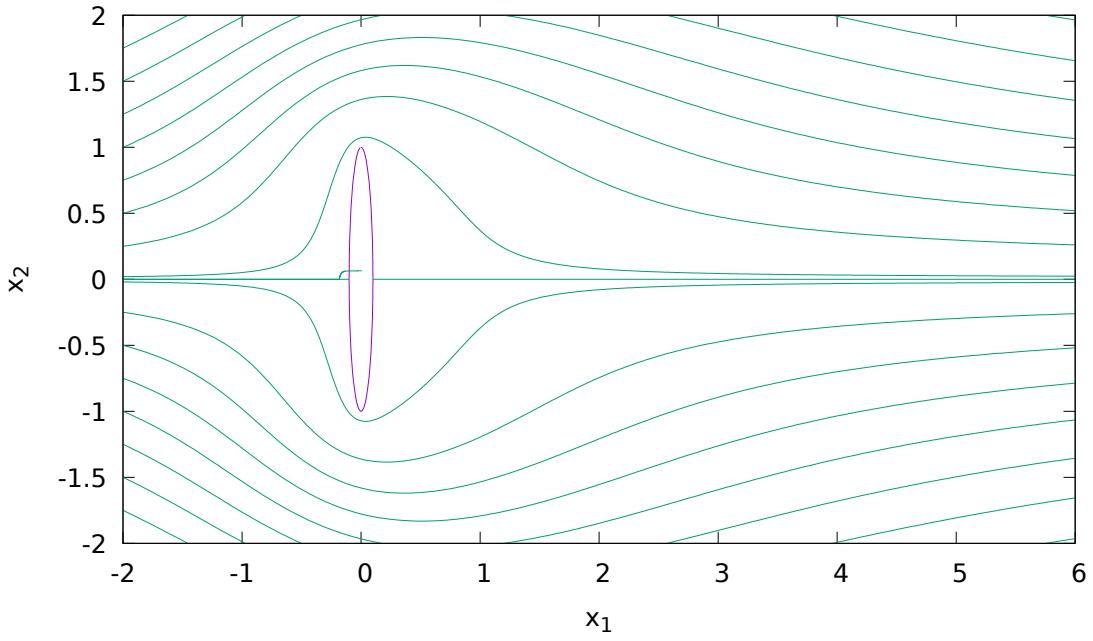

Figure 6.10: Streamlines past an elliptical cylinder with angle of inclination $\alpha = 90°$ and Reynolds number $Re = 1$.

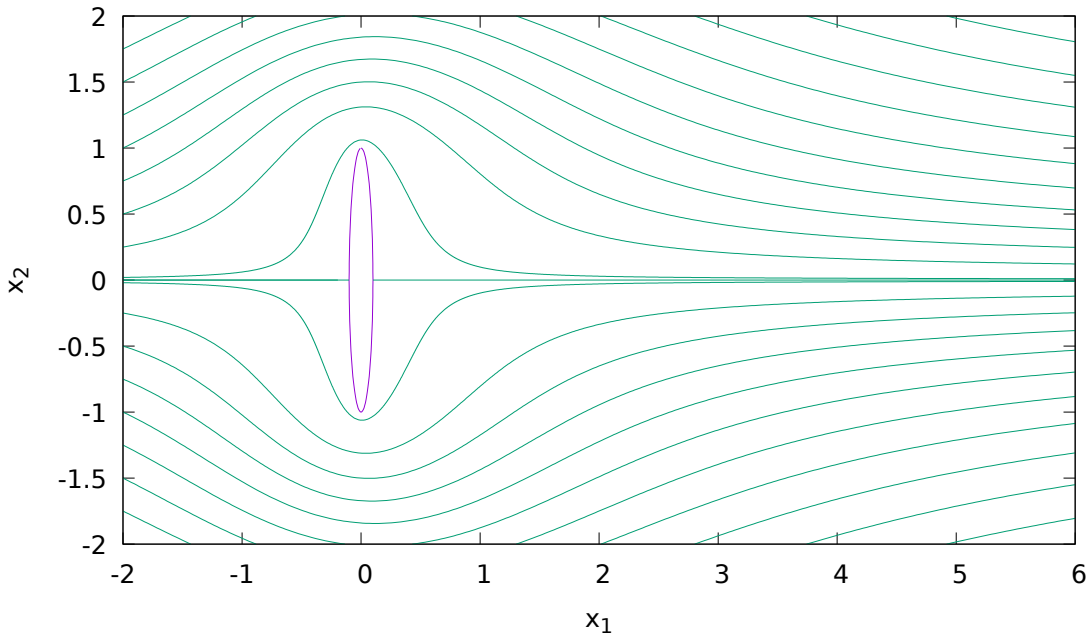

Figure 6.11: Streamlines past an elliptical cylinder with angle of inclination $\alpha = 90°$ and Reynolds number $Re = 0.1$.

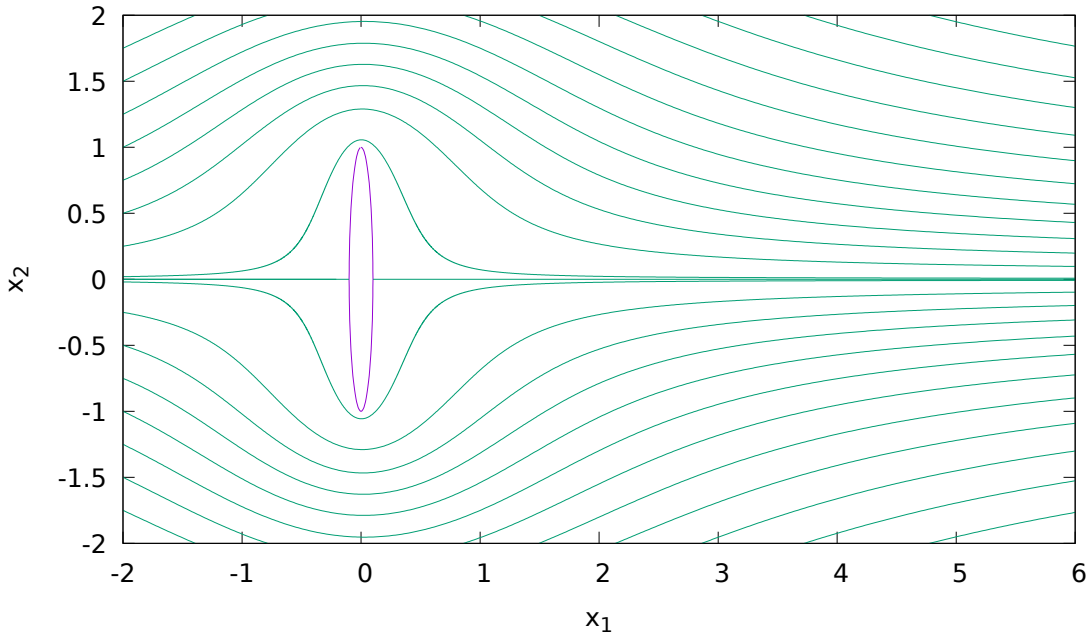

Figure 6.12: Streamlines past an elliptical cylinder with angle of inclination $\alpha = 90°$ and Reynolds number $Re = 0.01$.

handle more complicated geometries than the numerical method of Yano and Kieda ((Yano & Kieda, 1980)).

In the following results for figures (6.13) to (6.16), we consider the thickness ratio of the elliptic cylinder denoted by t, which is the ratio of the minor axis to major axis of the ellipse. The figures are shown for the drag coefficient against angle of attack α, varying from $0°$ to $90°$ for the ellipse. In figure (6.13), the Reynolds number is set to $Re = 0.1$. When $t = 1$, it can be seen that the drag coefficient remains constant irrespective of the angle α, it is true because that gives a circular cylinder. When $t = 0.1$ and $t = 0.5$ it can be seen that the drag coefficient reaches optimal when the angle is $90°$, this is expected when compared to the results of Yano and Kieda. In figure 6.14, the Reynolds number is now set to $Re = 1$ with the same angle of attack as in figure (6.13), it can be seen that the drag coefficient here is lower but it also reaches optimal drag values when the angle is $90°$. The drag coefficient here is lower than when the Reynolds number is $Re = 0.1$ which is expected.

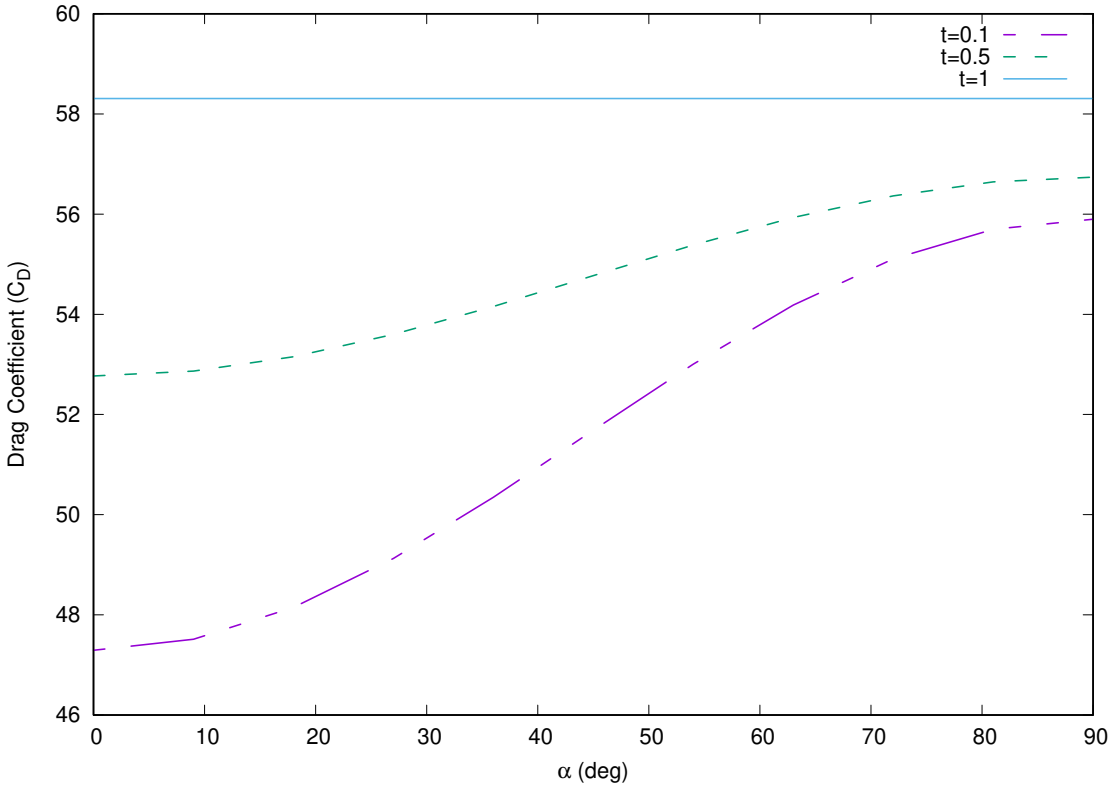

Figure 6.13: Drag coefficient C_D for an inclined elliptical cylinder at Reynolds number $Re = 0.1$ plotted against angle α for present result

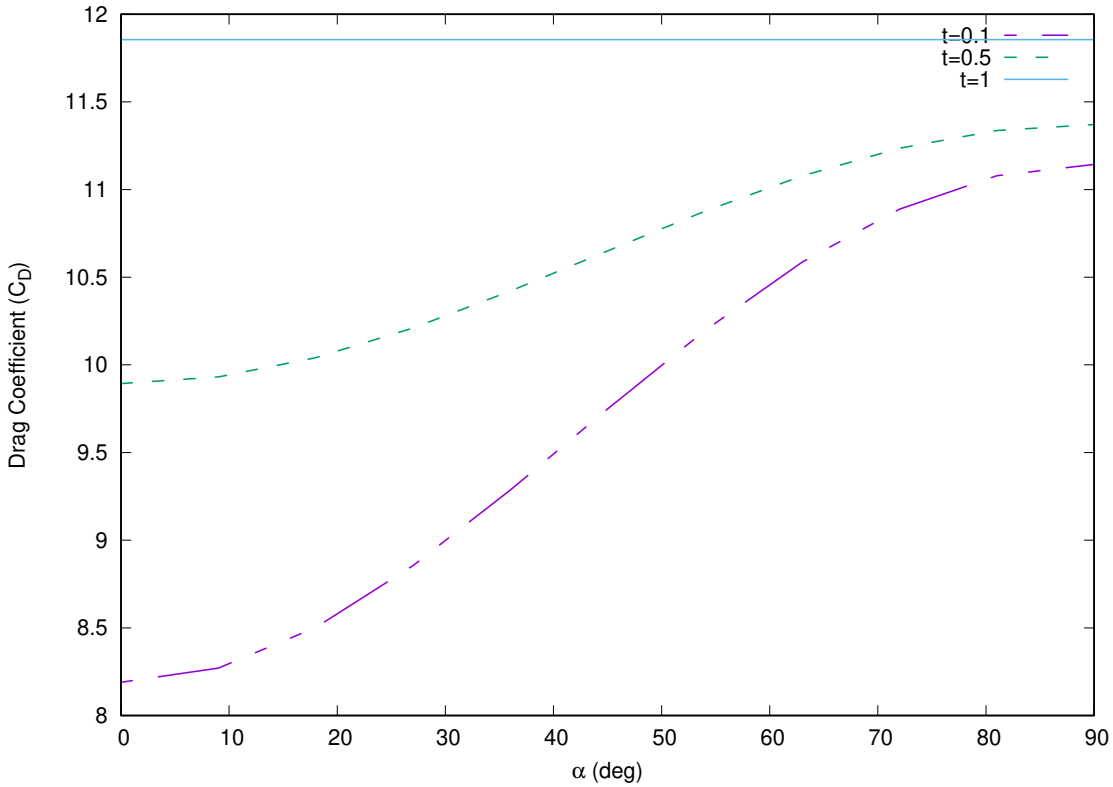

Figure 6.14: Drag coefficient C_D for an inclined elliptical cylinder at Reynolds number $Re = 1$ plotted against angle α for present result

Plotting the present results side by side with that of Lee and Leal, it can be seen from figure 6.15 and figure 6.16 that when the Reynolds number is $Re = 0.1$, the present result is closer to the result of Lee and Leal than when the Reynolds number is $Re = 1$, where b is the thickness ratio defined by Lee and Leal. Taking a closer look at our results with those of Lee and Leal and Proudman and Pearson, figure 6.15 and 6.16 give some insight for a flow past an elliptical body for Reynolds number $Re = 0.1$ and $Re = 1$ respectively. Both show an optimal drag coefficient when the angle reaches 90° for different Reynolds number and thickness ratio. Figure 6.15 shows clearly that at higher Reynolds number the difference is much greater. This is obviously what was expected because from previous results in Yano and Kieda when the drag coefficient was compared against Reynolds number, it was seen that as the Reynolds number increases, accuracy is greatly reduced, which is to say we can only get good comparison when the Reynolds number is very low (below $Re < 0.03$). It is good to be reminded that Yano and Kieda's results are based on an algorithms that assumes the position of singularities are in a prescribed manner (Yano & Kieda,

1980), while the present results can take any positioning of the singularities on the body boundary.

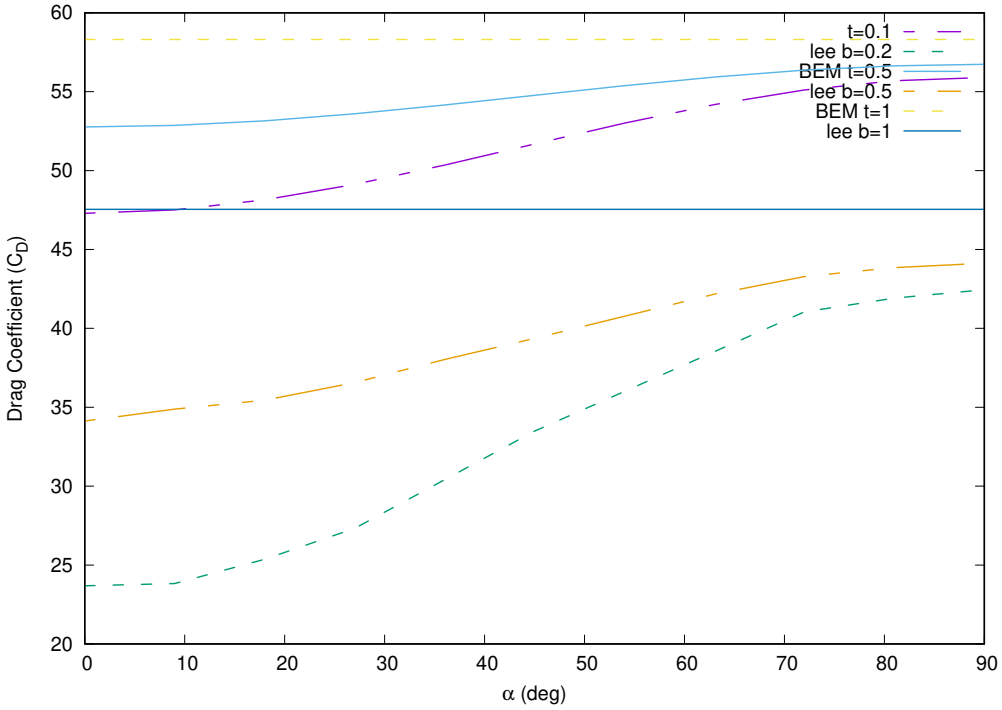

Figure 6.15: Drag coefficient C_D for an inclined elliptical cylinder compared for BEM and Lee and Leal both at Reynolds number $Re = 0.1$ plotted against angle α .

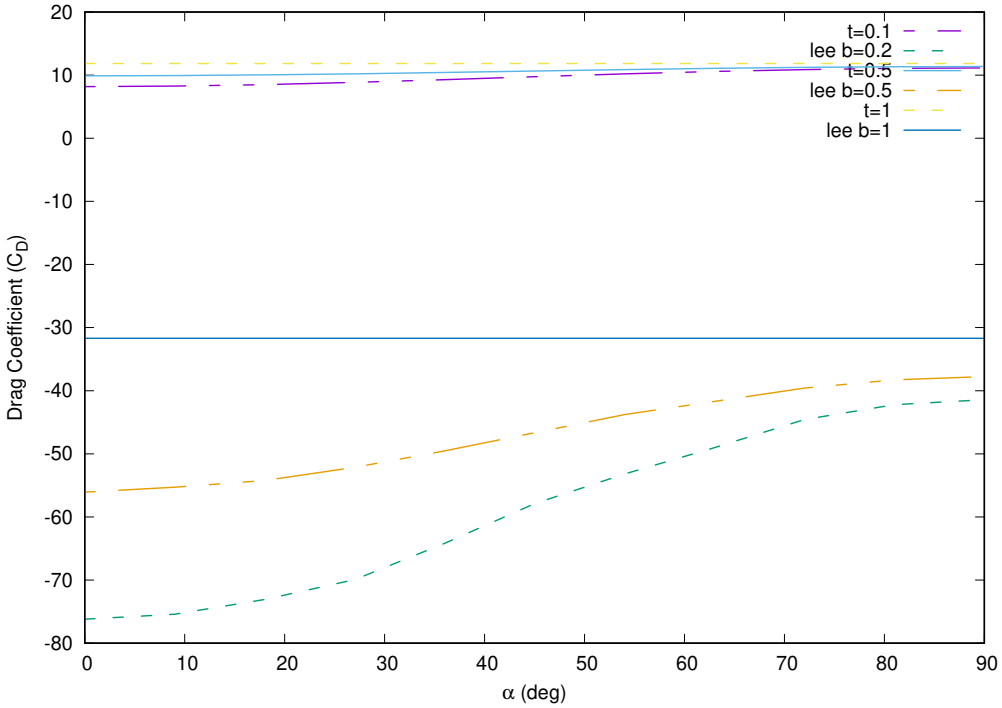

Figure 6.16: Drag coefficient C_D for an inclined elliptical cylinder compared between BEM and Lee and Leal both at $Re = 1$ plotted against angle α

6.4 Flow Past a Generic Tail-like Body

Referring back to section 3.3, it was seen that the flow is governed by the steady Stokes equation (3.35) because the time-dependent term is of lower order. In the far-field this is matched to the steady Oseen flow. Now the final result presented here is for a body in motion.

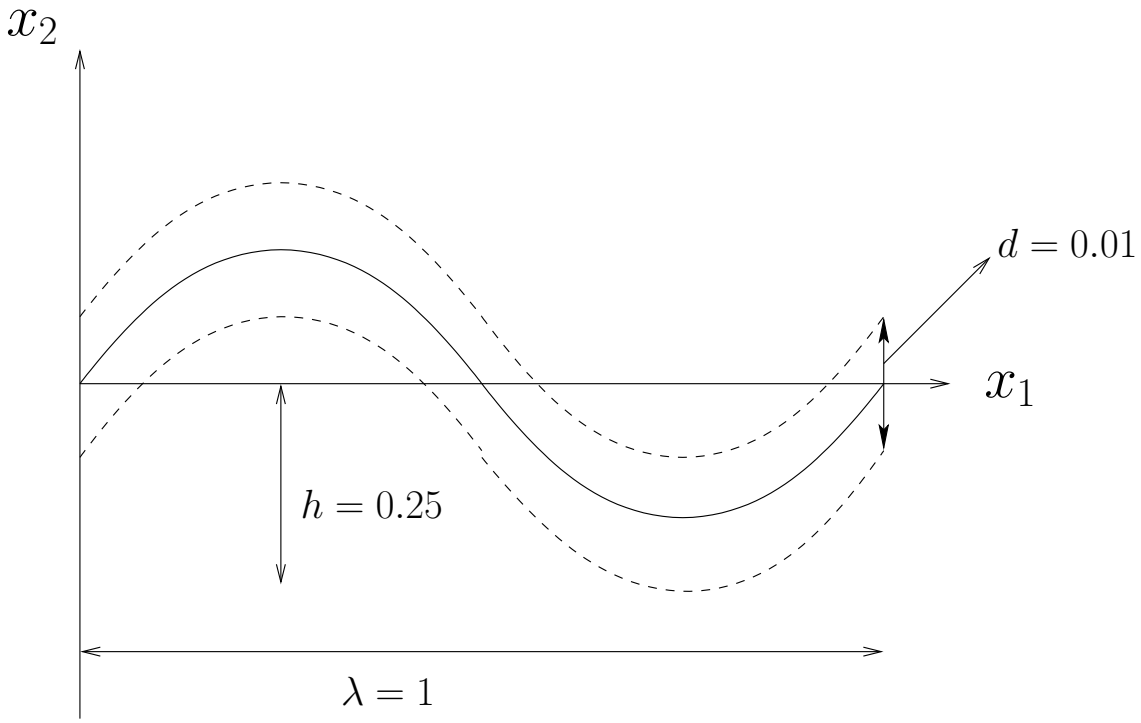

Figure 6.17: A generic tail-like structure with body thickness d, amplitude h and wavelength λ

6.4.1 Sensitivity Analysis of Parameters

To gain confidence on the model proposed for the generic tail-like body, local sensitivity analysis will be carried out on the parameters that will be use here. Sensitivity analysis referred to mathematical procedures set up to quantify the effects of variations in model output as a result of the model input (Link et al., 2018). Hence in this model, parameters representing the body thickness and amplitude shall be considered for different Reynolds number.

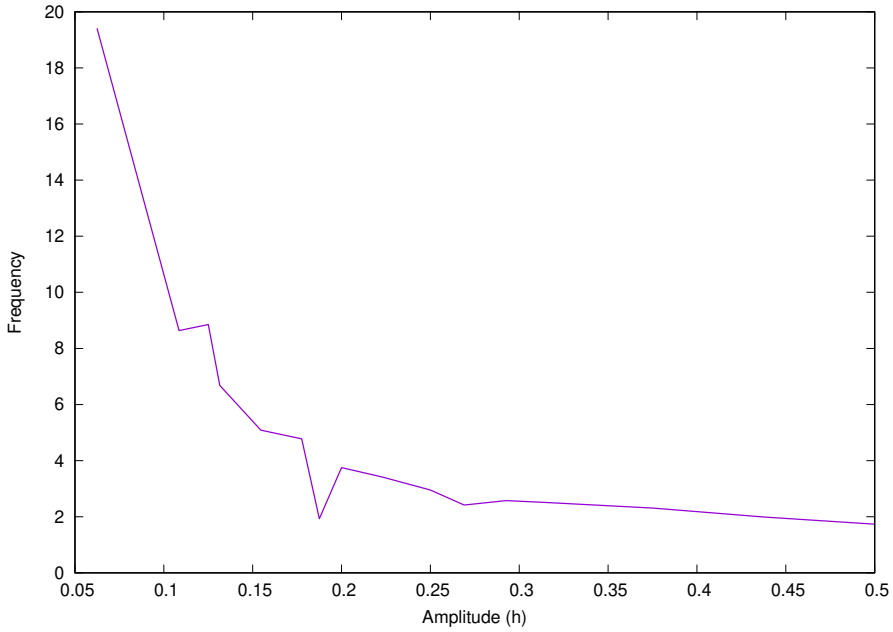

(a) The Amplitude of a moving body is compared against frequency at Reynolds number of $Re = 0.1$, with wavelength $\lambda = 1$ and body thickness $d = 0.01$

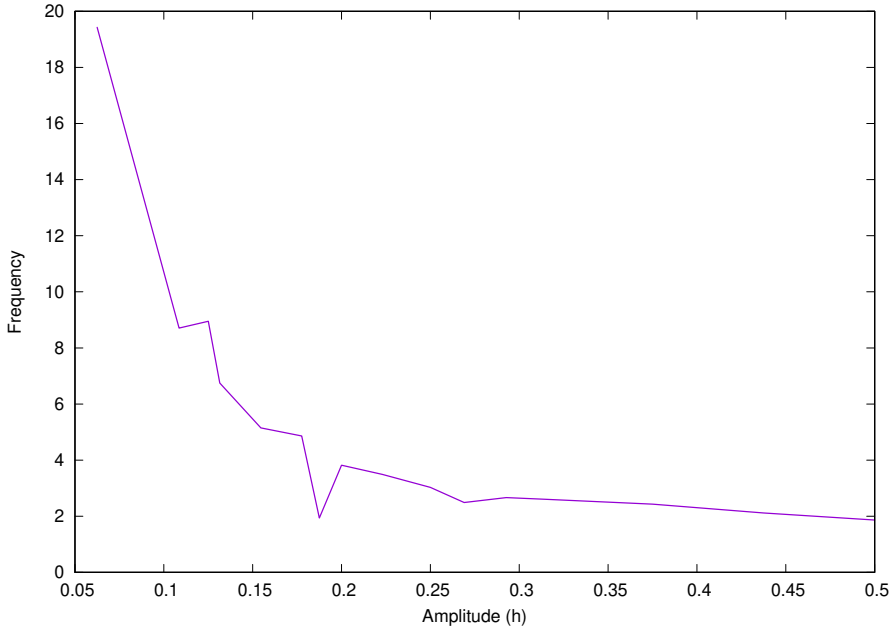

(b) The Amplitude of a moving body is compared against frequency at Reynolds number of $Re = 1$, with wavelength $\lambda = 1$ and body thickness $d = 0.01$

Figure 6.18: Local sensitivity analysis on body thickness for Reynolds number $Re = 0.1$ and $Re = 1$

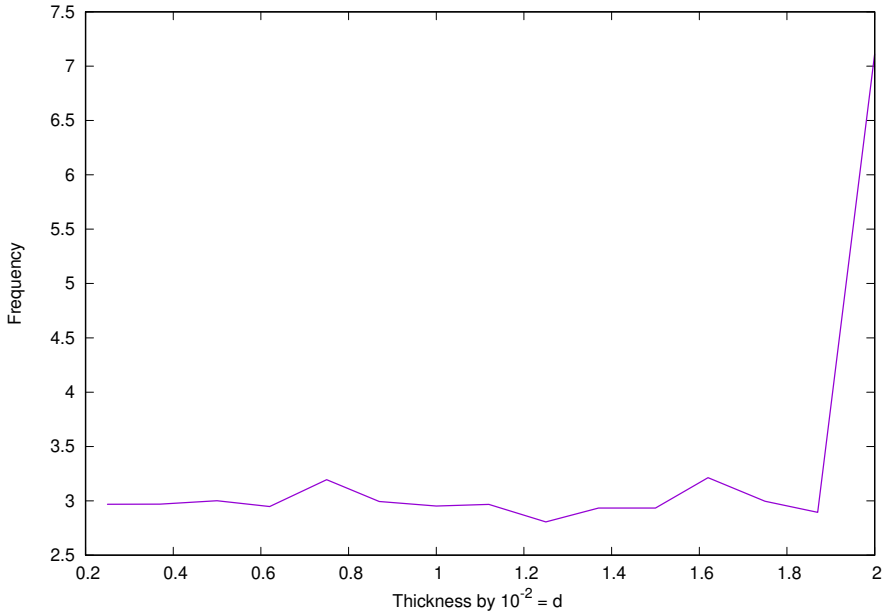

(a) The body thickness of a moving body is compared against frequency at Reynolds number of $Re = 0.1$, with wavelength $\lambda = 1$ and amplitude $h = 0.25$

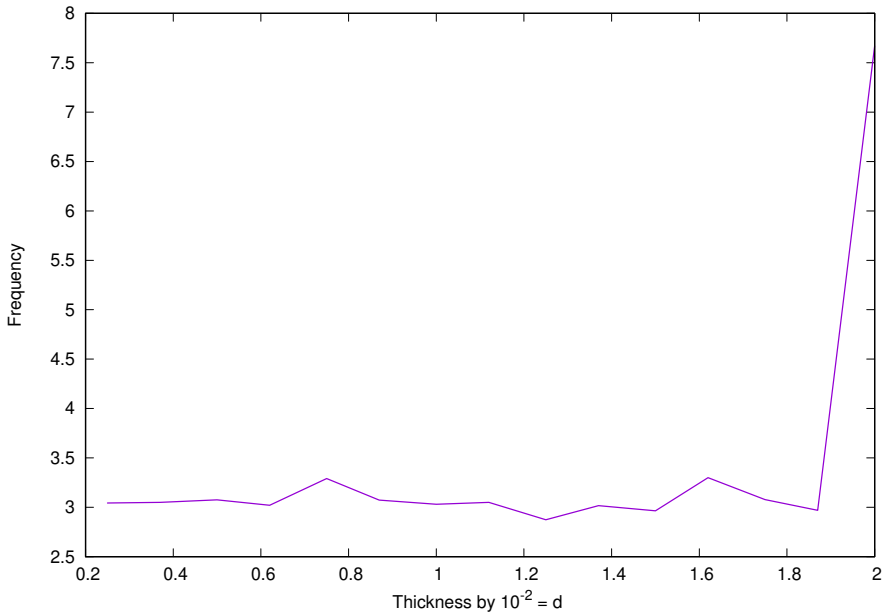

(b) The body thickness of a moving body is compared against frequency at Reynolds number of $Re = 1$, with wavelength $\lambda = 1$ and amplitude $h = 0.25$

Figure 6.19: Local sensitivity analysis on amplitude for Reynolds number $Re = 0.1$ and $Re = 1$

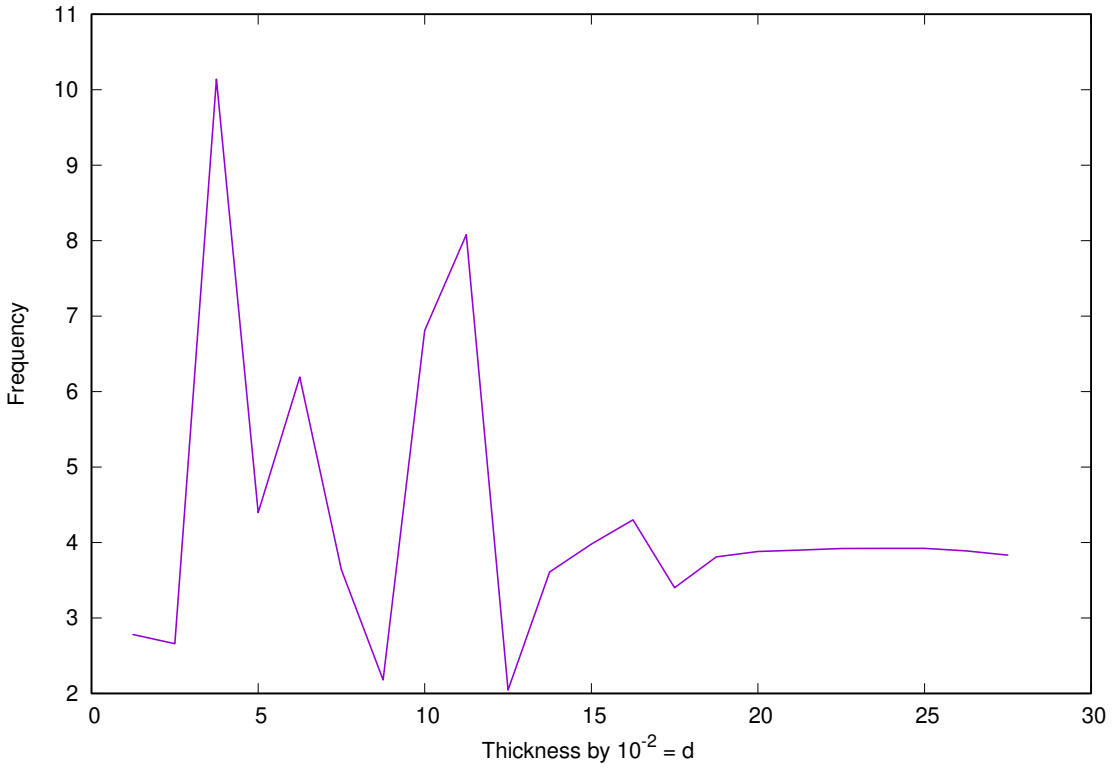

Figure 6.20: Varying the body thickness of a moving body compared against frequency at low Reynolds number of $Re = 0.01$, with wavelength $\lambda = 1$ and amplitude $h = 0.25$

Local sensitivity analysis for the body thickness (see figure 6.19) for Reynolds number $Re = 0.1$ and $Re = 1$ was carried out. It can be seen that changing the values of the Reynolds number did not affect values of the body thickness which is shown in figure 6.19a and 6.19b. The frequency required for a steady forward motion remains about 3 until the body thickness increases above 0.019. Similarly when considering the amplitude, by changing values of the Reynolds number it can be seen from figure 6.18 that there is no difference on the values of the amplitude. All these were check for wavelength ($\lambda = 1$), body thickness of $d = 0.01$, and amplitude ($h = 0.25$). To further verify, the value of the body thickness was increase from $d = 0.01$ to $d = 0.1$ and the difference is quite obvious as seen in figure 6.20. This shows that using the chosen body dimension, changing the Reynolds number does not have a significant effect, but as soon as the body thickness was changed the difference becomes clear.

6.5 Results of Flow Past a Generic Tail-like Body

Using the parameters stated above, BEM for a low Reynolds number flow is now tested to mimic a very small body in motion with a steady forward velocity. Consider a tail-like body with a sinusoidal centreline of wavelength λ, tail thickness d, amplitude h, and length $L = 1$ (see figure 6.17). We consider the steady forward motion obtained by changing the parameters h, d, λ, and Re about fixed baseline values of wavelength $\lambda = 1$, beating amplitude $h = 0.25$ to enable forward motion, thickness $d = 0.01$ of the body and Reynolds number $Re = 0.01$.

Let the sinusoidal wave pass down the body such that the centreline is given by

$$x_2 = h\sin(kx_1 - \omega t), \tag{6.5}$$

where $k = \frac{2\pi}{\lambda}$ and $\omega = 2\pi f$ where f is the wave frequency. At time $t = 0$, the top surface is given by

$$x_2 = h\sin(kx_1) + \frac{d}{2} \tag{6.6}$$

and the bottom surface by

$$x_2 = h\sin(kx_1) - \frac{d}{2} \tag{6.7}$$

The velocity given by

$$u_2 = \frac{dx_2}{dt} = -h\omega\cos(kx_1) \tag{6.8}$$

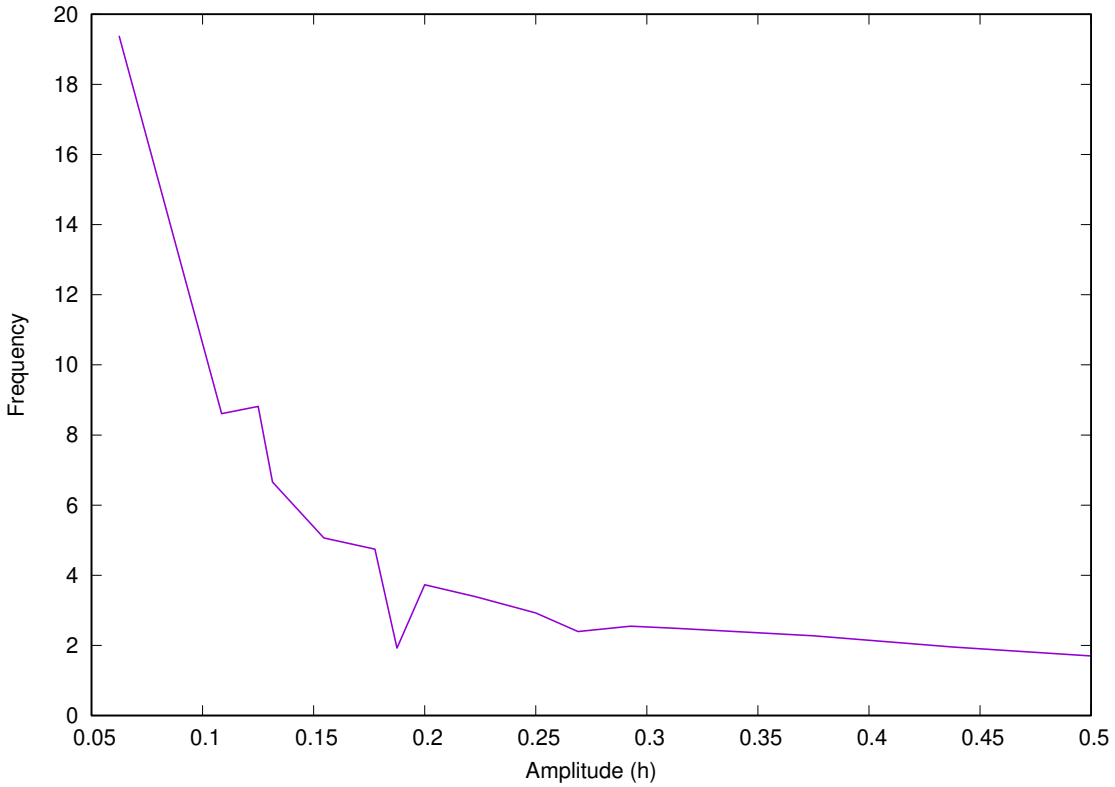

Figure 6.21: The Amplitude of a moving body is compared against frequency at low Reynolds number of $Re = 0.01$, with wavelength $\lambda = 1$ and body thickness $d = 0.01$

As can be seen that figure 6.21, as the amplitude gets smaller, the moving body has to beat more quickly in order to gain forward motion. Hence, it can be seen that once the amplitude reaches a certain optimal value (about $h = 0.175$), the beat frequency required to gain forward motion becomes less important as it approximately becomes constant with amplitude. Below the optimum amplitude, a higher beat frequency is required, and hence the organism must expend more energy for locomotion. The goal is to have zero drag force in order to get forward motion. Hence, the right choice of amplitude will have to be a value not less than $h = 0.175$ so as to require the least amount of energy for a beat frequency of about 2.

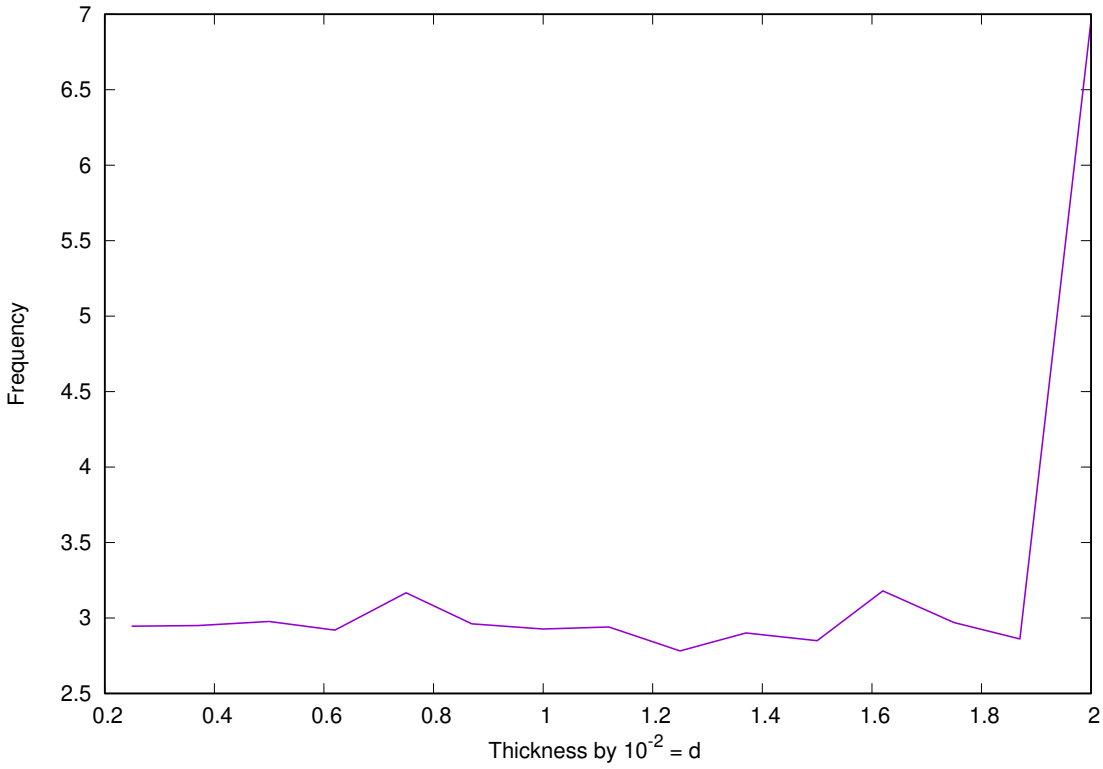

Figure 6.22: Body thickness d compared against frequency for a body in motion with low Reynolds number of $Re = 0.01$, wavelength $\lambda = 1$ and amplitude $h = 0.25$

Meanwhile, another important property to consider is the thickness of the body. From figure 6.22 it can be seen that when the thickness of the body is small, the frequency looks stable at about two, until the thickness reaches a critical value of about $d = 1.87 \times 10^{-2}$ when we noticed a great increase in the frequency. This shows that below the critical body thickness forward motion is easily achieved. It can be noted that energy input is directly related to frequency, and the minimum energy possible is required to have optimal motion of a body in viscous flow.

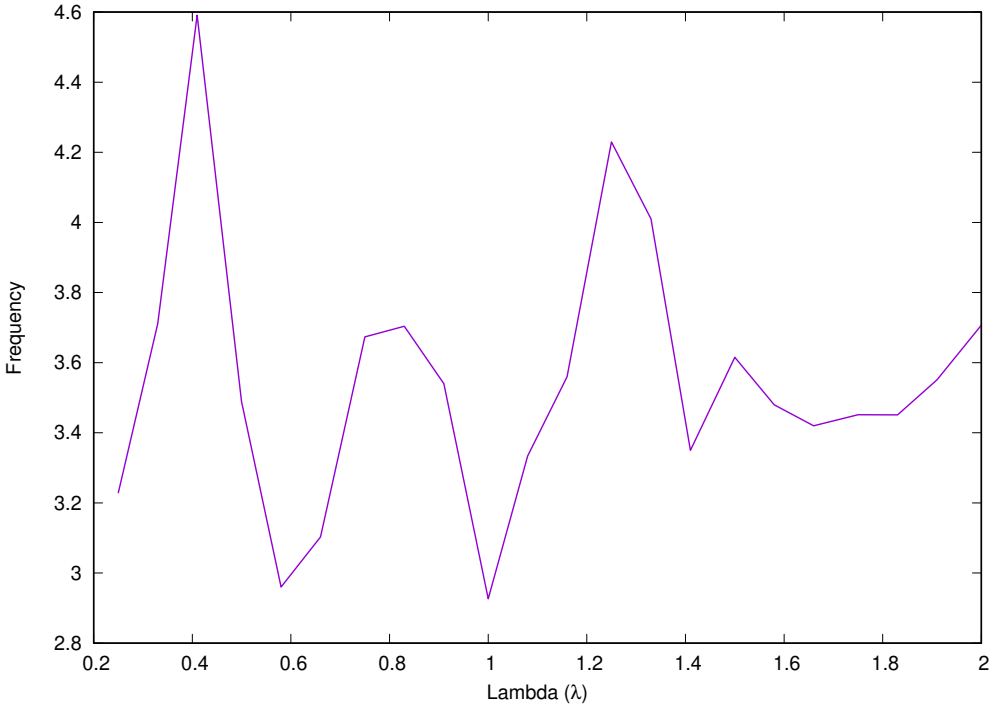

Figure 6.23: Wavelength compared against frequency for a moving body at low Reynolds number of $Re = 0.01$, body thickness $d = 0.01$ and amplitude $h = 0.25$

Considering the wavelength (Figure 6.23), it can be seen that lowest beat frequency is needed when the wavelength is about the value one. This matches with the body length of one and thus an optimal is expected at that point.

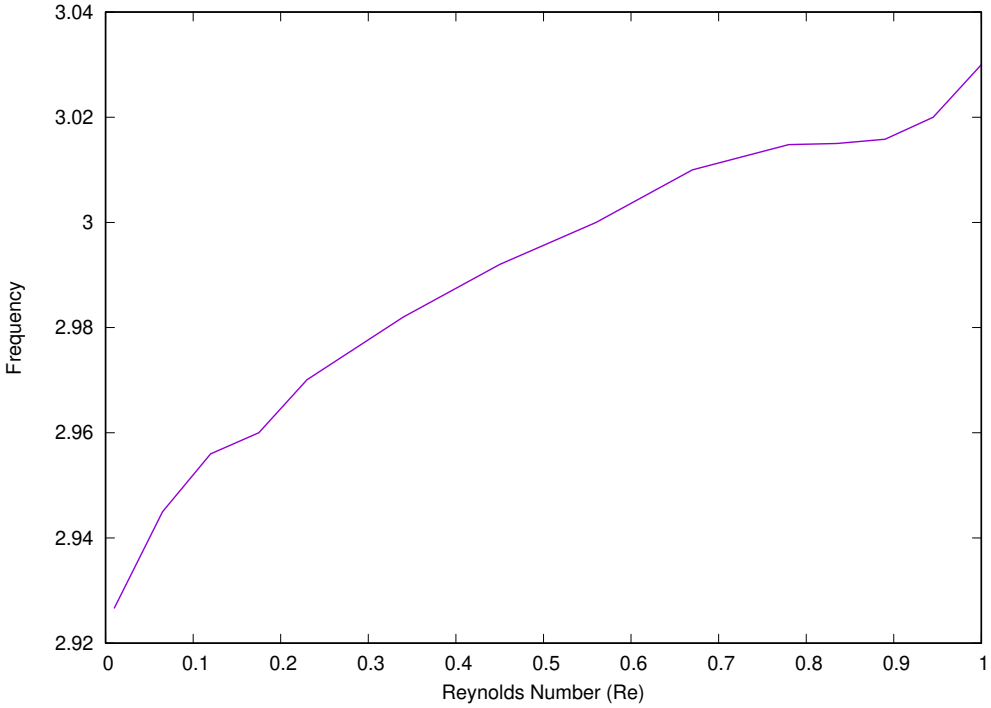

Figure 6.24: Reynolds number $Re = 1 \times 10^{-2}$ is varied and compared against frequency, with body thickness $d = 0.01$, amplitude $h = 0.25$, wavelength $\lambda = 1$ for a body in motion

In figure 6.24, the Reynolds number is plotted against the frequency. We can see that as the Reynolds number increases, the frequency also increases. This result is expected, especially since the model developed is for a steady viscous flow.

From the above illustrations for a body in motion, the effect of the amplitude, wavelength, Reynolds number and thickness of the body, on the frequency can be seen. The critical values expected to have a forward steady motion for a body in viscous flow regime were found. Namely, the amplitude was found to be about $h = 0.175$, wavelength $\lambda = 1$ and the thickness of the body be $d = 1.87 \times 10^{-2}$ for a Reynolds number of $Re = 0.01$. With these optimal values we can now take a real-life organism or a micro-robotic design and be able to model its motion in viscous fluid flow. One the advantages of this is that only the body boundary is discretised in an unbounded domain.

6.6 Summary of the Chapter

Main results for this thesis are discussed in this chapter. The first case that was considered was for a flow past a circular cylinder. It began with plotting streamlines for a flow past a circular cylinder for different Reynolds number $Re = 0.01$, $Re = 1$, and $Re = 4$ using BEM developed in this study. The drag coefficient was was then plotted against the Reynolds number for the results of Lamb, Lee and Leal and the present result for low Reynolds number $0 < Re < 0.3$ which shows present result and that of lamb align together while Lee and Leal diverge as Re increases. The second case considered was for a flow past an elliptical body, streamlines were also plotted for different values of Reynolds number. The drag coefficient was plotted against the angle of attack and for each figure, three different thickness ratio of the elliptic cylinder are considered. It was then compared with the result of Lee and Leal which shows large variation when the Reynolds number is high. The last case considered was to model a generic tail-like body shape. We were able to find the optimal values of body thickness, wavelength, amplitude, frequency, and Reynolds that is required for the body to have a forward motion. This is to mimic a micro-organism or any moving body swimming at low Reynolds number.

Chapter 7

Summary, Conclusions, and Future Work

7.1 Summary

General overview for this thesis is outlined. In chapter one, Boundary Integral Method (BIM) and Boundary Element Method (BEM) was introduced. This was followed by the aim and objectives of this studies, which is to provide accurate and non-complicated to use method for low Reynolds number. In chapter two, general literature review of past studies for flow past a circular cylinder was considered. Terms such as the Reynolds number, Green's function, and divergence theorem were defined and the classification of fluid under consideration in this thesis is stated. Chapter three introduced governing equations that were used, including the Navier-Stokes equation, continuity equation, Oseen equation, stokes equation, and their Green's integral representations. Chapter four introduced BEM for two dimensional body and a formulation for exterior problems using the Stokes and Oseen equations. Also in this chapter the analytic removal of the Green's function singularity was obtained and the chapter ended by outlining the step by step code implementation together with the flow chart that runs the numerical simulation. In chapter five, matched asymptotic expansion was presented for the Stokes flow near the body and Oseen flow far from the body. The results are validated using the benchmark

problem of flow past a circular cylinder in two dimensions and compared with other existing results of two dimensional flow. In chapter six, the model developed for flow past a circular cylinder is modified to describe flow past an elliptical cylinder and to also mimic a model of micro-organism in motion.

Studies of low Reynolds number flow for a viscous fluid past a body have been an active research field from the time of Osborne Reynolds in 1851 until today. In two dimensions, satisfying the boundary conditions both near the body surface and far away from the body has been a problem that researchers are still working to overcome. Review of past studies in that direction was presented here which included both analytical studies and numerical studies. The main limitation with all the previous results is that they were developed for a simple body geometry: once body geometry becomes complicated they become too complex to implement. It was seen that the different existing approaches presented do not agree with experimental results, particularly when the Reynolds number increases.

In this thesis, a novel numerical method was developed using BEM for a flow past a body in two dimensions at low Reynolds number. This novel numerical method was inspired by the matched asymptotic expansion by Chadwick (Chadwick, 2013). Our approach utilised point collocation weighting function, linear shape function, and two point Gaussian quadrature with analytic removal of the Greeen's function singularity for integration. The Green's integral representation of oseenlets is distributed over the boundary surface. The model is developed for an unbounded domain by matching the near field region with the far-field region by the method of matched asymptotic expansion used by Chadwick 2013. A computer programme developed in `Fortran 95` was used for testing the model through series of numerical simulations.

BEM for solving a two-dimensional steady flow past a circular cylinder has been presented. Our results compare favourably with the experiment of Tritton (Tritton, 1959), the analytical results of Lamb (Lamb, 1932), Kaplun (Kaplun & Lagerstrom, 1957), and Tomotika (Tomotika & Aoi, 1951), and the numerical results of Yano and Kieda (Yano & Kieda, 1980), Lee and Leal (Lee & Leal, 1986) and Proudman and Pearson (Proudman & Pearson, 1957) for the drag coefficient. Hence, our

method is uncomplicated and computationally efficient, yet robust in solving steady two-dimensional flow past a circular cylinder in an unbounded domain. Our results agree with the standard benchmark results and are an improvement upon existing models in the higher Reynolds number range, up to $Re = 4$ (other methods began to fail when Re approaches one). So our representation gives a better description of the flow field even outside the low-Reynolds number region of $Re < 1$. In particular, it gives better results than the matched asymptotic method of Kaplun (Kaplun & Lagerstrom, 1957). Our method is also able to deal with more complicated geometries. Finally, this method is applied to manoeuvring bodies such as a swimming organism with possible applications in micro robotics.

7.2 Findings From this Study

This thesis reviews different methods which include the discrete singularity method by Yano and Kieda (Yano & Kieda, 1980) with their results benchmarked with the analytic result of Lamb (Lamb, 1932), Kaplun (Kaplun & Lagerstrom, 1957) and the experiment of Tritton (Tritton, 1959) for the drag coefficient. It was revealed that when the Reynolds number is below one ($Re < 1$), there is good agreement, but when the Reynolds number is in the range 1 to 4 the analytical results do not align very closely with experiment, except the numerical studies presented by Yano and Kieda [17]. The analytical results work well for body surfaces with simple geometries, but as soon as the geometry becomes complicated, numerical approaches provide better basis for analysis. To apply to more complicated geometries, Lee and Leal [10] considered a matched asymptotic expansion method that used Green's integral representations of the velocity. Chadwick (Chadwick, 2013) takes this approach and matched Stokes and Oseen flow within a boundary integral formulation. It was found that the error is least if the matching boundary is on the body itself. Here, it is noted that this approach does not break down on the body boundary because in the formulation the oseenlet approximates to the stokeslet.

The boundary element method designed in this thesis is made such that the collocation point is chosen not to lie on the nodes so that the Green's function

singularity in the integral is more easily removed, because the singularity lies wholly within the element integration rather than divided across two elements. It was found that as the number of nodes are increased the collocation points will move closer to the boundary. The near field stokes flow and the far field oseen flow are matched in asymptotic expansion, this is then discretise using the present boundary element formulation. Results from this matching is in agreement with benchmarked results obtained through analytical and experimental studies for flow past a circular and elliptic cylinder. It was seen that the present formulation gives better results especially for the Reynolds number range ($0.01 < Re < 4$).

The last results presented which mimic a tail-like body shows that the variation of thickness of the body, the length of the body, wavelength of the flagella, and the Reynolds number of the supporting fluid all have a pronounced effect on the beat frequency required of the flagella to overcome the viscous forces of the fluid. Critical values have been identified beyond which the energy requirement to overcome these forces drastically increases. For example, a fluid with $Re = 0.01$, these critical values are $h = 0.175$, $d = 1.87 \times 10^{-2}$, and $\lambda = 1$. With the ability to calculate these critical values, mathematical modelling of micro-organisms and micro-machines through a viscous fluid is made possible using BEM, a key advantage of which is that discretisation is done only on the bounding surface, therefore allowing it to be extended to model a body of any arbitrary shape.

7.3 Recommendations and Future Studies

Results from this study show that modelling a body of any shape using BEM is possible. However, to mimic a real-life organism in motion, a three-dimensional model is required. Notwithstanding, this research provided a strong footing for advancing to a three dimensional problem. As a future study, this will be extended to three dimensions, and a specific real-life microorganism, and micro-robotics will be consider.

Furthermore, the present model can be extended for higher Reynolds number

above the present value considered in this thesis. Increasing the Reynolds number to $Re > 4$ and research on the computational size of the problem, then apply it to a generic body in motion, this time the research should consider a model of body in motion that is faster than microscopic level which will find many applications in environment, industry, and engineering. This can be research for both two and three dimensional cases.

If the boundary element model developed here can be extended to higher Reynolds number as mentioned above, then it can model flagellate-propelled micro-organism like planktons which in turn are very important in climate change by fixing carbon circle. Therefore understanding the motion of planktons, mathematical modelling will be useful in making predictions. Since planktons are at the base of the aquatic food chain, studying their dynamics is important for conservation of the aquatic ecosystem. Consequently, this interconnection has consequences for climate change. In industry, flagellate-propelled micro-organisms are used in biofuel production and the food processing industry, among other uses. Because of the importance flagella play in organisms, modelling using BEM is important.

Appendix A

Appendix

A.1 Summary of Publications

A.1.1 Published Work

B.C. Dang, and E.A. Chadwick (2019). BEM for Low Reynolds Number Flow Past a Steady Circular Cylinder in an Unbounded Domain. *Proceedings of the 12th UK Conference on Boundary Integral Methods UKBIM12.*

This paper presents a Boundary Element Method that solves a two–dimensional flow past a circular cylinder using the Oseen equation. We are able to verify the numerical method by benchmarking it with the standard flow past a circular cylinder. The method can be extended to a more general body shape.

A.1.2 Unpublished Work

1. **Uniform Flow Past a Closed Body at Low Reynolds Number Employing a Novel Matching in a Boundary Element Formulation.**
   Under Review.

   In this paper, a Boundary Element Method is developed for a flow past a circular cylinder. This method demonstrates that Oseen equation can be used

to model flow both near a body surface and far from the body surface. Since the discretisation is carried out only on the body boundary (as opposed to throughout the whole domain), modelling of a more generic body shape is possible.

2. **Mathematical Modelling for Motion in Viscous Fluid Flow in an Exterior Domain.** *In preparation for publication in a journal.*

   In this paper, a model for flow past a circular cylinder and flow past an ellipse is presented and benchmarked against the classical flow past a cylinder. The method is developed to model a generic tail-like moving body in a viscous flow. This model can be used for any body shape because the discretisation is carried out on the boundary only rather than within the domain of the body. The model has been verified against flow past circular cylinder and flow past an ellipse. Examples will be presented to mimic microscopic swimming in viscous fluid, micro-robotics, and plankton that assist in fixing the carbon circle.

References

Abel, N. (1823). Solution de quelques problemes a l'aide d'integrales definies. *Mag. Naturvidenskaberne*, *2*, 11–27.

Baretta-Bekker, J., Duursma, E., & Kuipers, B. (1992). Encyclopedia of marine sciences.

Batchelor, G. K. G. K. (1967). *An introduction to fluid dynamics.* Cambridge: Cambridge University Press.

Blazek, J. (2015). Chapter 3 - principles of solution of the governing equations. In J. Blazek (Ed.), *Computational fluid dynamics: Principles and applications (third edition)* (Third Edition ed., p. 29 - 72). Oxford: Butterworth-Heinemann. Retrieved from `http://www.sciencedirect.com/science/article/pii/B9780080999951000038` doi: https://doi.org/10.1016/B978-0-08-099995-1.00003-8

Brebbia, C. A. (2017). The birth of the boundary element method from conception to application. *Engineering Analysis with Boundary Elements*, *77*, iii - x. Retrieved from `http://www.sciencedirect.com/science/article/pii/S0955799716304453` doi: https://doi.org/10.1016/j.enganabound.2016.12.001

Causon, D., & Mingham, C. (2010). *Introductory finite difference methods for pdes.* Bookboon.

Chadwick, E. (2013). The far-field green's integral in stokes flow from the boundary integral formulation. *Computer Modeling in Engineering Sciences*, *96*(3), 177–184.

Chadwick, E. (2014). Viscous fluid dynamics: Lecture notes and tutorial sheet: Level 6. *Department of Mathematics, University of Salford*.

Cheng, A. H.-D., & Cheng, D. T. (2005). Heritage and early history of the boundary element method. *Engineering Analysis with Boundary Elements*, *29*(3), 268 - 302. Retrieved from http://www.sciencedirect.com/science/article/pii/S0955799705000020 doi: https://doi.org/10.1016/j.enganabound.2004.12.001

Day, M. A. (1990, Nov 01). The no-slip condition of fluid dynamics. *Erkenntnis*, *33*(3), 285–296. Retrieved from https://doi.org/10.1007/BF00717588 doi: 10.1007/BF00717588

Ehrenpreis, L. (1954). Solution of some problems of division: Part i. division by a polynomial of derivation. *American Journal of Mathematics*, *76*(4), 883–903.

Ehrenpreis, L. (1955). Solution of some problems of division: Part ii. division by a punctual distribution. *American Journal of Mathematics*, *77*(2), 286–292.

Eymard, R., Gallouët, T., & Herbin, R. (2000). Finite Volume Methods. In J. L. Lions & P. Ciarlet (Eds.), *Solution of Equation in (Part 3), Techniques of Scientific Computing (Part 3)* (Vol. 7, p. 713-1020). Elsevier. Retrieved from https://hal.archives-ouvertes.fr/hal-02100732 doi: 10.1016/S1570-8659(00)07005-8

Falkowski, P. (2012). The power of plankton. *Nature*, *483*(Suppl 7387), S17.

Fauci, L. J., & Dillon, R. (2006). Biofluidmechanics of reproduction. *Annu. Rev. Fluid Mech.*, *38*, 371–394.

Fawcett, D. (2014). Cilia and flagella. *Cells and Their Component Parts: Biochemistry, Physiology, Morphology*, 217.

Fishwick, N., & Chadwick, E. (2006). The evaluation of the far-field integral in the green's function representation for steady oseen flow. *Physics of Fluids*, *18*(11), 113101.

Gray, J. (2015). *Ciliary movement*. Cambridge University Press.

Hancock, G. J. (1953). The self-propulsion of microscopic organisms through liquids. *Proceedings of the Royal Society of London A: Mathematical, Physical and Engineering Sciences*, *217*(1128), 96–121. Retrieved from http://rspa.royalsocietypublishing.org/content/217/1128/96 doi: 10.1098/rspa.1953.0048

Hao, W., Hu, B., Li, S., & Song, L. (2018). Convergence of boundary integral

method for a free boundary system. *Journal of Computational and Applied Mathematics*, *334*, 128 - 157. Retrieved from http://www.sciencedirect.com/science/article/pii/S0377042717305769 doi: https://doi.org/10.1016/j.cam.2017.11.016

Henkel, R., Bittner, J., Weber, R., Hüther, F., & Miska, W. (1999). Relevance of zinc in human sperm flagella and its relation to motility. *Fertility and sterility*, *71*(6), 1138–1143.

Imai, I. (1951). On the asymptotic behaviour of viscous fluid flow at a great distance from a cylindrical body, with special reference to filon's paradox. *Proceedings of the Royal Society of London. Series A. Mathematical and Physical Sciences*, *208*(1095), 487–516.

Imai, I. (1954). A new method of solving oseen's equations and its application to the flow past an inclined elliptic cylinder. *Proceedings of the Royal Society of London. Series A. Mathematical and Physical Sciences*, *224*(1157), 141–160.

Kaplun, S., & Lagerstrom, P. (1957). Asymptotic expansions of navier-stokes solutions for small reynolds numbers. *Journal of Mathematics and Mechanics*, *6*(5), 585–593.

Katsikadelis, J. T. (2016). *The boundary element method for engineers and scientists: Theory and applications*. Academic Press.

Khalili, A., & Liu, B. (2017). Stokes' paradox: creeping flow past a two-dimensional cylinder in an infinite domain. , *817*, 374–387.

Kieda, A., & Yano, H. (1978). Approximate numerical solutions for two-dimensional potential flow problems. *Journal of Fluids Engineering*, *100*(1), 122–124.

Kress, N. (2019). Chapter 3 - seawater quality for desalination plants. In N. Kress (Ed.), *Marine impacts of seawater desalination* (p. 35 - 52). Elsevier. doi: https://doi.org/10.1016/B978-0-12-811953-2.00003-7

Lamb, H. (1911). Xv. on the uniform motion of a sphere through a viscous fluid. *The London, Edinburgh, and Dublin Philosophical Magazine and Journal of Science*, *21*(121), 112–121.

Lamb, H. (1932). Hydrodynamics.

Lee, S.-H., & Leal, L. G. (1986). Low-reynolds-number flow past cylindrical bodies of arbitrary cross-sectional shape. *Journal of Fluid mechanics*, *164*, 401–427.

Link, K. G., Stobb, M. T., Di Paola, J., Neeves, K. B., Fogelson, A. L., Sindi, S. S., & Leiderman, K. (2018, 07). A local and global sensitivity analysis of a mathematical model of coagulation and platelet deposition under flow. *PLOS ONE*, *13*(7), 1-38. Retrieved from https://doi.org/10.1371/journal.pone.0200917 doi: 10.1371/journal.pone.0200917

Longhurst, A., Sathyendranath, S., Platt, T., & Caverhill, C. (1995). An estimate of global primary production in the ocean from satellite radiometer data. *Journal of plankton Research*, *17*(6), 1245–1271.

Longhurst, A. R., & Harrison, W. G. (1989). The biological pump: profiles of plankton production and consumption in the upper ocean. *Progress in Oceanography*, *22*(1), 47–123.

Malgrange, B. (1956). Existence et approximation des solutions des équations aux dérivées partielles et des équations de convolution. In *Annales de l'institut fourier* (Vol. 6, pp. 271–355).

Montenegro-Johnson, T. D., Smith, A. A., Smith, D. J., Loghin, D., & Blake, J. R. (2012, Oct 29). Modelling the fluid mechanics of cilia and flagella in reproduction and development. *The European Physical Journal E*, *35*(10), 111.

Montenegro-Johnson, T. D., Smith, D. J., & Loghin, D. (2013). Physics of rheologically enhanced propulsion: different strokes in generalized stokes. *Physics of Fluids*, *25*(8), 081903.

Munson, B. R. (2002). *Fundamentals of fluid mechanics* (4th ed. ed.). New York ; Chichester: John Wiley.

Neill, S. P., & Hashemi, M. R. (2018). Chapter 8 - ocean modelling for resource characterization. In S. P. Neill & M. R. Hashemi (Eds.), *Fundamentals of ocean renewable energy* (p. 193 - 235). Academic Press. Retrieved from http://www.sciencedirect.com/science/article/pii/B9780128104484000082 doi: https://doi.org/10.1016/B978-0-12-810448-4.00008-2

Nonaka, S., Tanaka, Y., Okada, Y., Takeda, S., Harada, A., Kanai, Y., ... Hirokawa, N. (1998). Randomization of left–right asymmetry due to loss of nodal cilia generating leftward flow of extraembryonic fluid in mice lacking kif3b motor protein. *Cell*, *95*(6), 829–837.

Oseen, C. W. (1910). Stokes' formula and a related theorem in hydrodynamics.

Arkiv. Mat. Astron. Fysik, *6*, 20.

Oseen, C. W. (1927). Neuere methoden und ergebnisse in der hydrodynamik. *Leipzig : Akademische Verlagsgesellschaft m. b. H.*. Retrieved from `https://ci.nii.ac.jp/naid/10011544827/en/`

Parker, G. H. (1905). The movements of the swimming-plates in ctenophores, with reference to the theories of ciliary metachronism. *Journal of Experimental Zoology*, *2*(3), 407–423.

Pozrikidis, C. (1992). *Boundary integral and singularity methods for linearized viscous flow.* Cambridge: Cambridge University Press.

Pozrikidis, C. (2002). *A practical guide to boundary element methods with the software library bemlib.* CRC Press.

Pozrikidis, C. (2011). *Introduction to theoretical and computational fluid dynamics.* Oxford university press.

Proudman, I., & Pearson, J. (1957). Expansions at small reynolds numbers for the flow past a sphere and a circular cylinder. *Journal of Fluid Mechanics*, *2*(3), 237–262.

Rapp, B. E. (2017). Chapter 30 - finite difference method. In B. E. Rapp (Ed.), *Microfluidics: Modelling, mechanics and mathematics* (p. 623 - 631). Oxford: Elsevier. Retrieved from `http://www.sciencedirect.com/science/article/pii/B9781455731411500307` doi: https://doi.org/10.1016/B978-1-4557-3141-1.50030-7

Raymont, J. E. (1980). *Plankton and productivity in the oceans.* (Tech. Rep.).

Reynolds, O. (1883). An experimental investigation of the circumstances which determine whether the motion of water shall be direct or sinuous, and of the law of resistance in parallel channels. *Philosophical Transactions of the Royal Society of London*, *174*, 935–982. Retrieved from `http://www.jstor.org/stable/109431`

Shankar, P. N. (2007). *Slow viscous flows : qualitative features and quantitative analysis using complex eigenfunction expansions.* London: Imperial College.

Smith, D., Gaffney, E., Blake, J., & Kirkman-Brown, J. (2009). Human sperm accumulation near surfaces: a simulation study. *Journal of Fluid Mechanics*, *621*, 289–320.

Smith, S. H. (1987). A note on the stokes paradox. *Quarterly of Applied Mathematics*, *45*(3), 529–531.

Sommerfeld, A. (1908). Ein beitrag zur hydrodynamischen erklarung der turbulenten flussigkeisbewegung. *Atti Congr. Int. Math. 4th*.

Stokes, G. G. (1851). *On the effect of the internal friction of fluids on the motion of pendulums* (Vol. 9). Pitt Press Cambridge.

Strauss, W. A. (1992). *Partial differential equations*. John Wiley & Sons New York, NY, USA.

Suthers, I. M., & Rissik, D. (2009). *Plankton: A guide to their ecology and monitoring for water quality*. CSIRO publishing.

Tomotika, S., & Aoi, T. (1951). An expansion formula for the drag on a circular cylinder moving through a viscous fluid at small reynolds numbers. *The Quarterly Journal of Mechanics and Applied Mathematics*, *4*(4), 401–406.

Tritton, D. J. (1959). Experiments on the flow past a circular cylinder at low reynolds numbers. *Journal of Fluid Mechanics*, *6*(4), 547–567.

Verworn, M. (1891). Studien zur physiologie der flimmerbewegung. *Archiv für die gesamte Physiologie des Menschen und der Tiere*, *48*(1), 149–180.

Weber, T. S., & Deutsch, C. (2010). Ocean nutrient ratios governed by plankton biogeography. *Nature*, *467*(7315), 550.

White, F. M. (1991). *Viscous fluid flow.* McGraw.

White, F. M. (2011). *Fluid mechanics* (7th ed. ed.). New York: McGraw-Hill.

Whiteley, J. (2017). *Finite element methods: a practical guide*.

Witman, G. B. (1990). Introduction to cilia and flagella. In *Ciliary and flagellar membranes* (pp. 1–30). Springer.

Yano, H., & Kieda, A. (1980). An approximate method for solving two-dimensional low-reynolds-number flow past arbitrary cylindrical bodies. *Journal of Fluid Mechanics*, *97*(1), 157–179.

Zhu, L., Lauga, E., & Brandt, L. (2012). Self-propulsion in viscoelastic fluids: pushers vs. pullers. *Physics of fluids*, *24*(5), 051902.